Application of Phase Change Material to Improve Adiabatic Compressed Air Energy Storage System

Erwan Adi Saputro

A thesis submitted in fulfilment of the requirements for the degree of
Doctor of Philosophy in Chemical and Materials Engineering,
The University of Auckland, 2019.

Abstract

The use of renewable energy, such as wind and solar, has significantly increased in the last decade. However, these renewable technologies have the limitations of being intermittent; thus, storing energy in the form of compressed air is a promising option. In compressed air energy storage (CAES), the electrical energy from the power network is transformed into a high-pressure energy through a compressor. When the demand for electricity is high, the stored high-pressure air is used to drive a turbine to generate electricity. The advantages of CAES include high energy density and quality, but the efficiency is relatively low (about 50%) since a significant amount of the compression energy is lost as heat. Additionally, in the expansion process, this technology would require a non-renewable source of energy for heating the air to prevent frosting. To overcome this drawback, an adiabatic CAES (ACAES) system has been proposed by applying methods of storing the generated heat during compression.

The generated heat during compression is stored in the specific thermal storage system and is utilised to heat up the air during the expansion process. This method eliminates or limits the use of extra energy to heat the expanded air, usually needed in CAES system, which enhances the efficiency of the system by up to 70%. However, there are still challenges related to the selection of the thermal energy storage (TES) system needed in this application.

The thermal storage material should have large storage capacity and should be able to store/release the heat rapidly during compression and expansion. For that reason, this thesis aims to develop a new method for the ACAES system using microcapsule of phase change material (PCM) for thermal storage. The use of PCM is selected since it has high latent heat of melting and hence is able to store a large amount of heat within a narrow change of temperature. The microcapsules are not only needed to contain the PCM but also to provide the large surface Philoarea needed for the heat to be stored in or released from it at a very high rate. In addition, a specific goal of this research is to develop a model for a small ACAES, which requires solving energy equations in both air and container wall and validate the model experimentally.

A small CAES system has been designed for experimental purposes to validate the conceptual model. During the compression stage, the compressed air is stored into a 2L cylinder at 200 bar, while during the expansion stage, the compressed air is released to the environment. The results show that at the beginning of compression the air temperature rises from approximately 17°C to over 60°C, while it drops to -20°C during expansion.

The previous model is further improved to account for the presence of PCM microcapsules and then validated experimentally. In the presence of PCM microcapsules (Micronal® DS 5038X), the air temperature rises from 24°C to around 50°C during compression, which is lower than without PCM, since PCM absorbs some of the heat and stores it in the form of latent heat. While in expansion, the minimum temperature drops to only -2 °C compared to -20°C when operated without PCM, which indicates that PCM has efficiently transferred its stored heat to the air.

The effect of compression on physical and thermal properties of PCM microcapsules are investigated by comparing their characteristics before and after compression and for a number of cycles. Since air compression could crack the shell of the microcapsule, a metal-coating process, well-described in the thesis, is applied to prevent cracking of the polymer shell of the microcapsules and to improve their stability. Also to have a better understanding, two different PCMs are applied in this research: Micronal® DS 5038X and Microtek 24D, together with Microtek 24D metal-coated. All PCM microcapsules used in this research are analysed using differential scanning calorimetry (DSC), thermal gravimetric analysis (TGA) and scanning electron microscope (SEM), before and after 20 compression-expansion cycles. The results show that Micronal® DS 5038X has a better stability than Microtek 24D since these microcapsules are lumps of very small capsules. The performance of Microtek 24D is improved when metal coating is applied to the capsule.

The results disclosed in this thesis indicate that PCM microcapsules are able to successfully store the heat generated during compression and release it during expansion at a very high rate due to their large surface area. The developed model has successfully predicted both air and cylinder's wall temperature during compression and expansion processes.

Acknowledgements

First and foremost, I would like to express my appreciation to Professor Mohammed Farid for the warm welcome, active discussions, impactful advice and comments and the enthusiasm portrayed through my entire Ph.D. journey. It is my honour to be part of the world-class research group which is full of friendly individuals with great ideas.

I would like to thank Professor John Chen and Dr. Refat Al-Shannaq for their kind support and academic impact in my research. Additionally, all contributions from the technical and supporting staff at the Department of Chemical and Material Engineering, University of Auckland are greatly appreciated.

I also acknowledge Dive Doctor Company Ltd. for their kind support and assistance for the all experimental work conducted at their facilities.

I deeply appreciate the financial support from the doctoral scholarship provided by the Directorate General of Resources for Science, Technology and Higher Education (DG-RSTHE) of the Republic of Indonesia.

Most importantly, I would like to express my deepest gratitude to my lovely wife, son, and daughters for the tender care and endless encouragements in tandem with their incredible support. Also, to my parents for their material and spiritual support throughout this Ph.D. journey.

Table of Contents

Abstract ii

Acknowledgements iv

List of Tables viii

List of Figures ix

Nomenclature xi

Abreviations xii

Chapter 1. Introduction 1

1.1. Project Motivation 1

1.1.1 Energy storage definition and classification 1

1.1.2. Intermittent renewable energy sources 1

1.1.3 Compressed Air Energy Storage 5

1.2 Study Objectives 8

1.3 Thesis Structure 9

Chapter 2. Review of Thermal Storage on Adiabatic Compressed Air Energy Storage 11

Chapter Preface 11

2.1 Introduction. 11

2.2 Compressed Air Energy Storage 13

2.3 Thermal Energy Storage 15

2.4 Application of Thermal Energy Storage on ACAES 16

2.4.1 ACAES with sensible heat energy storage 16

2.4.2 ACAES with latent heat energy storage 19

2.5 Summary 27

Chapter 3. Performance of a Small-Scale Compressed Air Energy Storage 28

Chapter Preface 28

3.1 Introduction 29

3.2 Theory 30

3.3 Methods 32

3.3.1 Experimental procedure 32

3.3.2 Theoretical modelling 33

3.4 Results and Discussion 35

3.4.1 Pressure evaluation during the charging and discharging process. 35
3.4.2 Basic calculation for adiabatic compression and expansion 36
3.4.3 Heat transfer analysis 37
3.4.4 Temperature evaluation during charging and discharging process. 39
3.4.5 Summary of the experimental measurements 41
3.5 Summary 42
Chapter 4. A Novel Approach of Heat Recovery system in Compressed Air Energy Storage 43
Chapter Preface 43
4.1 Introduction 44
4.1.1 Development of adiabatic compressed air energy storage (ACAES) 44
4.1.2 Encapsulation of phase change material 46
4.2 Theoretical Modelling 47
4.3 Experimental Method 49
4.4 Results and Discussion 50
4.4.1 Thermal Properties of phase change material (Micronal® DS 5038X). 50
4.4.2 Pressure change during charging and discharging processes. 52
4.4.3 Heat transfer analysis 53
4.4.4 Temperature evaluation during charging and discharging process. 56
4.5 Summary 58
Chapter 5. Performance of metal and non-metal coated phase change materials microcapsules when used in compressed air energy storage system 59
Chapter Preface 59
5.1 Introduction 59
5.2 Experimental work 61
5.2.1 Materials 62
5.2.2 Preparation of metal coated PCM microcapsules 62
5.2.3 Surface activation of PCM microcapsules 62
5.2.4 Electroless plating 63
5.2.5 Air compression process 63
5.2.6 PCM microcapsules Characterizations 64
5.2.6.1 Particle size distribution (PSD) 65
5.2.6.2 Differential Scanning Calorimetry (DSC) 65
5.2.6.3 Scanning Electron Microscope (SEM) 65

5.3 Result and Discussion 66
5.3.1 Thermal performance of ACAES system. 66
5.3.2 PCM microcapsules life assessment 70
5.3.2.1 Particle size distribution (PSD) 70
5.3.2.2 DSC analysis of PCMCs 71
5.4 Scale-up challenges for CAES. 76
5.4.1 Technology aspect. 76
5.4.2 Economic aspect 76
5.4.3 Proposed large scale design using PCM Microcapsules as TES. 77
5.5 Summary 78
Chapter 6. Conclusions and Future Research Work 79
6.1 Author's Contributions 79
6.2 Conclusions 79
6.3 General Conclusion 80
6.4 Recommendations for Future Research Work 81
References 82
Appendices 90

List of Tables

Table 1. 1 Worldwide installed electrical energy storage capacities. Adapted from [9] 3
Table 1. 2 Technical parameters for various energy storage systems. Obtained from [10-12] 4
Table 1. 3 Development status for various energy storage systems, obtained from [9]. 5
Table 1. 4 Technical data of the existing CAES plants [19, 22] 7
Table 2.1 Candidates for sensible heat material for ACAES application 18
Table 2.2 Comparison of PCM, Adapted from [70, 87] 20
Table 2.3 Latent heat of storage materials as a candidate for TES on ACAES and their temperature ranges 21
Table 2.4 Some international PCM companies available worldwide. 26
Table 3.1 The specification of the small cylinder 33
Table 3.2 Adiabatic compression and expansion 37
Table 3.3 Temperature change at 100 bar 41
Table 3.4 Temperature change at 200 bar 41
Table 5. 1: Thermo-physical properties of PCM microcapsules used in this study. 62

List of Figures

Figure 1.1 Global cumulative installed wind capacity 2000-2015.Adapted from [6]. 2
Figure 1.2 Worldwide cumulative capacity installed solar PV 2000-2014. Adapted from [8].3
Figure 1.3 Schematic process of CAES plant, Adapted from [2]. 6
Figure 2.1 Approximated renewable energy share of overall energy consumption, 2015 [42]. 12
Figure 2.2 Simplification of constant pressure energy storage. 14
Figure 2.3 The basic principle of ACAES with Active thermal storage system, Simplified from [32, 34]. 17
Figure 2.4 Basic principles of ACAES with the passive thermal storage system, simplified from [19]. 17
Figure 2.5 Classification of PCM [70, 71, 84-86]. 19
Figure 2.6 Concentrated solar power plant integrated system with TES using PCM [41]. 22
Figure 2.7 CAES integrated system with TES using PCM (ACAES). 23
Figure 2.8 Cascade PCM for TES system on ACAES[78]. 24
Figure 2.9 Simplification of proposed ACAES system 25
Figure 3.1 Experimental set-up 32
Figure 3.2 Pressure change during charging, storing and discharging processes; 100 bar (a) and 200 bar (b). 36
Figure 3.3 Heat transfer coefficient for mixed convection during charging process at 100 bar (a) and 200 bar (b) 38
Figure 3.4 Heat transfer analysis for mixed convection during discharge process at 100 bar (a) and 200 bar (b). 38
Figure 3.5 Measured and predicted air and cylinder's wall temperatures during charging process, (a) 100 bar and (b) 200 bar. 39
Figure 3.6 Measured and predicted air and cylinder's wall temperatures discharge process, (a) 100 bar and (b) 200 bar. 40
Figure 4.1 The simplified process of adiabatic CAES with sensible heat storage: (a) passive system and (b) active system. 45
Figure 4.2 The simplified process of ACAES with latent heat storage as TES. 45
Figure 4.3 Experimental flow scheme design. 49
Figure 4.4 DSC analysis for Micronal® DS 5038X. 51

Figure 4.5 Particle size analyser result for Micronal® DS 5038X. 51
Figure 4.6 Pressure change during charging and storing processes, with PCM (a) and without PCM (b). 52
Figure 4.7 Pressure change during discharging processes with PCM (a) and without PCM (b). 53
Figure 4.8 Heat transfer coefficient during the charging process with PCM (a) and without PCM (b). 54
Figure 4.9 Heat transfer coefficient during the discharging process with PCM (a) and without PCM (b). 55
Figure 4.10 Air and wall temperature comparison between simulation and experimental study on charging process for the system with PCM (a) and system without PCM (b).....56
Figure 4.11 Air and wall temperature comparison between simulation and experimental study on discharging process for system with PCM (a) and system without PCM (b).....57
Figure 5.1 Schematic setup of ACAES.....64
Figure 5.2 Flow chart diagram of the experimental steps.....66
Figure 5.3 Temperature and pressure profiles at fast and slow air expansion. 67
Figure 5.4 Air and wall temperatures variations during air compression/expansion-first cycle 68
Figure 5.5 Air and wall temperature variations during air compression/expansion-20x cycles 69
Figure 5.6 Particle size distribution before and after 20x cycles. 70
Figure 5.7 DSC measurements of (a) Micronal DS 5038X and (b) Microtek 24D before and after 20x cycles 72
Figure 5.8 DSC measurements of metal-coated Microtek 24D PCMCs before and after 20x cycles.....73
Figure 5.9 Micronal 5038X metal-coated. 74
Figure 5.10 SEM images of (A) original Micronal DS 5038X PCMCs (B) Micronal DS 5038X PCMCs-20x cycles (C) original non-metal-coated Microtek 24D PCMCs (D) non-metal-coated Microtek 24D PCMCs-20x cycles (E) original metal-coated Microtek 24D PCMCs and (F) metal-coated Microtek 24D PCMCs-20x cycles 75
Figure 5.11 Application of PCM Microcapsule at CAES, (a) integrated with air storage, (b) special thermal storage facility. 77

Nomenclature

Symbol	Description	Unit
A	Surface area	m^2
C_p	Heat capacity at constant pressure	j/kg K
Cp_a	Heat capacity of air	j/kg K
Cp_t	Heat capacity of cylinder	j/kg K
Cp_p	Heat capacity of probe cylinder	j/kg K
Cp_{pcm}	Heat capacity of PCM based on Cp effective	j/kg K
C_v	Heat capacity constant volume	j/kg K
D_o	Outside diameter	m
D_i	Inside Diameter	m
G	Gravitational acceleration	m/s^2
Gr	Grashof number	
h	Convection Heat transfer coefficient	W/m^2 K
h_1	Convection Heat transfer coefficient for cylinder's wall	W/m^2 K
h_2	Convection Heat transfer coefficient for probe cylinder	W/m^2 K
K	Thermal conductivity	W/m K
k	C_p/C_v = 1.4 for an ideal gas	
L	The length of the cylinder	m
m	Mass	kg
mf	mass flowrate	kg/s
m_t	Mass of cylinder	kg
m_1	Mass of air at initial time	kg
m_2	Mass of air at final time	kg
$\dot{m}_{in}$	mass flow rate entering the storage unit	kg/s
$\dot{m}_{out}$	mass flow rate out from the storage	kg/s
N	Number of moles	mole
Nu	Nusselt number	
P_1	Initial pressure	Bar
P_2	Final pressure	Bar
Pr	Prandtl number	
R	Universal gas constant (8.314 J/mol K)(286.9 J/Kg K)	
Ra	Rayleigh Number	
Re	Reynolds Number	
T′	Ambient temperature	K
T_{a1}	Temperature of air in initial time process	K
T_{a2}	Temperature of air in final time process	K
T_{c1}	Temperature of cylinder in initial time process	K
T_{c2}	Temperature of cylinder in final time process	K
T_{p1}	Temperature of probe cylinder in initial time process	K
T_{p2}	Temperature of probe cylinder in final time process	K
T_a	Temperature of air	K
T_w	Temperature of cylinder's wall	K
T_{eq}	Equilibrium Temperature	K
Q	Energy	J
Q_{air}	Energy in the air system	J
$Q_{cylinder}$	Energy in the cylinder system	J
U_1	Internal energy in the initial process	J
U_2	Internal energy in the final process	J
V_{air}	volume of air	m^3
V	Volume	m^3
W_C	compression power	watt
W_t	Expansion power	watt
β	Volume expansivity	1/K
ρ	Density	kg/m^3
M	Dynamic viscosity	kg/ms
ϒ	Kinematic viscosity	m^2/s

Abreviations

ACAES	Adiabatic Compressed Air Energy Storage
CAES	Compressed Air Energy Storage
DSC	Differential Scanning Calorimetry
EASE	European Association for Storage of Energy
PCM	Phase Change Material
PHS	Pumped Hydro Storage
SEM	Scanning electron microscope
TES	Thermal Energy Storage
VLAB	Vented Lead Acid Battery
NGCC	Natural Gas Combine Cycle
SMES	Superconducting Magnetic Energy Storage
HTF	Heat Transfer Fluid
RTD	Resistance Temperature Detector
NaS	Sodium Sulphur
Li-ion	Lithium-ion battery
VRB	Vanadium redox
LA	Lead Acid Battery
Ni-Cd	Nickel Cadmium Battery

Chapter 1. Introduction

1.1. Project Motivation

1.1.1 Energy storage definition and classification

Research on energy storage has been ongoing for the last decades. A complete classification of energy storage is given by the European Association for Storage of Energy. Energy storage technology can be classified under five headings, based on the form of energy storage: chemical energy storage, electrical energy storage, electrochemical energy storage, mechanical energy storage and thermal energy storage (TES). Mechanical energy storage is further divided into three main groups: kinetic energy storage (Flywheel), potential energy storage (pumped hydro storage [PHS]), and compressed air energy storage (CAES). TES can be divided further into three sub-classifications: sensible heat storage, latent heat storage and thermochemical storage [1]. Electrical energy storage can be defined as a conversion process by which electrical energy, taken from a power network, is transformed into a form which can be re-converted to electricity when needed [2].

1.1.2. Intermittent renewable energy sources

The rapid growth of renewable energy requires improvements in energy storage facilities to increase their efficiency and to reduce costs. There are a number of reasons for storing energy. For instance, some energy sources, such as wind and solar power are available only intermittently, energy needs to be transferred to various areas; or there is a fluctuation in power consumption over different hours, days, months, or even years. As a consequence, it is essential to have a way of saving and storing energy [3-5].

Even though wind and solar have high intermittency, in recent years, there has been a significant increase in capacity of installed wind and solar power stations that will account for an increase in the need for energy storage. Figures 1.1 and 1.2 illustrate the installed capacity of the wind and solar energy globally.

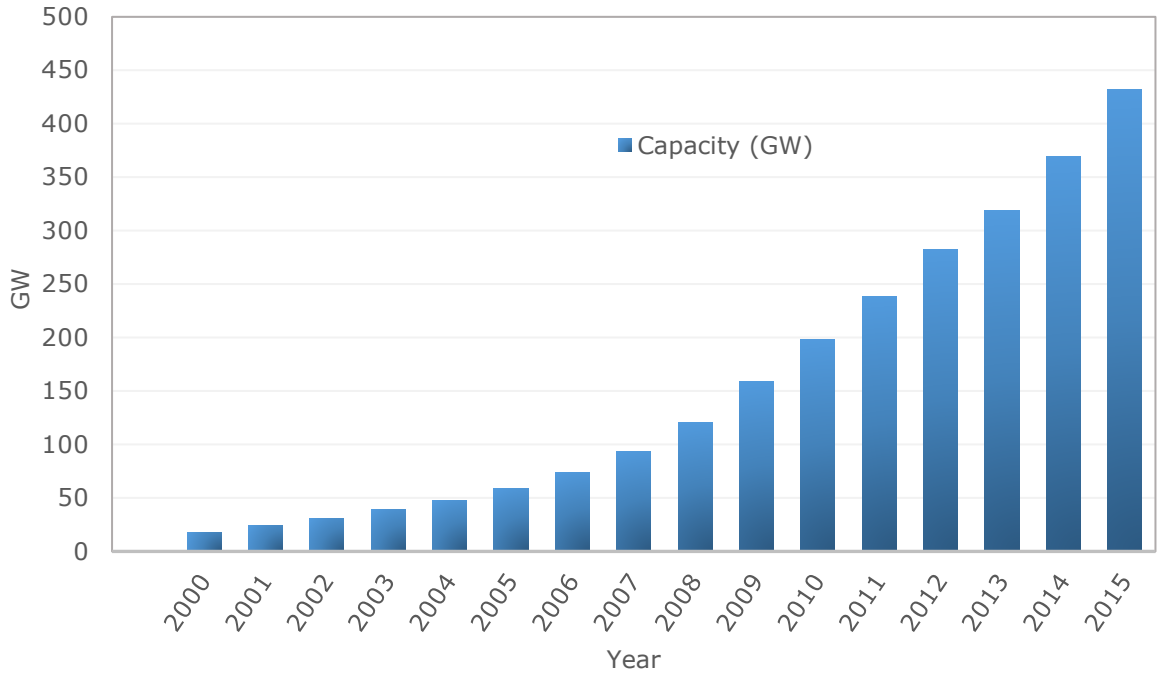

Figure 1.1 Global cumulative installed wind capacity 2000-2015.Adapted from [6].

As seen in Figure 1.1, installed wind capacity has increased significantly over the last decade. In 2015 the capacity of installed wind power was 432.4 GW. According to the Global Wind Energy Council (GWEC), the top 10 countries for installed wind systems are: China (33.6%), USA (17.2%), Germany (10.4%), India (5.8%), Spain (5.3%), United Kingdom (3.1%), Canada (2.6%), France (2.4%), Italy (2.1%), and Brazil (2.0%) [6]. In 2015, China installed 30.5 GW of wind power, making it the world leader in the installation of wind power systems. In 2015, USA and Germany added new installations of wind power of around 13.6 GW and 9.5 GW respectively. Both Brazil and India added 4 GW, with other countries contributing no more than 2 GW.

The other renewable energy source is solar, and globally, solar PV installations have increased dramatically (Figure 1.2). It is interesting to note that, in 2004, solar power capacity was less than 10 GW; however, this had increased to 178.39 GW as of 2014. In Europe, the UK and Germany are the leading markets for solar PV. In the Asia Pacific region, Korea and Australia had the same levels of solar PV installations, with more than 1 GW in 2014 [7].

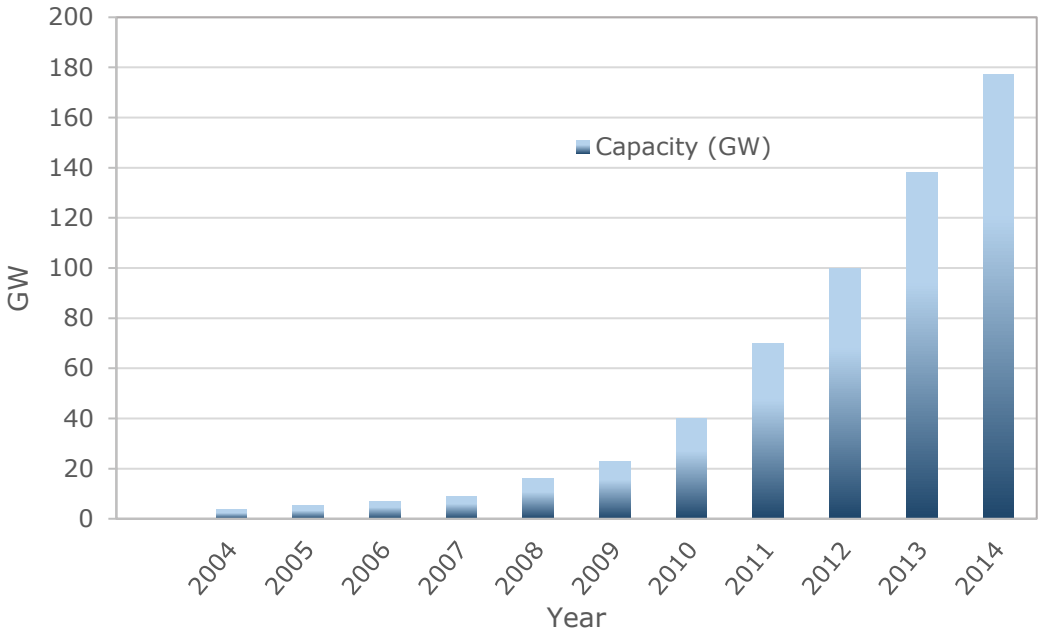

Figure 1.2 Worldwide cumulative capacity installed solar PV 2000-2014. Adapted from [8].

Based on the growing renewable power generation reported in Figures 1.1 and 1.2, there will be a growing need for storage systems to ensure efficient grid operation. The most commonly used energy storage systems in the world, presently, are detailed in Table 1.1. It shows that 99% of worldwide energy storage capacity comes from PHS, followed by CAES and battery storage [9]. Thus, while it is a distant second largest energy storage system, CAES may be an ideal system for future development of renewable energy storage. PHS stores and produces the electricity by moving water between two reservoirs at different elevations while the battery store and produce the electricity by chemical reaction [5, 9]. The CAES system is discussed in the next section.

Table 1. 1 Worldwide installed electrical energy storage capacities. Adapted from [9]

Energy storage	MW	%
Pumped hydro	127000	99.32
Compressed air energy storage	440	0.34
Sodium-sulphur battery	316	0.25
Lead-acid battery	35	0.03
Nickel-cadmium battery	27	0.02
Flywheels	25	0.02
Lithium-ion battery	20	0.02
Redox-flow battery and other	3	0.003

Since energy storage function and application may be different, storage system selection will depend on many factors; for example, geographic and technological factors (e.g., energy density, power rating, lifetimes, and other technical parameters). The technological parameters of several kinds of energy storage facilities, including CAES and these parameters are summarised in the following table:

Table 1. 2 Technical parameters for various energy storage systems. Obtained from [10-12]

	Energy Density (Wh/kg)	Power Rating (MW)	Lifetimes (years)	Durability (cycle)	Efficiency
PHS	0.5-1.5	100-5000	40-60	12,000-30,000+	75-85
CAES	20-60	3-400	20-60	30,000+	50-89
LA	30-50	0.001-50	5-15	500-1200	70-92
NI-Cd	50-75	1-40	10-20	2000-5000	60-65
NaS	150-240	0.05-8	10-15	1000-2500	80-90
Li-ion	75-200	0.1	5-15	1000-10000	85-90
VRB	10-50	0.3-15	5-15	13000+	75-85
Flywheel	5-130	0.002-20	15-20	1,000,000+	80-99
SMES	0.5-5	0.1-10	20+	100,000	95-98
Super Capacitor	2.5-15	0.3	20+	1,000,000+	90-95
TES	80-250	0.1-300	10-40	2000-4000	50-90

As seen in Table 1.2, CAES has some benefits over other storage systems. Firstly, if the battery is excluded because of its need of recycling, CAES has higher energy density than PHS. Secondly, its power rating is higher than all other storage systems except PHS. Indeed, it also has a long lifetime, similar to that of PHS. The lifecycle of CAES can be more than 30,000 cycles, and the efficiency of this storage can be as high as 89%. However, CAES also has some disadvantages (Table 1.3). The major drawback of CAES is that it is hard to find a suitable location for storage. This technology needs to be set up near salt caverns or rock mines that have the capacity to store air under high pressure [2]. Another problem in conventional CAES is the requirement of fuel for heating the expanded low-temperature air before it can be used for electricity generation since significant temperature drop occurs during expansion [13].

Table 1. 3 Development status for various energy storage systems, obtained from [9].

	Maturity	Advantages	Disadvantages
PHS	Mature	large capacity, low cost	Huge area, destroys local vegetation
CAES	Developed	Available large and small capacity	Specific site required
LA	Commercial	Low capital cost	Toxic, require recycling
NI-Cd	Commercial	High power	Toxic, require recycling
NaS	Commercial	High energy density and efficiency	Toxic, require recycling
Li-ion	Commercial	High energy density and efficiency	Toxic, require recycling
VRB	Developing	High capacity	Short lifetime
Flywheel	Developed	High capacity and efficiency	Low energy storage,
SMES	Developed	High capacity and efficiency	High cost
Super Capacitor	Developing	Long life cycle, high efficiency	Low energy density, toxic
TES	Developed	High energy density	Low efficiency

According to Mason and Archer [14], a wind-CAES system has a lower CO_2 emission and lower fuel consumption compared to a wind-NGCC. CAES also has a fast start-up time that makes it suitable for wind power because that is one of the requirements for storage of energy from wind and solar energy [14, 15]. The fact that wind farms are usually located at a far distance from housing areas is one of the reasons to consider wind-CAES system [15]. A comparative analysis has been done through several energy storages systems for gathering power from the wind sources. This analysis was based on load shifting, distribution support, and power quality. The results show that small-scale CAES is slightly better than other storage systems (PHS, flywheels, and SMES) [16]. The comparison of energy and economic analysis for solar power, PV-micro CAES, and PV only, has been made for residential use. It was found that an integrated CAES+PV (PV size 15 kW) provides an electrical saving of 21,572 kWh/y (6,788 €/y) while for PV system alone (PV size 33 kW) it was only 18,666 kWh/y (4,229 €/y) [17].

1.1.3 Compressed Air Energy Storage

CAES is used in power plants to store energy in the form of compressed air. During off-peak hours this plant uses electrical power to compress air, and when the electricity is needed during peak hours, this plant uses the compressed air to run gas turbines to generate electricity [2, 18, 19]. In this technology, after the compression, the air is cooled and subsequently stored in an underground cavern. During the discharge process, the air temperature drops during expansion, and hence it has to be heated using fuel before it is transmitted to the turbine [2, 18]. The schematic diagram of such a system can be seen in Figure 1.3.

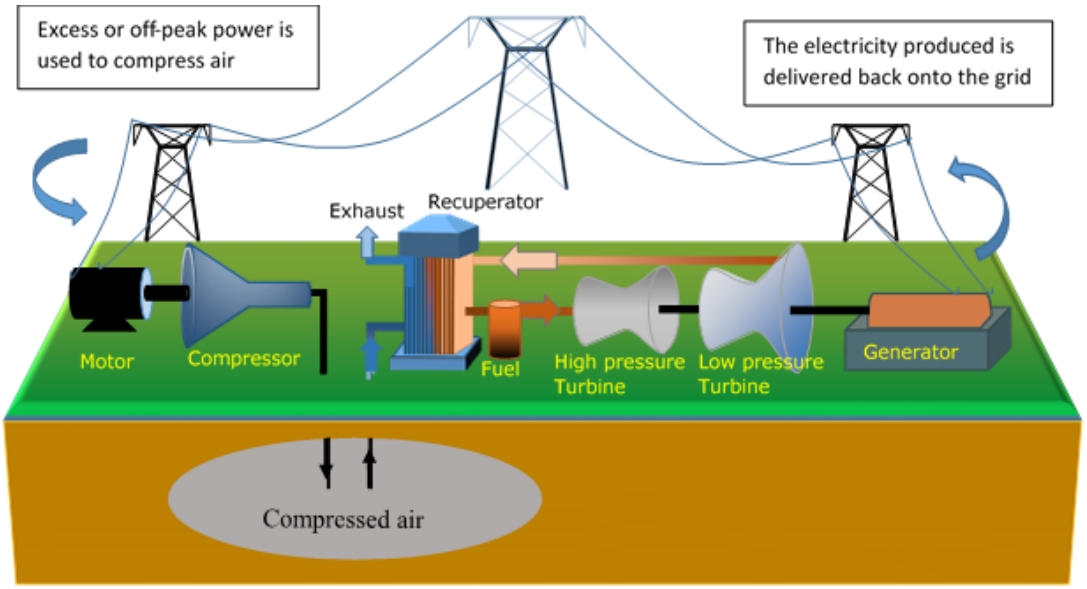

Figure 1.3 Schematic process of CAES plant, Adapted from [2].

CAES was invented and patented by Stal Laval in 1949, and since then, CAES has been a subject of much interest for decades [20]. However, it was not until 1978 that the first CAES power plant was deployed in Huntorf, Germany. Initially, this plant has a power rating of 290 MW, which then recently was increased to 320 MW [19]. The second CAES plant was established in 1991 in McIntosh, Alabama, USA. The power rating of this plant is 110MW. Both power plants use salt caverns as their air storage system [21, 22].

Another CAES project was started in Norton, Ohio (USA) in 2001. Unfortunately, this project was delayed due to lack of technological support. In 2009, it was continued by First Energy Generation Corp; nevertheless, in 2013 the project was terminated for economic reasons [23]. In 2003, a new CAES facility was started in Iowa USA by the Iowa Stored Energy Park project. Unfortunately, in 2011 this project was also canceled due to geographic issues [24]. So far, there are three main identifiable factors to explain why these projects have not been completed and why no more CAES power plants have been established: geological structure, financial resources, and technological resources.

Table 1. 4 Technical data of the existing CAES plants [19, 22]

Parameter	Huntorf (Germany)	McIntosh AL (USA)
Build year	1978	1991
Compression		
Max input power	62 MW	53 MW
Charging time	8-12 hours	41-53 hours
Max mass flow rate	108 kg/s	94 kg/s
Unit	2	4
Storages		
Cavern pressure range	46-72 bar	46-75 bar
Cavern volume	310,000 m3	538,000 m3
Expansion		
Max output power	321 MW	110 MW
Discharging time	2 hours	24-26 hours
Max mass flow rate	455 kg/s	154 kg/s
Fuel	Gas	Gas/Oil
Recuperator	No	Yes
Heat rate	5,800 kJ/kWh	4,300 kJ/kWh
Roundtrip efficiency	42%	54%

Table 1.4 shows the technical parameter for the existing conventional CAES plants in Germany and USA. Both plants use salt caverns as air storage chambers, and both facilities use fuel to heat up the air before entering the turbine. Neither plant has a heat-storage facility. The main difference between the plants is the use of a recuperator system in McIntosh plant. This system uses the hot air from the lower pressure expander to preheat the air from storage thus decreasing the fuel consumption by about 25%. As a result, the round trip efficiency of McIntosh plant is higher than the Huntorf plant [19, 22].

The need for extra heat in CAES plants makes the efficiency of the system relatively low. Also, in the expansion process, when fuel is used to provide extra heat, carbon dioxide emissions will not sustain the process as an environmentally friendly process [25, 26].

To overcome this drawback, an adiabatic CAES is designed by applying TES into the system. Thermal storage is introduced to store the heat generated during compression for later use

during expansion. This thermal storage is important as it can minimise the use of non-renewable sources of energy and enhance the efficiency of this system up to around 70% [12, 25, 27-31]. As a result, extensive research is conducted to improve the adiabatic CAES (ACAES) system through the application of sensible energy storage. Common sensible heat-storage materials that are incorporated with ACAES include oil [32-34], water [30, 35, 36], rock bed [28, 37, 38] and ceramic material[39].

The use of phase change material (PCM), which has high storage density, has been limited in this application. For PCM to be used in ACAES, it should have a high thermal conductivity for it to absorb and release the heat at very high rates. A promising method of providing such an increase in the effective thermal conductivity of PCM is by encapsulation or impregnation in a graphite matrix. Alternatively, PCM encapsulation, in micro- and nano-scales, can increase heat transfer rate dramatically due to the large heat transfer area provided by the micro- or nano-capsules [40, 41]. For that reason, a novel approach of using PCM microcapsules to store and release thermal energy in ACAES is investigated and explained in this thesis.

1.2 Study Objectives

The objectives of the study were as follows:

1. To conduct a comprehensive literature review on energy storage, especially on ACAES systems, including their design strategies as proposed in the literature.
2. To conduct a comprehensive literature review on PCMs and select the most suitable method for their encapsulation in ACAES systems.
3. To develop a mathematical model for a small ACAES system by solving energy equations in both the air and the container's wall to describe the thermal effect during compression and expansion process in air storage.
4. To design and construct a small-scale ACAES system for experimental purposes and to validate the conceptual model.
5. To use PCM microcapsules as TES material for capturing the heat generated during compression and releasing it during expansion.
6. To apply a metal coating to the microcapsules to improve the performance of the PCM microcapsules utilised in this research.
7. To identify the stability of the microcapsules used in the system, specifically measuring any change in the morphology and thermal characteristic of it.
8. Scale up of the research outcome.

1.3 Thesis Structure

The thesis comprises six chapters which are based on a series of scientific papers, either accepted or submitted to an international conference and international journals. Some parts of these chapters may overlap, particularly in the introduction and method sections. The chapters are structured as follows:

Chapter 1: Introduction. This chapter gives an elementary account of the need for energy storage for managing the quality and stability of power networks, especially the intermittency of renewable energy (wind and solar). Additionally, this chapter describes the differentiation, benefits, and drawbacks of energy storage. This chapter also gives an overview of the development of and current issues with one particular energy storage system: conventional CAES. Furthermore, the background and the objective of the study are clarified in this chapter.

Chapter 2: Review of Thermal Storage on Adiabatic Compressed Air Energy Storage. This chapter explains adiabatic CAES (ACAES), a more modern technology than the conventional CAES as described in Chapter 1. This chapter provides an overview of ACAES, especially thermal storage systems, by explaining the basic design of ACAES and comparing the availability of different thermal storage materials. Additionally, in this chapter, the current issues associated with the use of thermal storage in ACAES, including materials, working principles and system characterisation are also elaborated.

Chapter 3: Performance of a Small-Scale Compressed Air Energy Storage (CAES). Understanding the thermal behaviour in compressed air storage is essential, thus the development of a theoretical model for the compression and expansion processes and the design of small-scale CAES are presented in this chapter. The steady-state analysis as well as the dynamic analysis, to predict the transient change of temperature inside the cylinder, both for air and cylinder's wall temperature behaviour are discussed in this chapter. The model and experimental study are based on a small CAES using a high-pressure cylinder (200 bar, 2 L). This chapter is based on published paper in the *International Journal of Energy Research* with the title "Performance of a Small-Scale Compressed Air Storage (CAS)".

Chapter 4: A novel approach of heat recovery system in Compressed Air Energy Storage (CAES). The CAES system is improved to an ACAES system and explained in this chapter. Also, it presents a novel approach whereby TES is applied to the small CAES system by using PCM. The PCM used in this system is Micronal® DS 5038X in the form of microcapsules. The advantages of using microcapsules are explained in this chapter. A more complicated

conceptual model, due to the accommodation of PCM properties and their behaviour, is also clarified in this chapter. This chapter is based on a published paper in the *Journal of Energy Conversion and Management*, with the title "A novel approach of heat recovery system in Compressed Air Energy Storage (CAES)".

Chapter 5: Performance of metal and non-metal coated phase change materials microcapsules when used in compressed air energy storage system. The microcapsules are assessed in this chapter describes the physical and thermal characteristics of the PCM microcapsules utilised in this project. Two different PCMs are applied in this research: Micronal® DS 5038X and Microtek 24D, together with Microtek 24D metal coated. All PCM microcapsules used in this research, before and after 20 compression-expansion cycles, are analysed using particle size analyser (PSD), differential scanning calorimetry (DSC), and scanning electron microscope (SEM), and discussed in detail in this chapter. This chapter is based on submitted paper to the *Journal Applied Thermal Engineering*.

Chapter 6: Conclusions. The major findings are summarised in this chapter by addressing the key points in the results and discussion in each chapter. The recommendations for further investigation of thermal storage in the ACAES system, especially using PCM, are also described in this chapter.

Chapter 2. Review of Thermal Storage on Adiabatic Compressed Air Energy Storage

Chapter Preface

The continuous increase in power generation from intermittent renewable energy makes energy storage very important to balance the supply and demand of electricity. CAES is one of the prospective energy storage methods in the future. This technology has been commercialised on a large scale (>100MW) by the Huntorf Plant in Germany and McIntosh plant in the USA. The efficiency of this commercial CAES is around 50%. To improve the efficiency up to around 70%, an adiabatic CAES (ACAES) system has been proposed and developed in many parts of the world by applying TES. Although the utilisation of TES in ACAES can increase the efficiency of the process, by recovering the generated heat during compression, there are still challenges related to the selection of the thermal storage system in this application. Hence, this chapter reviews the current issues associated with the use of thermal storage in ACAES, including materials, working principles, and system characterisation.

2.1 Introduction.

Power consumption is increasing along with the increase of population, necessitating improvements in the electricity grid managements [27]. Fossil fuel remains at the top of the energy share (around 78%), followed by renewable energy (19.3%) and nuclear (2.4%) (Figure 2.1)[42]. To contain global warming, the use of fossil fuel should be reduced and replaced by renewable energy sources. Therefore, cost-effective and efficient renewable energy methods are attracting much interest.

The focus on renewable energy has grown vigorously since the early 2000s [43]. In 2016, most of the countries around the world have indicated their intention to make progress by moving toward the implementation of a successful renewable energy policy. Under the Paris Agreement, 117 countries submitted their first nationally determined contributions for renewable energy, and some countries have targeted plans to set up new renewable energy facilities in the next few years [42]. Moreover, on a worldwide basis, the share of renewable

energy is about 19.3%, mainly from wind and solar, and this will continue to increase in the future.

Globally, the use of solar photovoltaic (PV) has dramatically increased from 137GW in 2013 to 303GW in 2016. In 2016, China added 34.5 GW, followed by the US (+14.8 GW), Japan (+8.6 GW), UK (+2GW) and Germany (+1.5GW). Some other countries have also added to the capacity of PV; however, this is of an order of not more than 1 GW (Italy, Australia, Spain) [42]. It is not only solar energy that has shown a significant increase in usage; wind energy has also followed the same trend. Wind energy grew by around 55GW during 2016 (approximately 12% increase from the previous years) so in 2016 the total capacity was around 487 GW worldwide. In addition, more than 90 countries have been utilising wind for power generation [42].

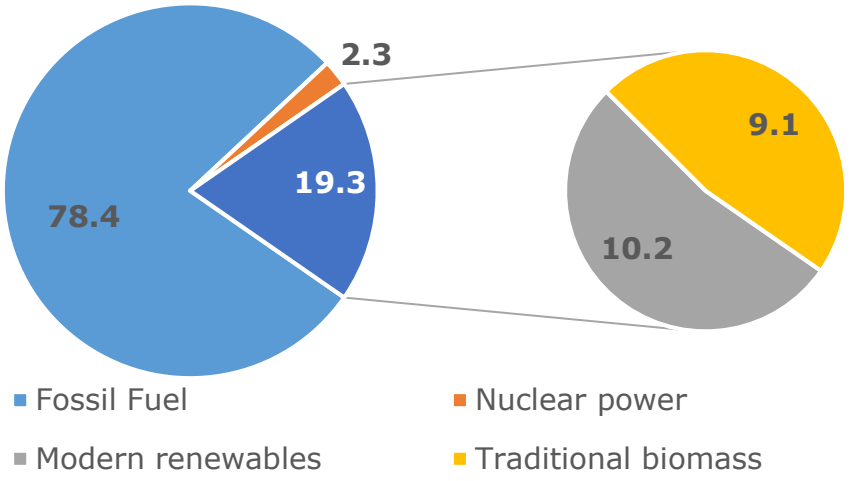

Figure 2.1 Approximated renewable energy share of overall energy consumption, 2015 [42].

Despite the rapid growth of renewable energy, especially solar and wind energy, which is likely to continue in the following years, all types of renewable energy have drawbacks regarding intermittency. To cope with this intermittency, energy storage can be the most efficient way to eliminate or minimise the fluctuation of power generation and maintain its stability in the power network. Many kinds of electrical energy storage systems are commercially available, such as PHS, batteries, and CAES. CAES has some benefits compared with other types of energy storage. Firstly, CAES is environmentally friendly compared to batteries which needs to be recycled, thus causing cost and environmental limitations. For example, CAES has been reported to sustain for more than 20 years compared to less than 12 years for VLAB (vented lead-acid battery) [44]. The installation and the commissioning of CAES also seem to be faster

than VLAB [44]. The lower capital cost of CAES and the capacity limitation of the other forms of electrical energy storage (flywheels, super capacitors, fuel cells, and batteries), will make CAES more attractive in the near future [29, 45].

There have been several investigations into the use of CAES to store wind energy [15, 16, 45-50]. It works by using surplus energy from wind farms to compress air and store it in a specific storage system. During shortage of energy, the CAES system takes over the role of generating electricity [15, 16, 45-51]. In addition to being used for storing wind energy, CAES has been used to save solar energy produced in the form of electricity from PV since solar energy is not available all day and sometimes for longer due to weather conditions [29, 52-54].

2.2 Compressed Air Energy Storage

According to the availability of the heating system in any process, CAES can be categorised into two types: conventional and advanced CAES. The conventional type (Figure 1.3), which is also called diabatic CAES, is well developed, while the advanced or adiabatic CAES (ACAES) is still in the research and development stage. Diabatic CAES requires heat to increase the temperature of the compressed air before it is used to drive the turbine for power generation. In contrast, adiabatic CAES does not require additional heat because the heat generated during compression is stored and utilised to heat the air in the expansion process [19, 55-57].

The diabatic CAES is comprised of three steps: compression, storage, and expansion. Initially, during the time of low demand for electricity, the electricity is used to run a compressor to compress air to a specified pressure. The air is then cooled down and stored at close to ambient temperature in a cavern or specific storage unit. When there is a high demand for electricity, the compressed air is released and used to drive a gas turbine to generate electricity. Before entering to the gas turbine, the air needs to be heated up using fossil fuel or coal [2, 18, 19, 44]. Presently, two diabatic CAES plants have been developed and commercialised. The first is located in Huntorf (1978), Germany and the second is in McIntosh (1991), USA. Both technologies (Huntorf and McIntosh) use salt caverns for air storage with an overall efficiency of 42% and 54%, respectively [19, 21, 23]. Since they use natural gas, a non-renewable source of energy, for heating the air, which emits carbon dioxide[12], the heating process is seen as the main drawback of these conventional CAES systems.

Many variants of CAES systems are introduced in the last decade to improve their performances, such as: adiabatic CAES, constant pressure CAES, isothermal CAES and liquefied air energy storage (LAES).

Constant pressure CAES maintains constant pressure inside the chamber during the discharging process to prevent temperature drop. This technology uses two storage chambers, one for air pressure and the other for water (Figure 2.2). The chamber is filled with water and during the compressing process the compressed air will occupy the chamber pushing the water to the other chamber. In the discharge process the water flows back to the air chamber sustaining the pressure constant by displacing air space with water. [58].

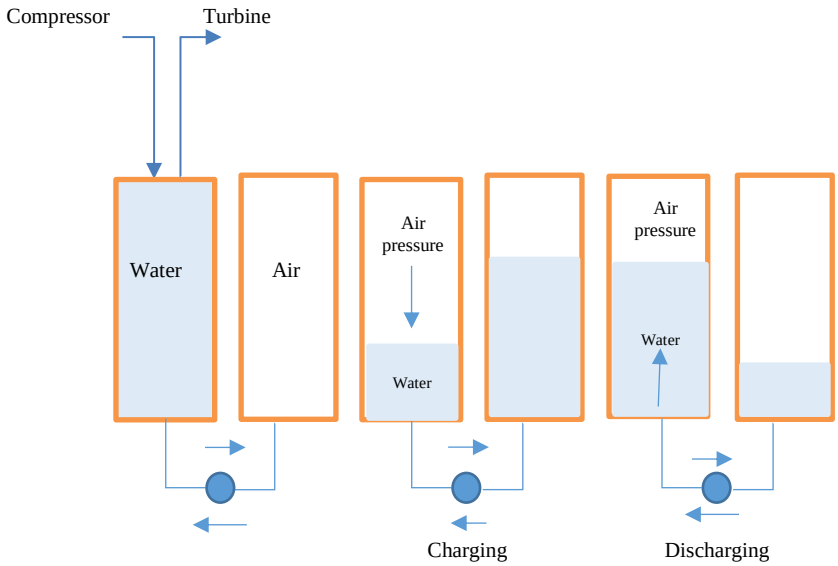

Figure 2.2 Simplification of constant pressure energy storage.

Another variant of CAES is isothermal CAES [59-61]. Constant temperature operation eliminates the use of fuel or thermal storage during discharge and hence improves process efficiency. A company (Sustain X Inc.) in New Hampshire, USA, has demonstrated some technological approaches for isothermal CAES. This technique injects water into the compressed air storage for transferring heat from air to water during charging, and transferring heat from water to air during discharging to maintain constant temperature [62]. The company claims that this technology is more efficient than the conventional CAES. This method will allow direct contact between water and air, making it different from the proposed design in the previous section.

LAES technology is similar to conventional CAES. The difference is that in LAES the air will be stored in the form of liquid. [63-65]. The phase change from gas to liquid makes the process more complicated than CAES.

Among those variants, adiabatic CAES (ACAES) seems to provide a suitable solution to overcome the drawback of conventioanl CAES. The ACAES system does not require additional heat for the heating process. The generated heat during compression is stored in a material and is utilised to heat up the air during the expansion process [19, 55-57]. The utilisation of heat from the compression process will eliminate or limit the use of fuel in the CAES system, which enhances the efficiency of this system by up to around 70% [12, 25, 27-31, 66, 67].

In ACAES, the heat-storage media should be able to absorb and release the heat of compression/ expansion safely and efficiently. Furthermore, the selection of the thermal storage system in the adiabatic compressed air energy storage depends on the characteristics and performance of the system. Therefore, this chapter identifies and compares the characteristics of the different TES material that could be useful in the designing of ACAES.

2.3 Thermal Energy Storage

Storing of thermal energy can be accomplished in many ways according to the applications. The methods and material used depend greatly on the input and output temperature [12]. According to its operation, TES can be classified into two categories: active and passive systems. In the active system, the thermal storage medium flows through a heat exchanger to absorb or release the heat into the storage media, while passive thermal storage uses a heat transfer fluid (HTF) medium as the heat carrier for transferring heat into and from the static thermal storage medium [12, 68-70]. In general, TES systems can be categorised into three main classes: sensible heat, latent heat and thermochemical storage [4, 68].

In simple terms, a sensible heat-storage system involves the increase in temperature of a substance as it absorbs heat and a temperature decrease as it releases heat [68]. The energy stored in the sensible heat material is a function of the change in temperature, specific heat capacity and the mass of the material [71]. The benefits of sensible heat storage include relatively fast charging and discharging rates, with a thermal process efficiency in the range of 50% to 90% [12]. In addition, this heat-storage method is already developed, and the low-cost material for sensible heat storage is readily available [71]. However, if the temperature swing

is limited, then the storage density will be limited too, resulting in large volumes of storage and some of them are corrosive.

In latent heat-storage, the energy is stored in the form of latent heat of melting, which is the energy required to convert a solid to a liquid. The materials used in this process are referred to as the phase change materials (PCMs)[68]. Apart from having 75 to 95% efficiency, the main benefit of latent heat storage is that it has a higher storage density compared to the sensible heat storage and the ability to provide energy at nearly constant temperature. As a result, it requires a lower volume of material compared to sensible heat storage in order to store the same amount of energy. However, it has a limitation in the rate of heat transfer that can be achieved due to the low thermal conductivity of most PCMs. Thus, it requires a heat transfer enhancement. Additionally, most of the PCMs are flammable and relatively expensive [4, 12].

Another type of TES is thermochemical storage, in which the energy is stored and released based on a reversible chemical reaction. Among the types of energy storage, this technology offers the highest storage capacity. Nevertheless, the main challenges in this technology include the necessity for an advanced reactor suitable for a specific reaction and chemical stability. Therefore, it is less developed compared to the other two types of TES [4, 71-74].

2.4 Application of Thermal Energy Storage on ACAES

The operating process of the existing designed ACAES has temperature ranges from 50 to 600 °C [39] and can be categorised into high (500 – 600 °C), medium (400 °C), and low (80 – 200 °C) temperature ACAES [28, 30, 75]. Since this technology starts from environment temperature, which is around 25°C, it has a wide temperature range that provides a significant amount of heat that could be stored and utilised during the discharging process. Currently, according to the type of thermal storage material in ACAES, the proposed designs could be divided into two sub-systems: ACAES with sensible heat storage and ACAES with latent heat storage.

2.4.1 ACAES with sensible heat energy storage

Various studies have reported that sensible heat as TES combined with CAES has a good performance. Commonly, the sensible heat materials that are used to incorporate with CAES include: oil [32-34], water [30, 35, 36], rock bed [28, 37, 38] and ceramic [39]. While water and oil usually follow an active thermal system (Figure 2.3), rock bed and ceramic follow a passive thermal system (Figure 2.4).

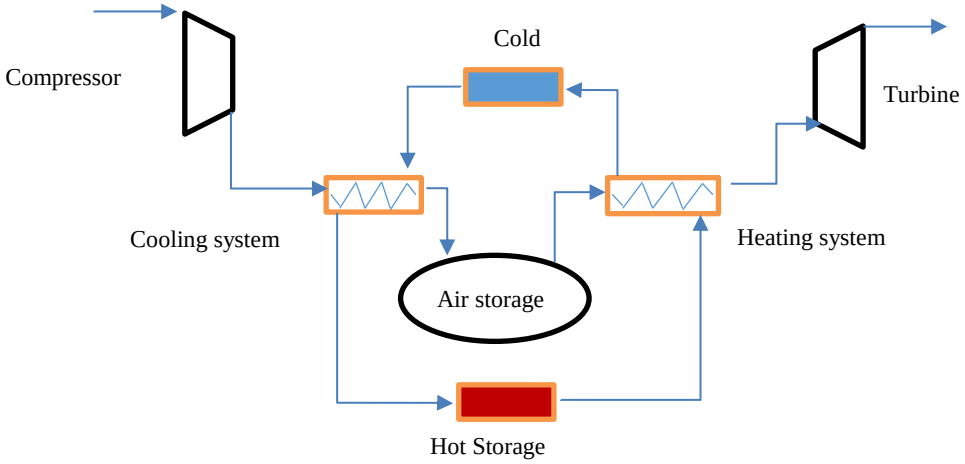

Figure 2.3 The basic principle of ACAES with Active thermal storage system, Simplified from [32, 34].

Regarding the active thermal system for ACAES (Figure 2.3), the compressor first compresses the air and generates heat during the process. The hot air from the compression process flows through a heat exchanger, and heat is transferred to a thermal fluid carrier, either water or oil. This process increases the temperature of the carrier and decreases the temperature of the compressed air. Next, the hot fluid is transported to a storage unit which is high-temperature one. In the discharge process, the hot fluid from the high-temperature storage unit is passed to another heat exchanger to heat up the air cooled by expansion before entering the turbine. The thermal fluid carrier becomes cold as the air temperature increases [23].

As shown in Figure 2.3, this type of ACAES uses two separate cylinders for heat and cold storage. Although the most common HTF used in this system is water or oil [30, 32-36, 76], molten salt can also be used as HTF [57].

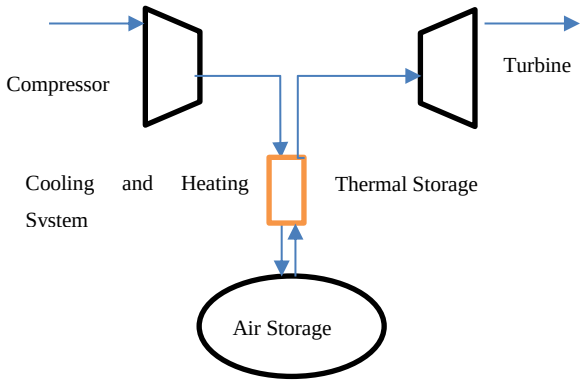

Figure 2.4 Basic principles of ACAES with the passive thermal storage system, simplified from [19].

The ACAES with the passive thermal storage system that uses sensible heat requires only one cylinder for hot and cold storage (Figure 2.4). In this technology, the heat-storage medium is used for cooling and heating, at different times. During the charging process, the heat-storage medium absorbs the heat generated during the compression process, and later in the discharging process, the cooled air during expansion is heated using the stored energy. Rock bed or ceramic is usually used as TES material in this system [37, 38]. A high volume of TES and a highly efficient turbine in this type of technology can acquire a 70% roundtrip efficiency without any fuel consumption [15]. The prospective of sensible heat materials for ACAES are summarised in Table 2.1.

Table 2.1 Candidates for sensible heat material for ACAES application

Material	Type	Temperature Range (^{O}C)	Density (kg/m^3)	Average specific heat (kJ/kg K)	Thermal conductivity 25^{O}C (W/mK)	Estimated cost (Solid:US$/kg) (Liquid:US$/L)	Ref.
Rock	solid	20 to 300	2560	1.3	1	n.a	[69, 71]
Concrete	solid	20 to 400	2200	0.85	1.5	0.05	[12, 69]
Cast Iron	solid	Up to 400	7200	0.56	37	1	[12, 69]
NaCl	solid	Up to 500	2160	0.85	7	0.15	[12, 69]
Silica fire bricks	solid	Up to 700	1820	1	1.5	1	[12, 69]
Water	liquid	0-100	1000	4.2	0.61	n.a	[12, 69]
Engine oil	liquid	Up to 160	888	1.8	0.12	0.3	[12, 71]
Synthetic oil	liquid	250-350	900	2.3	0.11	3	[12, 69]
Silicone oil	liquid	300-400	900	2.1	0.1	5	[12, 69]
Liquid sodium	liquid	270-530	853	1.3	71	2	[12, 69]
Propanol	liquid	Up to 97	800	2500	0.154	91.5	[71, 77]
Ethanol	liquid	Up to 78	790	2400	0.176	107	[71, 77]
octane	liquid	Up to 126	704	2400	0.137	277	[71, 77]
Isopentanol	liquid	Up to 148	831	2200	n.a	76	[71, 77]
Isobutanol	liquid	Up to 100	808	3000	n.a	70	[71, 77]
Butanol	liquid	Up to 118	809	2400	0.154	102	[71, 77]

(n.a : Not available)

As shown in Table 2.1, the sensible heat materials can cover a wide range of storage temperatures corresponding to applications with different pressures.

2.4.2 ACAES with latent heat energy storage

The application of latent heat storage using PCM seems to be more viable compared to sensible heat storage because the PCM has a higher energy density, which translates to the requirement of smaller storage volume [78]. Although PCM has a good prospective market in building applications through energy saving, peak-load shifting and reducing daily temperature fluctuation [79-83], only a few studies have been reported on its use in ACAES system. PCM may be classified as shown below in Figure 2.4.

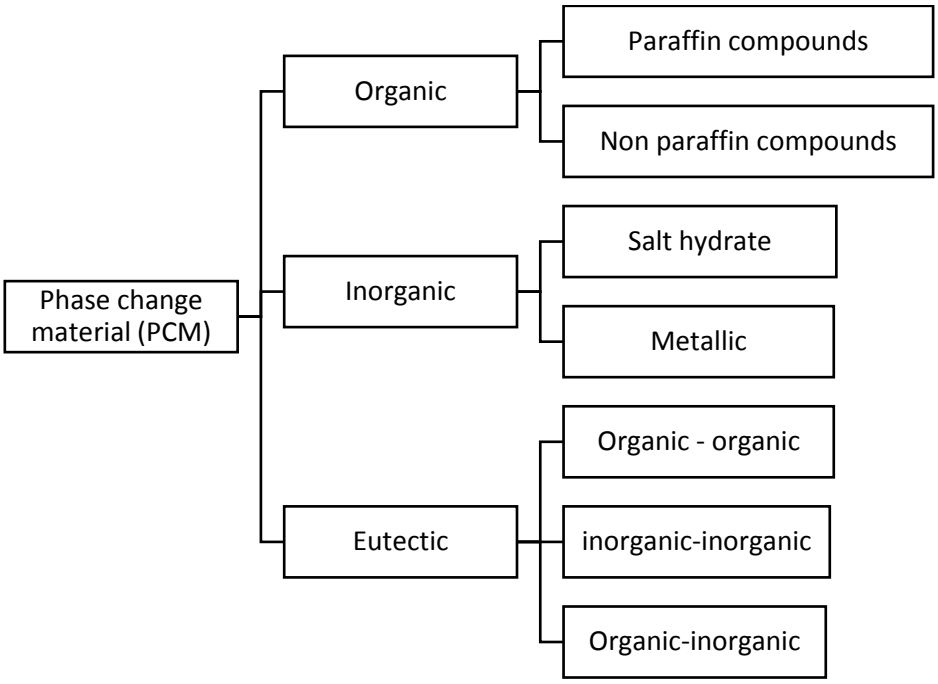

Figure 2.5 Classification of PCM [70, 71, 84-86].

As shown in Figure 2.5, the three common types of PCMs that could be used for ACAES systems include organic, inorganic and eutectics compounds. Organic PCM consists of paraffin and non-paraffin/fatty acids and esters, while inorganic PCMs are made up of salt hydrates and metals. Organic materials have certain advantages including moderate latent heat, being non-corrosive, chemically stable and non-toxic [4]. Conversely, flammability and low thermal conductivity are drawbacks of most organic materials. Inorganic compounds have a higher thermal conductivity, higher latent heat, are non-flammable and cost-effective [4]. However, they suffer supercooling and phase segregation and hence must be used with care. Table 2.2 shows the advantages and disadvantages of the different PCMs.

Table 2.2 Comparison of PCM, Adapted from [70, 87]

	Organic	Inorganic	Eutectics
Advantages	• No phase segregation • Non-corrosive • Cost-effective • Self-nucleating • Chemically and thermal stable • Available in wide temperature range • Recyclable	• Moderate cost • Non-flammable • Low volume change • High volumetric storage density • Higher thermal conductivity	• High energy density • Sharp melting point
Disadvantages	• Low energy density • Flammable • Low thermal conductivity	• Phase segregation • Corrosion • Thermal instability • Sub-cooling	• Limited availability

Based on Table 2.2, both the organic and inorganic PCMs have benefits and drawbacks. Additionally, the potential candidate of PCM as thermal storage on ACAES is listed in Table 2.3. Organic PCMs are prospective materials for ACAES system due to their moderate thermal storage density and long-term stability with minimum supercooling and no phase segregation [4, 88]. However, organic PCMs have a major limitation of low thermal conductivity (0.24 W/m K). The limitation does not introduce a serious problem when applied in buildings; however, it will cause a major limitation if applied in the ACAES system, since the compression and expansion in this process could happen within a short period, requiring high-heat transfer rates. This limitation of low thermal conductivity can be solved by encapsulating it in microcapsules or by impregnating it in porous graphite of very high thermal conductivity [89, 90]. Microcapsules can also be coated with metals to strengthen their structures of the microcapsule and improve their contact thermal conductivities [91].

Table 2.3 Latent heat of storage materials as a candidate for TES on ACAES and their temperature ranges

ACAES Temperature Range	Material	Transition Temperature (°C)	Heat of Fusion (kJ/kg)	Ref.
Low (Under 200 °C)	Paraffin wax	64	173.6	[4]
	Polyglycol E360	22	127.2	[4]
	Water to ice	0	335	[92]
	$AlCl_3$	192	280	[92, 93]
	$MgCl_2 . 6H_2O$	117	168.6	[4]
	$Mg(NO_3)_2 . 6H_2O$	89	162.8	[4]
	$Ba(OH)_2 . 8H_2O$	48	265.7	[4]
	Palmitic acid	64	185.4	[4]
	Capric acid	32	152.7	[4]
	Naphthalene	80	147.7	[4]
Medium (200-400 °C)	$LiNO_3$	250	370	[92]
	Na_2O_2	360	314	[92]
	KNO_3–KOH	214	83	[94]
	KNO_3–$NaNO_3$	222	110	[94]
	LiBr–$LiNO_3$	228	279	[94]
	$CaCl_2$–$LiNO_3$	238	317	[94]
	Bismuth	271–271.4	53.3	[93]
High (Above 400°C)	Aluminium	661	388	[78]
	Zinc	419	112	[78]
	50LiOH/50LiF	427	512	[92, 93]
	$KClO_4$	527	1253	[92, 93]
	LiH	699	2678	[92]
	LiF	868	932	[92]
	NaF	993	750	[92]
	MgF_2	1271	936	[92]
	Si	1415	1654	[92]
	46.3Al–4.6Si–49.1Cu	571	406	[93]
	88%Al, 12%Si	576	560	[93]
	$MgCl_2$	714	452	[87]

Encapsulated phase change salt has prospective outcome when used to store the heat energy from the concentrated solar power plant by designing the integrated system as shown below [41]:

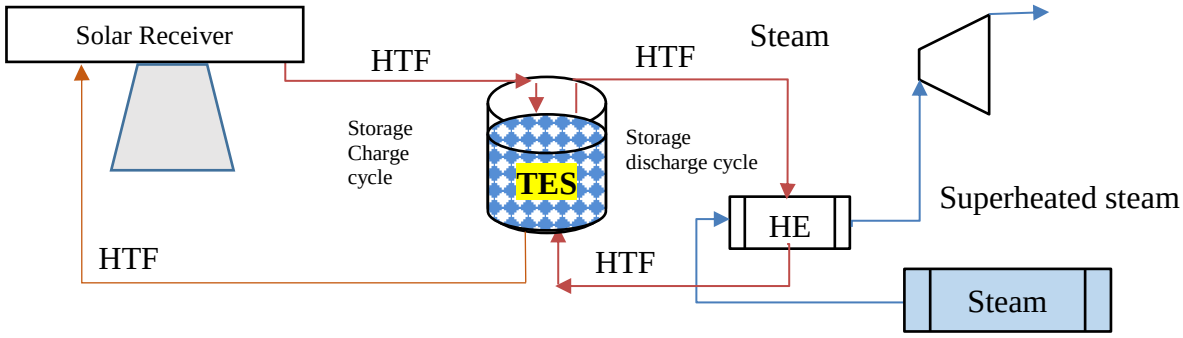

Figure 2.6 Concentrated solar power plant integrated system with TES using PCM [41].

As Figure 2.6 illustrates, during the charging process, the HTF collects the heat energy from the heat receiver and transmits the heat to the encapsulated PCM then stores it in the form of latent heat in the TES. For the duration of the discharging process, the HTF collects the heat from the TES and then transfers the heat to the steam system through the heat exchanger. In this method, the encapsulated PCM salt is sodium nitrate [41]. This research concludes that the salt should have the heat of fusion about 200 kJ/kg and the optimum diameter of salt capsules should be between 10mm to 15mm. Furthermore, it is being clarified that these kinds of capsules which have lifetimes more than 30 years which correspond to 10,000 thermal cycles [41].

Some major benefits of molten salts include being inexpensive, having high thermal stability, and low vapour pressure. The low vapour pressure makes the storage design easier without the need for using pressurised cylinder. Furthermore, the two functions of molten salts are that the salts serve as a storage medium and as a heat transfer medium [95]. Some chloride salts ($MgCL_2$, KCl, and NaCl) have latent heat above 350 kJ/kg, while pure inorganics salts are based on hydroxides and nitrates which have a melting temperature of 300-350°C, their latent heat is in the range of 95 and 172 kJ/kg [96]. The high-temperature PCMs are not only suitable for concentrated solar power, but they may also be applied to high-temperature adiabatic CAES.

Encapsulated salt could also be applied to any CAES system as follows:

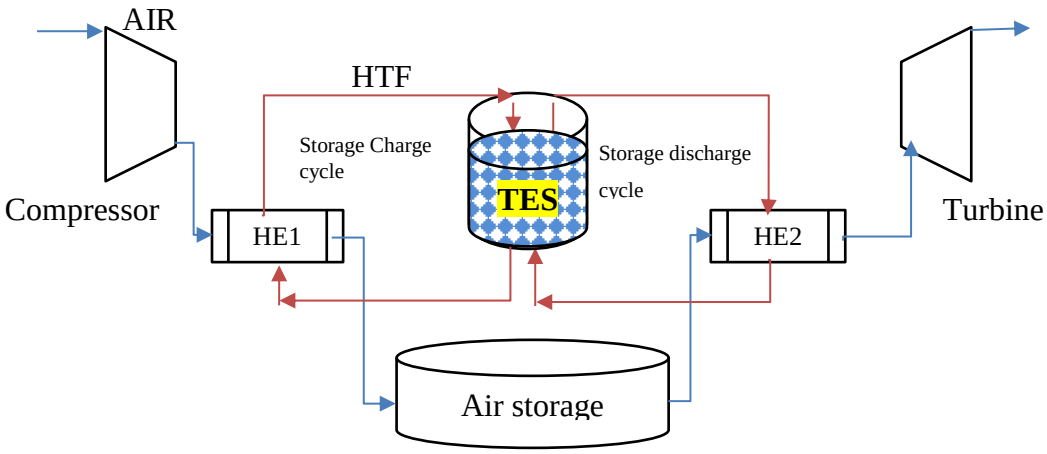

Figure 2.7 CAES integrated system with TES using PCM (ACAES).

Figure 2.7 represents the CAES system connected with a TES system using a packed bed of encapsulated PCM. During the charging process, the HTF, which absorbs heat from the compressed hot air through the heat exchanger 1 (HE1), is pumped through the storage cylinder which contains a packed bed of PCM capsules, transferring the stored heat to the capsules through direct contact by occupying the space between the capsules. Next, the HTF exits the cylinder and return to HE1.

During the discharging process, the high-temperature HTF from the TES is transported to the heat exchanger 2 (HE2) to heat the cold air before progressing into the turbine for generating electricity. Afterward, the HTF, which has low-temperature exits from HE2, returns to the TES cylinder. Thus, this system stores the energy in the encapsulated PCM both in the form of sensible and latent heat in addition to the thermal stored as sensible heat in the HTF and used to transfer the heat from and to the heat-storage cylinder. The HTF and PCM material can vary depending on the operating temperature.

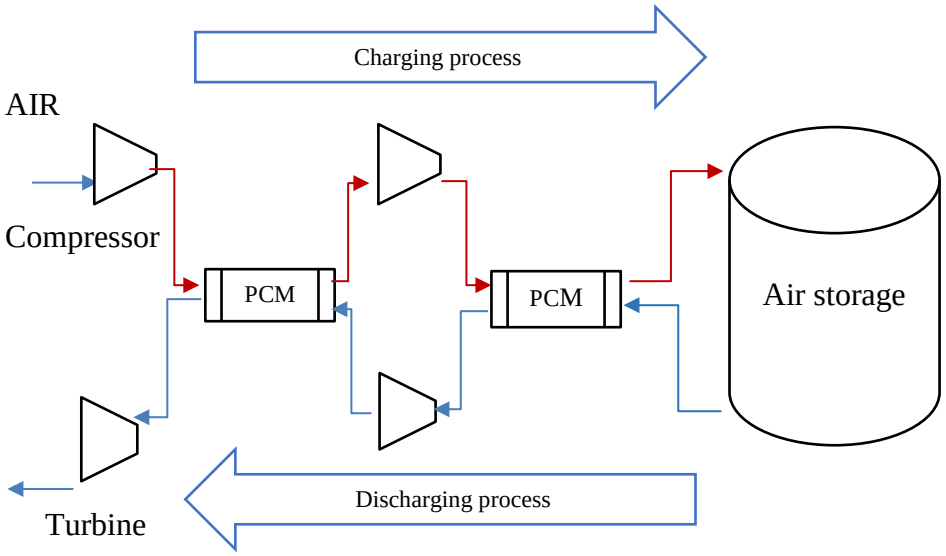

Figure 2.8 Cascade PCM for TES system on ACAES[78].

In order to develop the heat-storage facilities and increase their efficiencies, two or more different types of PCMs can be used as TES in the ACAES system. As shown in Figure 2.8, two PCMs are occupied to store the heat from the compression process. There are two stages of compression, and each stage has one PCM to absorb the heat that is generated. The two PCMs have different melting temperatures according to the temperature generated in the compression process. In the discharging process, the air gets heated by the stored latent heat inside the thermal storage system. This method is called "cascade PCM system". The utilisation of the PCM cascade can enhance the efficiency of the system rather than work with one PCM which covers a large temperature range [78]. Some of the PCMs shown in Table 2.3 could be suitable for this design of ACAES.

Another configuration of ACAES is the use of the combination of heat storage and air storage. In this technology, the storage facility of ACAES is usually in the form of latent heat (PCM). The heat from the compression process is stored in a PCM which is placed inside along the inner wall surface or outside the wall surface. During the charging process, the PCM absorbs heat, while in the discharging process, the heat is released into the air [97]. This process is illustrated in Figure 2.9(A) and (B).

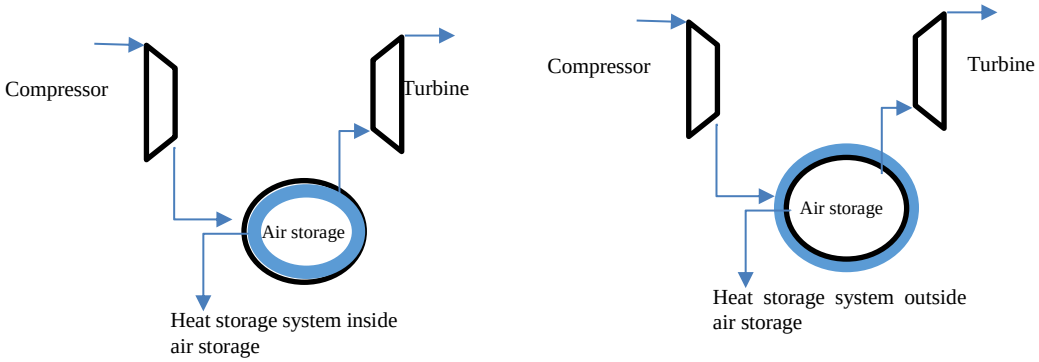

(A) (B)

Figure 2.9 Simplification of proposed ACAES system

In the adiabatic CAES systems (Figure 2.9 A and B), the PCM is usually used as a heat-storage medium. The major criteria for selecting PCMs include physical, technical and economic considerations. Initially, physical properties are considered in the selection of PCM, for example, the suitable phase-change temperature, the heat-storage capacity, consistency (stable performance over a large number of cycles) and material cost [98].

Castellani et al. [97] studied the expansion process in adiabatic CAES according to Figure 2.9(A). They used RT18HC as the TES material, which has a total volume 0.28 L in the form of an encapsulated plastic disc with a thickness of around 5mm. It was placed inside the cylinder, and the system was operated at a pressure in the range of 20 and 30 bar. Thermal performance of the system with and without PCM were compared. For the 20 bar operations, their experiments showed that the expanding air temperature would drop by 25.2°C (from 27.7°C to 2.5°C) when PCM was not used, while the temperature dropped to 11°C (from 24°C to 13°C) when PCM was used. The corresponding temperature drops at 30 bar were 34.8°C and 30.5°C, respectively. Their conclusions revealed that the latent heat could minimise the temperature drop during the expanding process and make the operational air temperature at the near-isothermal conditions [97].

In terms of the configuration shown in Figure 2.9 (B), the heat-storage medium is placed outside the cylinder, specifically on the outer surface. The advantage of this method is that the PCM material will not undergo pressurisation and hence reduce the risk of damage to the encapsulated PCM. However, heat transfer in this design is limited by the cylinder's wall thermal conductivity, which could restrict heat transfer from the air to the thermal storage

medium. This problem may be solved by adding fins inside the cylinder to provide more heat transfer area, needed to enhance heat transfer process. This method seems to be the preferred alternative for future design as it has not been reported in the literature.

Table 2.4 Some international PCM companies available worldwide.

Commercial Name	Company website	Available range temperature (°C)	Number of listed PCM on website	Reference
PureTerm	www.puretemp.com	-37 to 151	27	[99]
Rubitherm	www.rubitherm.eu	- 9 to 90	44	[100]
Crodatherm	www.crodatherm.com	5 to 53	6	[101]
Cristopia	www.cristopia.com	-64 to 140	6	[102]
TEAP	www.teappcm.com	-58 to 1100	24	[103]
Climsel	www.climator.com	-21 to 70	11	[104]
EPS	www.pcmproducts.net	-100 to 885	142	[105]

Presently, there is a wide range of commercialised PCM products available worldwide (Table 2.4). Generally, for PCM to be suitable for any application, it should have an appropriate melting temperature, melt congruently, be safe, non-corrosive, and chemically stable [4].

In addition, for ACAES application, PCM should have a high thermal conductivity in order for it to absorb and release the heat at very high rates. Some promising methods that could provide an increase in the effective thermal conductivity of PCM is encapsulation or impregnation in a graphite matrix. In the PCM, encapsulation, including macro, micro and nanoencapsulation, can increase the heat transfer rate dramatically due to its large heat transfer area and provide better direct contact between HTF and PCM capsule [40, 41]. Furthermore, the use of metal coating could raise the bulk PCM microcapsules' thermal conductivity from 0.189 to 2.41 W/mK [91].

Another possibility to improve heat transfer is by impregnating the PCM with a high thermal conductivity matrix. Mills et al. [89] impregnated PCM into graphite matrix by submerging the matrices in liquid paraffin wax (Rubitherm, RT42) at 80 °C with different submerging time (5 to 60 min). The relationship between heat conduction direction and compression direction are taken into account in this research. The results show that the thermal conductivity of PCM increases significantly from an initial value to approximately 20-60 times on the parallel

sample, while in the perpendicular sample the thermal conductivity increases approximately 30–130 times [89]. For instance, when paraffin is impregnated in graphite, its thermal conductivity increases from 0.24W/mK up to 4.70 W/mK [106]. The use of metal coating could raise the bulk PCM microcapsules' thermal conductivity from 0.189 to 2.41 W/m K [91].

2.5 Summary

This chapter explains the variation of the basic system of ACAES, especially in terms of thermal energy storage mechanisms, their differences, and characteristics, which can be summarised as follows:

- Based on the storage media, thermal energy storage can be divided into three categories; sensible heat (water or oil), latent heat, and chemical reaction heat storage. Up to now, only sensible and latent heat storage have been used in a prototype of ACAES system.
- The use of latent heat storage to store the heat generated from the compression process is essential. Otherwise, thermal efficient of the system will be unacceptably low. However, the low thermal conductivity of most PCMs requires more work to be done to ensure that the PCM can absorb and release the generated and absorbed heat at sufficiently high rates.

Chapter 3. Performance of a Small-Scale Compressed Air Energy Storage

Chapter Preface

The use of renewable energy, such as wind and solar, has significantly increased in the last decade. However, these renewable technologies have the limitation of being intermittent; thus, storing energy in the form of compressed air is a promising option. In CAES, the electrical energy from the power network is transformed into a high-pressure storage system through a compressor. Then, when the demand for electricity is high, the stored high-pressure air is used to drive a turbine to generate electricity. The advantages of CAES are its high energy density and quality, and environmentally friendly process.

At the existing facilities of the University of Auckland, New Zealand, an air cavern is not available; thus, a high-pressure cylinder is used to store the compressed air, which could provide an excellent opportunity for small-size applications. There is limited literature available on the temperature and pressure profiles in a typical high-pressure cylinder during charging and discharging processes. Therefore, this research investigates how temperature and pressure inside a high-pressure cylinder changes during charging and discharging processes. It will provide a better understanding for heat transfer in such a system. Furthermore, it will provide the necessary information for the design of an efficient small-scale CAES. In this work, air is compressed to a maximum pressure of 200 bar and stored in a 2-L cylinder, which is fully fitted with a pressure transducer and a thermocouple suitable for high-pressure measurements. The charging and discharging process is theoretically modelled, and the results are compared with the experimental measurements, showing a good agreement. The heat balance in the system is used to validate the steady-state condition, while dynamic analysis is used to predict the transient change of compressed air and the cylinder's wall temperatures. Theoretical modelling is undertaken by solving the differential equations describing the transient change in temperature of both air and cylinder's wall. The results of this study show that air temperature rises from 24°C to 60°C at 100 bar and from approximately 17°C to over 60°C at 200 bar. During the discharging process, the air temperature drops from ambient to 5°C at starting pressure of 100 bar and to -20°C at starting pressure of 200 bar.

This chapter based on published paper: Saputro EA, Farid MM., Performance of a small-scale compressed air storage (CAS). Int J Energy Res. 2018; 1–10

3.1 Introduction

Storing electricity is an important step in a power network, and it can be done in many ways, either in large- or small-scale storage. Since renewable energy, such as wind and solar, are intermittent in nature, energy storage is needed [2, 42, 107]. Globally, there has been an upsurge in wind energy capacity from approximately 200 GW in 2010 to 487 GW in 2016 [42]. Also, solar power use has increased from 137 GW in 2013 to 303 GW in 2016 [42]. To support renewable energy growth, an efficient and reliable energy storage system must be developed.

CAES is a promising energy storage method that could be applied to wind and solar energy and is available on large and small scales. In CAES, the electrical energy from the power network is transformed into a high-pressure air system through a compressor. Then, when the demand for electricity increases, high-pressure air is released to run a turbine generating electricity [2, 18, 107]. On a large scale, the existing CAES technology capacity is 440 MW worldwide [9]. The first CAES power plant was deployed in Huntorf, Germany. Initially, this plant had a power rating of 290 MW, which was recently increased to 320 MW [19]. The second CAES plant was established in 1991 in McIntosh, Alabama, USA. The power rating of this plant is 110MW. Both power plants use salt caverns as their air storage system [21, 22].

Regarding the storage system, Kushnir et al. [108] reported the calculation of the temperature and pressure behavior in an air storage cavern. In this analysis, the heat transfer coefficient was assumed to be constant and the wall cavern was at an isothermal condition. It seemed to be an acceptable assumption since the wall cavern would have experienced only a small temperature change which can be neglected. According to their energy balance analysis, the predicted temperature showed a good agreement with the measured data from the Huntorf plant [108]. Xia et al.[109] simplified the analysis by assuming that wall cavern temperature remained constant. Their result showed reasonable agreement of better than 80% when compared to Huntorf plant data. They claimed that such deviation was possibly due to inaccurate prediction of heat transfer coefficient and the used value of rock thermal effusivity [109].

Apart from large scale CAES, small-scale CAES is starting to gain interest and seems to have great potential in the future [110-113]. The advantage of this technology is that it is easy to set up in different areas, both aboveground and underground. Vongmanee and Monyakul [114] proposed a system for small-scale aboveground CAES storage, which was connected to an induction generator. The study simulated a medium-scale CAES system with an air storage volume of 20,000 L and a pressure of 10 bar. The total compression time was 200 min and the

total expansion time was 50 min. The power output was approximately 3.84 kW. To improve this system, they suggested increasing the pressure by adding another compression stage. Others suggested installing a high-efficiency compressor to minimize air leak so that the system become more efficient and cost effective [115].

In another study, Zhang et al. [116] suggested a small-scale CAES using steel pipe piles underground. Surplus solar power was used to compress the air, which was stored in hollow steel pipes buried underground. At night, the compressed air system took over for electricity generation. Further studies include that of Kiliç et al [112] who designed a small-scale CAES with an energy storage capacity of 2 kWh, and Khamis et al. who designed a small-scale CAES using a micro-turbine and an electricity generator combined with a DC-AC converter producing 6 to 8 volts AC output.

Despite a considerable amount of research reported on small-scale CAES, there is the need for more work to understand the thermal effect during the compression and expansion process, especially in regards to the effect of the cylinder's wall. This chapter reports experimental measurements and a comprehensive theoretical model for a high-pressure compressed air cylinder storage system. In specific, this chapter is to investigate the temperature variations during charging and discharging process in a small compressed air storage. Most previous investigators have ignored the change in the cylinder's wall temperature, unlike the model developed in this work. The temperatures of both the air and the wall of the storage cylinder during compression and expansion are predicted and compared with the experimental measurements conducted in this work. This chapter also presents a unique analysis of the performance of a special temperature sensor, capable of operating at such high pressure (200 bar), since such a sensor could have a very slow-response time.

3.2 Theory

To simplify the thermodynamic analysis, the majority of researchers have assumed that the cavern's wall is at a constant temperature or the cavern is adiabatic [109, 118]. This approach is true due to the fact that the change in the cavern's wall temperature is usually small compared to the change in air temperature. However, in a small-scale CAES using cylinder, the cylinder wall's surface area per unit volume is large and hence the thermal mass of the wall is significant, thus it must be included in the analysis. In any CAES system, three main parts can be analysed through thermodynamic perspectives: the compressors, the turbines and the air storage chamber for the charging and discharging processes.

Based on the above argument of ignoring the wall effect and on the assumption that air behaves as an ideal gas with a constant specific heat, the temperature change with increased pressure and mass of air entering the cylinder can be written as follows:

$$\frac{T_1}{T_2} = \left(\frac{P_1}{P_2}\right)^{\frac{k-1}{k}} \quad \text{..... (1)}$$

$$m = \frac{PV}{RT} \quad \text{..... (2)}$$

$$k = \frac{C_p}{C_v} \quad \text{..... (3)}$$

where T_1 and T_2 are the initial and final temperatures of air, P_1 and P_2 are the initial and final pressure, m is the mass of air entering the cylinder, V is the volume of the cylinder, R is the gas constant, and C_p and C_v are the heat capacities at constant pressure and constant volume respectively [30, 113, 118, 119].

The compression power (W_c) can also be calculated as follows:

$$W_C = \frac{k}{k-1}(RT_1)\left[\left(\frac{P_2}{P_1}\right)^{\frac{k-1}{k}} - 1\right] \quad \text{..... (4)}$$

While the expansion work (W_t) can also be calculated from the equation below:

$$W_t = \frac{k}{k-1}(RT_1)\left[1 - \left(\frac{P_1}{P_2}\right)^{\frac{k-1}{k}}\right] \quad \text{..... (5)}$$

In order to account for heat transfer between the compressed air and the cylinder's wall during charging and discharging processes, the first law of thermodynamics is applied [119, 120].

$$\Delta E = \Delta U + \Delta W + \Delta Q \quad \text{..... (6)}$$

where ΔE is the total energy stored in the chamber, ΔU is the change in internal energy, ΔW is the work done by air and ΔQ is the heat transfer into or from the environment. The heat exchange between the air and the cylinder's wall can be expressed as follows:

$$Q = h\ A\ (T_c - T_a) \quad \text{..... (7)}$$

where Q is the total rate of heat transferred between the air and the cylinder's wall, h is air heat transfer coefficient, A is cylinder surface area, and T_c and T_a are the cylinder's wall and air temperatures respectively.

3.3 Methods

3.3.1 Experimental procedure

The main equipment in this research consists of a high-pressure compressor, a big cylinder (25L), a small cylinder (2L), a data logger and a personal computer. The experiment configuration is shown in the following diagram, Figure 3.1.

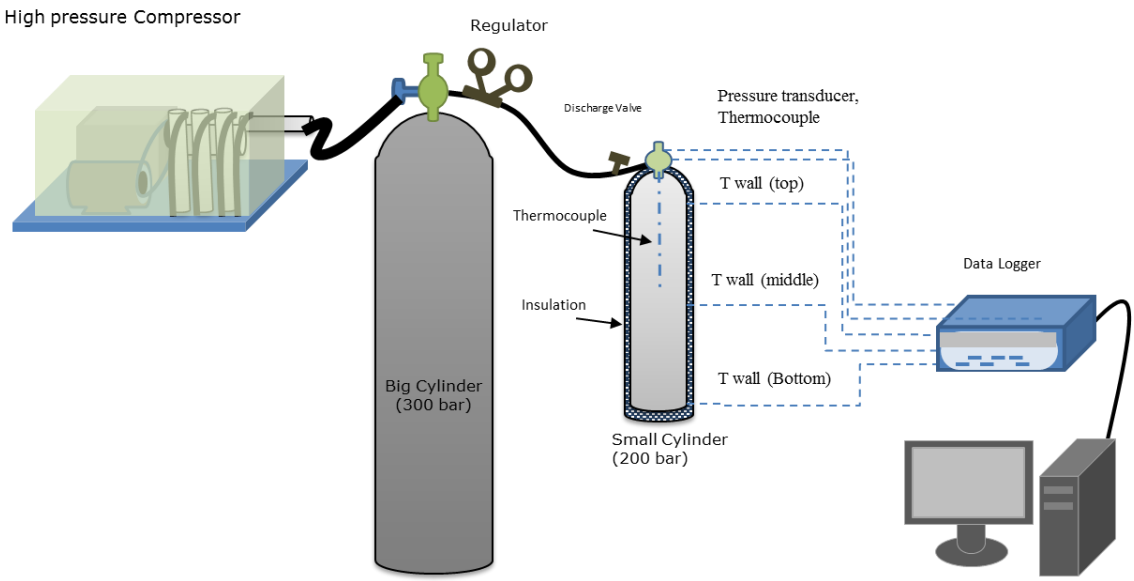

Figure 3.1 Experimental set-up

To acquire the experimental data, the test rig is equipped with temperature and pressure sensors. The pressure transducer is installed to measure pressure inside the cylinder. Three thermocouples are assembled to measure the temperature of the cylinder's wall, at the bottom, middle and top of the cylinder. The air temperature inside the cylinder is measured accurately by an RTD PT 100, type TR33 provided by WIKA Instrument Ltd. The sensor can measure liquid or gas media temperature in the range of -50 to +250 °C with pressure up to 270 bar. It is made from very thin platinum film which is applied to a ceramic carrier and stainless-steel case (WIKA data sheet). This platinum sensor has very good accuracy and stability compared to other materials [121].

In the charging process, the high-pressure air (300 bar) is stored first in the big cylinder (25 L), which acts as the compressor in the process. It was possible to get an almost constant pressure

feed to the small cylinder, since it is significantly smaller in size than the big cylinder. The maximum allowable design pressure of the small cylinder is 230 bar. During the discharge process, the air was released from the 2 L high-pressure cylinder to the environment.

3.3.2 Theoretical modelling

A simulation programme is written to predict compressed air and cylinder's wall temperatures when air is compressed to 100 and 200 bar. The system is assumed as a closed-end system. The compressed air from the big cylinder, which acts as a compressor, is transported and stored into the small cylinder, then released from the small cylinder during discharge. The cylinder was insulated so the assumption of no heat loss or gain from the environment is reasonable (the calculated heat loss is included in the appendix).

The small cylinder (2L) used to store the compressed air, which is commercially available in the market, having the following specifications (Table 3.1):

Table 3.1 The specification of the small cylinder

Description	Unit	Value
Outside diameter (Do)	cm	9.8
Inside diameter (Di)	cm	8.8
Length (l)	cm	40
Weight (m)	kg	3.6
Heat capacity (Cp)	kJ/kg	0.5
Volume (V)	m^3	0.002
Material		Steel

According to the first law of thermodynamics, the steady-state air energy balance based on adiabatic system may be described as follows [122]

$$\Delta(mU) = H'\Delta m \quad \text{..... (8)}$$

$$(m_2U_2 - m_1U_1) = H'(m_2 - m_1) \quad \text{..... (9)}$$

where m_1 and m_2 are the initial and final mass of air, U_1 and U_2 are internal energies at the initial and final conditions and H' is the enthalpy of the air entering the system.

As noted earlier, thermal mass of the cylinder's wall cannot be ignored and must be included in the energy balance. This has been done as shown below:

Air heat balance:

$$m_2\,U_2 - m_1\,U_1 + \left\{\left(m\,C_p\right)_t\right\}\left(T_{t_2} - T_{t_1}\right) + \left\{\left(m\,C_p\right)_p\right\}\left(T_{p_2} - T_{p_2}\right) = (C_V T' + RT')(m_2 - m_1) \quad \ldots\ldots\ldots\ldots\ldots (10)$$

Specifically:

- $(C_v T' + RT')(m_2 - m_1)$: energy input from the air entering the cylinder.
- $(m_2\,U_2 - m_1\,U_1)$: energy accumulation in the compressed air.
- $\left\{\left(m\,C_p\right)_c\right\}\left(T_{c_2} - T_{c_1}\right)$: energy accumulation in the cylinder's wall.
- $\left\{\left(m\,C_p\right)_p\right\}\left(T_{p_2} - T_{p_1}\right)$: energy accumulation in the thermocouple probe.
- T_{a_1} and T_{a_2} are the initial and final air temperatures.
- T_{c_1} and T_{c_2} are the initial and final temperatures of the cylinder's wall.
- m_1 and m_2 are initial and final mass of air in the cylinder.
- $\left(m\,C_p\right)_c$ is the mass and heat capacity of the cylinder.

Cylinder heat balance:

$$h_1\,A_1\left[\left(\frac{T_{a_2}+T_{a_1}}{2}\right) - \left(\frac{T_{t_2}+T_{t_1}}{2}\right)\right]\Delta t = \left(m\,C_p\right)_t\left(T_{t_2} - T_{t_1}\right) \quad \ldots\ldots\ldots\ldots (11)$$

Specifically:

- $h_1\,A_1\left[\left(\frac{T_{a_2}+T_{a_1}}{2}\right) - \left(\frac{T_{t_2}+T_{t_1}}{2}\right)\right]\Delta t$: energy transferred from the air to the cylinder.
- $\left(m\,C_p\right)_c\left(T_{c_2} - T_{c_1}\right)$: energy accumulation in the cylinder's wall.
- h is the heat transfer coefficient.
- A_1 is the cylinder surface area and Δt is the time interval.

As we have noted earlier, a unique sensor (RTD PT 100) is used to measure air temperature inside the high-pressure cylinder (200 bar). This sensor is specially designed to handle a high-pressure system. It is 310 mm long, 6 mm in diameter, and has an overall mass of 89.35 g. Due to the probe sensor having a large mass, the slow response time of this sensor must be taken into account in the analysis. For this reason, an additional energy balance, to account for heat transfer between air and probe must be included [equation (12)].

$$h_2\,A_2\left[\left(\frac{T_{a_2}+T_{a_1}}{2}\right) - \left(\frac{T_{p_2}+T_{p_1}}{2}\right)\right]\Delta t = \left(m\,C_p\right)_{probe}\left(T_{p_2} - T_{p_1}\right) \quad \ldots\ldots\ldots\ldots (12)$$

where $h_2\,A_2\left[\left(\frac{T_{a_2}+T_{a_1}}{2}\right) - \left(\frac{T_{p_2}+T_{p_1}}{2}\right)\right]\Delta t$ is the energy transferred from air to the probe and $\left(m\,C_p\right)_p\left(T_{p_2} - T_{p_1}\right)$ is the energy accumulation in the thermocouple probe and A_2 is the probe surface area.

According to Raju and Khaitan [123], the heat transfer coefficient in this system is quite challenging since both forced and natural convection play significant role in heat transfer between air and cylinder's wall.

Khusnir et al.[108] and Xia et al.[109] simplified the heat transfer by using a constant value of heat transfer coefficient, whereas Raju and Kumar Khaitan [123] proposed a heat transfer coefficient function of mass flow rate. Xia, Zhou [109] reported a value of 30 W/m^2K for the heat transfer coefficient (h), according to their system (59 bar in the air storage chamber). Raju and Khaitan [123] proposed the following equation for air heat transfer coefficient:

$$h = 0.2356 + 0.0149\,[\dot{m}_{in} - \dot{m}_{out}]^{0.8}\ (W/m^2\,K) \qquad \ldots\ldots\ldots\ldots\ldots\ldots\ldots\ldots\ (13)$$

where, $\dot{m}_{in}$ represents the mass flow rate entering the storage unit from compressor and $\dot{m}_{ou}$ is the mass flow rate out from the storage entering the turbine. The heat transfer coefficient is different in each CAES system as it depends on pressure, temperature, and the geometry of cylinder. In this chapter, a different approach for the calculation of h is followed as described in the following section.

3.4 Results and Discussion

3.4.1 Pressure evaluation during the charging and discharging process.

The following graphs show the pressure variations during charging process. As seen in Figure 3.2, the pressure increases rapidly from 1 bar to approximately 100 bar in 8 s, meanwhile to achieve 200 bar it takes about 15 s.

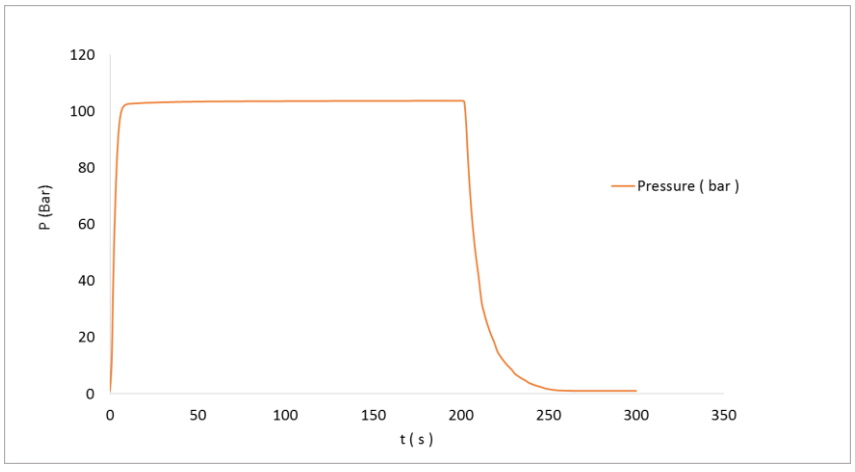

(a)

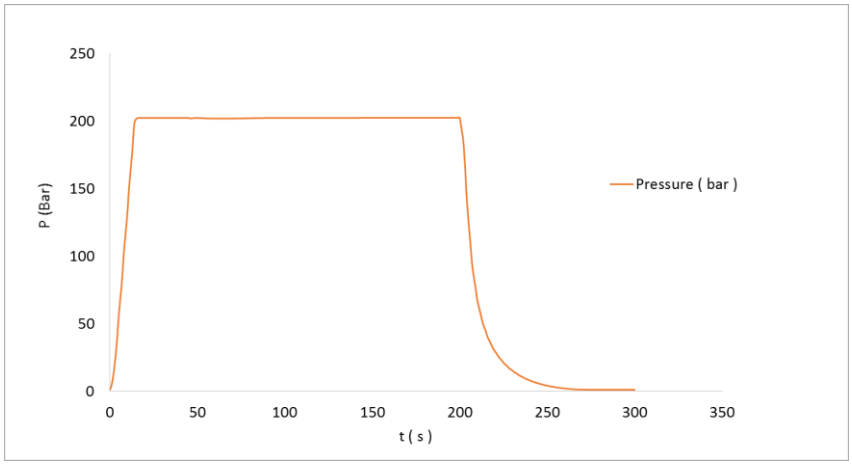

(b)

Figure 3.2 Pressure change during charging, storing and discharging processes; 100 bar (a) and 200 bar (b).

In the discharging process, the high-pressure air is released from the cylinder into the environment. As seen in Figure 3.2, the pressure drops fast at the beginning of the process and remains constant when it is close to ambient pressure. The discharging times for the 100 bar and 200 bar are around 45 s and 60 s, respectively.

3.4.2 Basic calculation for adiabatic compression and expansion

In this project, the pressure ratio ($r=P_2/P_1$) is set to 100 and 200. In the air-compression process, the temperature can rise dramatically; meanwhile, during the expansion process, the air temperature drops significantly. Table 3.2 gives the final temperature and temperature rise for adiabatic air compression and expansion when the initial temperature is set to environment condition 300 K (26.85 °C). In the adiabatic system, the heat transfer between the air and its environment is ignored, which can be true only if the compression and expansion are extremely fast to be able to influence the cylinder's wall. According to equation (1), the final temperature of adiabatic compression can reach higher than 1000K and during the expansion can drop to -200 K, which of course never happens in practice. This equation is based on air only without any storage tank. The big thermal mass of the air chamber (cylinder system or cavern) will prevent such change in air temperature. In fact, compressors usually have a cooling system that prevents air temperature from increasing dramatically.

Table 3.2 Adiabatic compression and expansion

Adiabatic compression				
Pressure ratio, *r*	**1**	**50**	**100**	**200**
Final temperature, K	300	914.8	1114.6	1354.1
Temperature rise, K	0	614.8	814.6	1054.1
Adiabatic expansion				
Pressure ratio, *r*	**1/200**	**1/100**	**1/50**	**1**
Final temperature, K	66	80.7	98.4	300
Temperature drop, K	-234	-219.3	-201.6	0

3.4.3 Heat transfer analysis

In this work, the heat transfer coefficient (air to wall) is calculated based on mixed forced and natural convection. In the charging process, both temperature of the probe and the cylinder's wall, are assumed to be heated by mixed convection. The equation is based on an experiment conducted by Woodfield, Monde [124]:

$$Nu_{mix} = 0.56\ Re^{0.67} + 0.104\ Ra^{0.352} \quad \text{..... (14)}$$

Nu is the Nusselt number, Re is the Reynolds number, and Ra is the Rayleigh number.

At the end of charging process, there will be no air flow and heat transfer is assumed to be governed by natural convection only. The following correlation is used to describe heat transfer between air and cylinder's wall [125]:

$$Nu = 0.55\ Ra_L^{1/4} \quad \text{..... (15)}$$

On the other hand, the following equation [126] is used to describe natural convection between probe and air since it simulates that geometry better:

$$Nu_L = \frac{4}{3}\left[\frac{7\ Ra_L\ Pr}{5\ (20+21Pr)}\right]^{1/4} + \frac{4(272+315Pr)H}{35\ (64+63Pr)D}, \quad D \leq \frac{35\ L}{Gr_L^{1/4}} \quad \text{..... (16)}$$

The predicted heat transfer coefficient is shown in Figure 3.3.

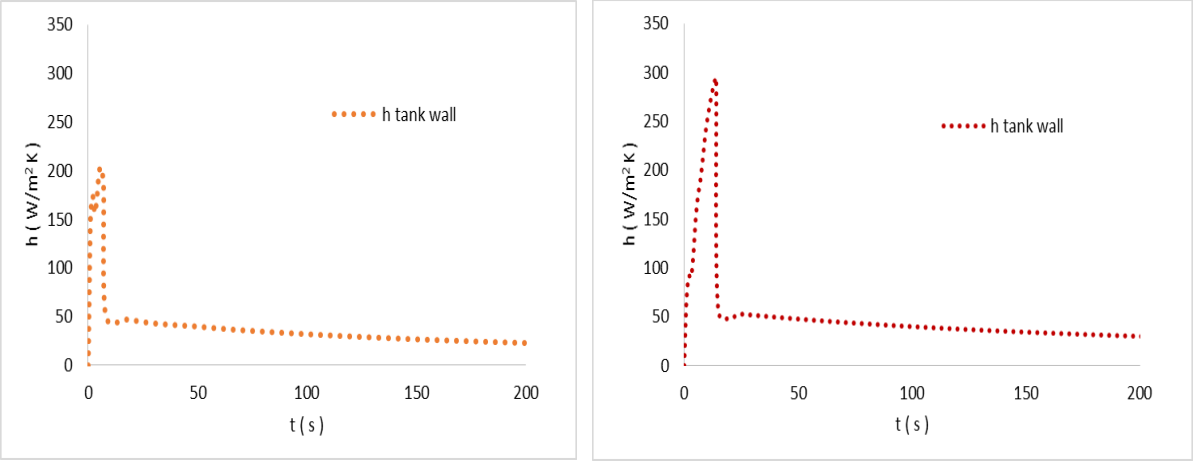

(a) (b)

Figure 3.3 Heat transfer coefficient for mixed convection during charging process at 100 bar (a) and 200 bar (b).

An accurate determination of the heat transfer coefficient can be very problematic as many aspects need to be considered. As seen in Figure 3.3, the heat transfer coefficient increases rapidly in the first couple of seconds, it can increase to around 200W/m^{2}K in 4s at 100 bar and increase to around 300W/m^{2}K in 10s at 200 bar. This rapid increase in heat transfer coefficient is mainly due to forced convection. After reaching the targeted pressure and airflow is stopped, the heat transfer coefficient drops to around 50 W/m^{2}K, as controlled by natural convection alone and continues to decrease until the air temperature is in equilibrium with the cylinder temperature.

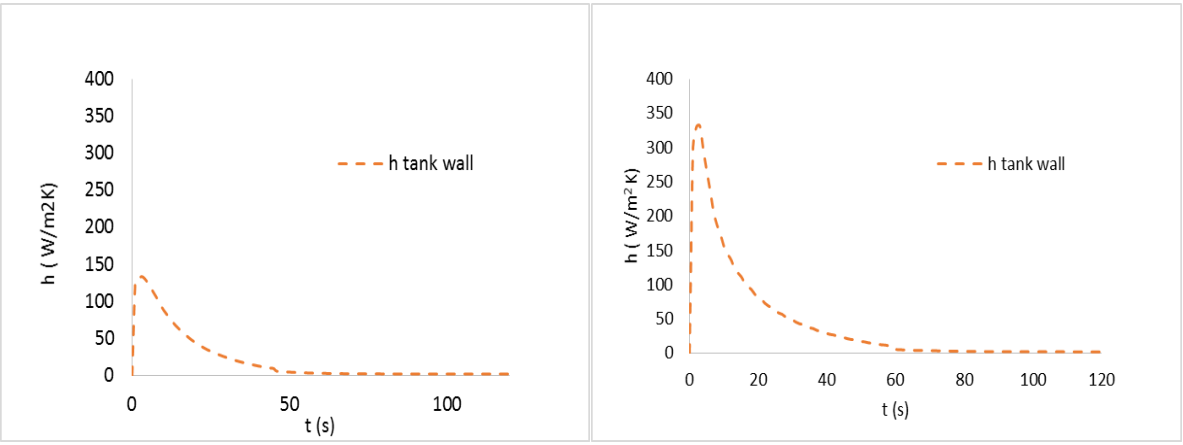

(a) (b)

Figure 3.4 Heat transfer analysis for mixed convection during discharge process at 100 bar (a) and 200 bar (b).

The change in the heat transfer coefficient during discharge is similar. The results show that the heat transfer coefficient for 100 bar system drops from about 140 W/m^{2}K initially to around 2 W/m^{2}K when the discharging process is completed (Figure 3.4 [a]). The corresponding change in the 200 bar system is from 300 W/m^{2}K to 2 W/m^{2}K (Figure 3.4[b]). The heat transfer coefficient is lower during discharge due to the low air temperature caused by expansion.

3.4.4 Temperature evaluation during charging and discharging process.

In this section, the measured and predicted air and cylinder's wall temperatures are reported and discussed.

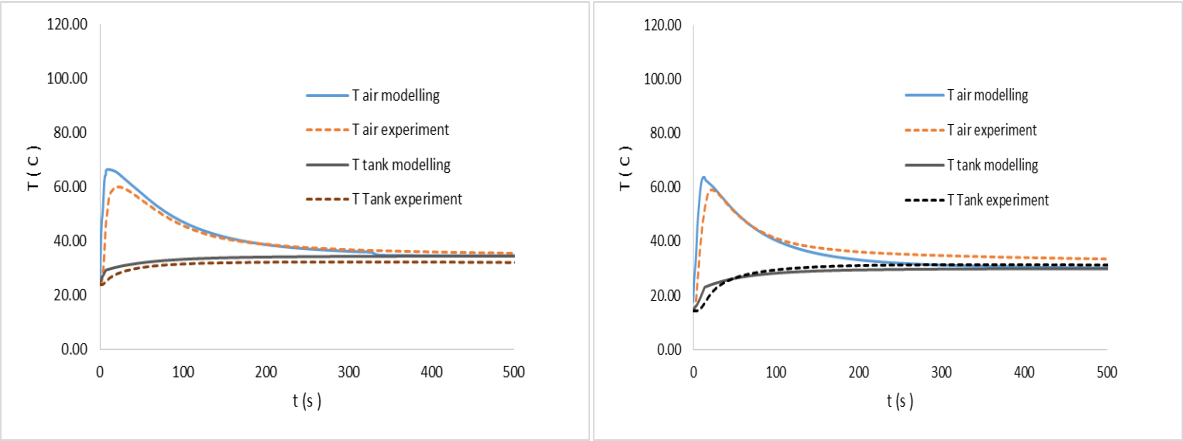

(a) (b)

Figure 3.5 Measured and predicted air and cylinder's wall temperatures during charging process, (a) 100 bar and (b) 200 bar.

Figure 3.5 shows the variation in measured and predicted air and average cylinder's wall temperatures during the charging process. It can be seen that, at the beginning of the process, air temperature rises rapidly. At 100 bar, air temperature rises from 24°C to 60°C while at 200 bar it rises from approximately 17°C to over 60°C. The air temperature drops close to the wall temperature, as the system approaches equilibrium.

The disagreement between measured and predicted temperatures is very small. In the modelling, the air temperature is assumed to be uniform inside the cylinder; however, in reality, air temperature inside the cylinder can vary along the cylinder height due to buoyancy. In the experimental system built for this work, the use of more than one temperature sensor was not an option, due to safety and to minimise potential leaks.

The measured and predicted cylinder's wall temperatures are also in a good agreement. At the beginning of the charge process, the wall temperature gradually increases due to heat being received from the compressed air. At 100 bar, the wall temperature increases from 25°C to approximately 33°C, while at 200 bar, the wall temperature rises from approximately 15°C to 28°C.

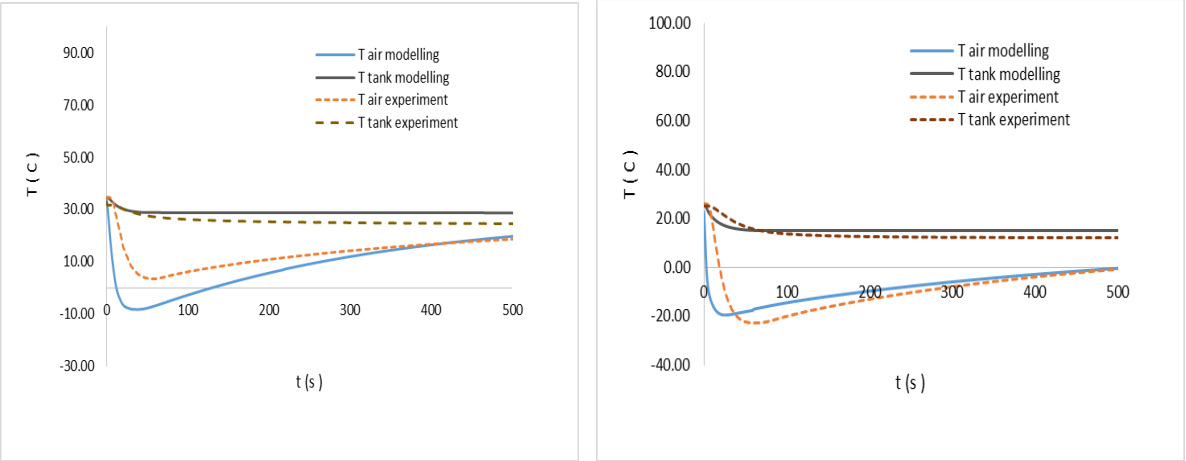

(a) (b)

Figure 3.6 Measured and predicted air and cylinder's wall temperatures discharge process, (a) 100 bar and (b) 200 bar.

Figure 3.6 shows the measured and predicted air temperatures during the discharging process. Initially, the air temperature drops to approximately 5°C for the starting pressure of 100 bar and reduces to -20°C for the starting pressure of 200 bar. The heat transfer from the cylinder's wall is quite low compared to the cooling effect caused by the expansion process. A similar cooling effect phenomenon is also reported by Woodfield, Monde [124] for hydrogen expansion, which showed a drop in temperature from 30°C to -30°C in 10s for 100 bar system.

There are two possible reasons for the disagreement between the measured and predicted air temperature shown in Figure 3.6. As noted earlier, air temperature is measured in the middle of the cylinder, which may not represent average air temperature accurately. Also the air valve, shown in Figure 3.1, is kept fully opened while discharging, making the system not fully insulated.

3.4.5 Summary of the experimental measurements

The following tables summarise the experimental measurements conducted on the small-scale compressed air storage.

Table 3.3 Temperature change at 100 bar

Parameter	**n - experiment**				
Pressure	100 bar				
n-experiment	1	2	3	4	5
Ambient temperature (°C)	27.2	24.95	23.34	22.3	21.87
Charging time (s)	14	9	9	10	10
Maximum air temperature (°C)	58.5	59.87	58.29	54.8	54.59
Δ T charging (°C)	31.3	34.92	34.95	32.5	32.72
Initial T discharging (°C)	33.5	34.66	32.8	35.4	32.8
Discharging time (s)	78	46	35	35	38
Minimum temp (°C)	5.34	3.5	7.7	7.7	7.9
Δ T discharging (°C)	28.16	31.16	25.1	27.7	24.9

Table 3.4 Temperature change at 200 bar

Parameter	**n – experiment**				
Pressure	200 bar				
n-experiment	1	2	3	4	5
Ambient temperature (°C)	17.27	9.5	14.23	18.3	17.07
Charging time (s)	15	13	15	10	10
Maximum air temperature (°C)	58.37	46.7	58.97	60.61	59.81
Δ T charging (°C)	41.1	37.2	44.74	42.31	42.74
Initial T discharging (°C)	31.8	25.7	17	26.4	27
Discharging time (s)	1650	904	2046	60	63
Minimum temp (°C)	5	0.7	-7.16	-22.64	-22.24
Δ T discharging (°C)	26.8	25	24.16	49.04	49.24

Tables 3.3 and 3.4 show air temperature change inside the high-pressure cylinder during charging and discharging. Charging time needed to increase pressure from 1 bar to 100 or 200 bar is kept the same. Discharging time is the time required to decrease air pressure to 1 bar from the initial pressure of 100 or 200 bar. The maximum and minimum air temperatures are the maximum or minimum value of the air inside the cylinder during the charging or discharging process.

In this work, the change in the charge time was limited while the discharge time varied significantly (from fast discharge under 100s to slow discharge with more than 1000s). The effect of discharge time or discharge rate can be seen very clearly from the data shown in Tables 3.3 and 3.4. At fast discharge, the air shows a significant drop in temperature (Δ T almost 50°C) compared to (Δ T around 25 °C) for slow discharge. During fast discharge, heat transfer from the cylinder's wall is not sufficiently fast enough to transfer heat to the air.

3.5 Summary

Based on the experimental and theoretical analysis conducted in this work on a small-scale CAES system, the following conclusions may be drawn:

- The air and wall temperature in a high-pressure cylinder are predicted successfully when compared to measured value, for both charge and discharge processes. At the beginning of compressing (100 bar), air temperature rises dramatically up to around 60 °C and drops significantly to around -10 °C during the discharging process.
- The best method to describe heat transfer during charging and discharging processes is a mix forced and natural convection, followed by natural convection after flow is stopped. In the 100 bar system, h rises to around 150 W/m^2K at the beginning of the compressing process and drops to around 2 W/m^2K when the compressing process is completed. Meanwhile, in the 200 bar system, it rises to around 300 W/m^2K at the beginning of the compression .
- When CAES is applied in a small scale system, similar to the system employed in this work, cylinder's wall must be included in the thermal analysis.
- Temperature sensors used in such high-pressure system have high thermal mass and hence would have poor time response, and hence requiring careful analysis.

Chapter 4. A Novel Approach of Heat Recovery system in Compressed Air Energy Storage

Chapter Preface

CAES is a useful means of storage since the stored compressed air can be used at any time as a source of mechanical energy for power production. However, if the heat generated during compression is not utilised, the process efficiency will be low, and consequently, additional heat is required to avoid frost formation during the expansion process. The generated heat during compression can be stored in the form of sensible heat in the wall of the high-pressure cylinder at an elevated temperature. However, this method is undesirable due to (1) less air can be compressed at higher temperatures and (2) heavy insulation would be required to prevent heat loss to the environment over extended time. A solution to this problem is to use PCM which has a melting temperature close to ambient, hence the heat could be stored as latent heat of melting. PCMs have low thermal conductivity and hence require large contact area with the compressed air so as to be able to release its latent heat rapidly during rapid expansion. This could be achieved through the use of microencapsulated PCM, which provides very large surface area. In this work, a high-pressure cylinder (2 L, 200 bar) was used for air storage while the commercial microcapsules, Micronal® DS 5038X, were used as the latent heat-storage material. Both theoretical simulation and experimental measurements made on the system show that the use of PCM microcapsules reduces the maximum increase in air temperature from approximately 45°C to 27°C (150 gram, Micronal® DS 5038X) during charging, while during discharging, the maximum decrease in temperature was reduced from 48°C to 28°C, which prevented air temperature from dropping to below 0°C.

This chapter based on published paper: Saputro, E.A. and M.M. Farid, A novel approach of heat recovery system in compressed air energy storage (CAES). Energy Conversion and Management, 2018. 178: p. 217-225

4.1 Introduction

4.1.1 Development of adiabatic compressed air energy storage (ACAES)

Energy storage systems are required to provide stable energy production from intermittent energy sources, such as wind and solar [4, 91]. One well-known energy storage method is CAES. This type of energy storage is suitable for both renewable and non-renewable energy sources [14]. In this system, the excess electricity is used to generate compressed air during low electricity demand, and the compressed air, through expansion, can run a turbine to generate electricity during peak demand period [13].

To my knowledge, there are only two large-scale CAES. In 1978, the first CAES power plant, was built in Huntorf, Germany, provided a power rating of 290 MW with 41% efficiency. The second CAES plant was established in 1991 in McIntosh, Alabama, USA. The power rating of this plant was 110MW, and its efficiency was 54%. Both power plants used salt caverns as their air storage systems [16]. Both of these technologies are based on what is known as "diabatic CAES".

The primary motivation to improve diabatic CAES lies in the fact that diabatic CAES requires additional energy to heat up the air before it is supplied to the turbine. The adiabatic CAES does not require additional heat during power generation through expansion, as it incorporates thermal storage in its system [55, 57]

There are two types of TES methods that are commonly used: sensible heat storage and latent heat storage. In the sensible heat-storage system, two designs have been investigated. The first design uses water or oil as the sensible heat-storage media and carrier. The heat transfer process will occur in a heat exchanger as illustrated in Figure 4.1 (a) [23, 76]. The second design uses rock bed or ceramics as thermal storage materials, as shown in Figure 4.1 (b) [3]. The first design follows a passive storage system while the second follows an active storage system.

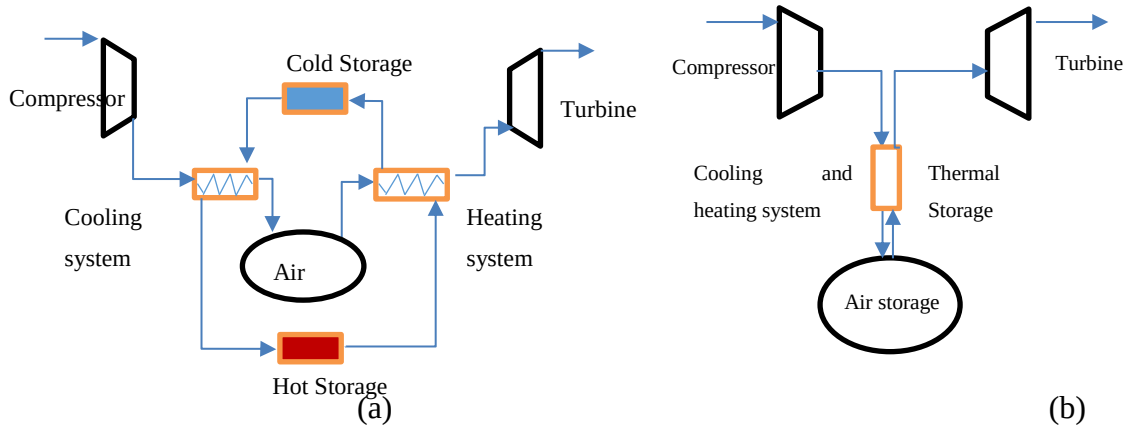

Figure 4.1 The simplified process of adiabatic CAES with sensible heat storage: (a) passive system and (b) active system.

Alternatively, the heat-storage facility of adiabatic CAES (ACAES) can also be in the form of latent heat. In this method of storage, the heat generated from compression will be stored in a PCM through its latent heat of melting. In the charging process, the PCM absorbs the heat, while discharging it during expansion [97]. Such integration between air storage and thermal storage is illustrated in Figure 4.2.

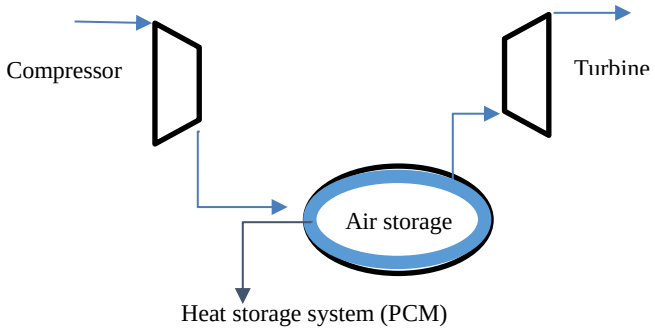

Figure 4.2 The simplified process of ACAES with latent heat storage as TES.

Castellani et al. [97] studied the expansion process in ACAES. They used RT18HC, which is a commercial type PCM for TES, in a cylinder of 1.12 L in volume, operating at 20 and 30 bar. Their experiment showed that without PCM, the expanding process at 20 bar experienced a temperature drop of 25.2°C (from 27.7°C to 2.5°C). Meanwhile, with PCM, the temperature drop was only 11°C (from 24°C to 13°C). However, for the 30 bar operations, the temperature drop during expansion was 34.8°C without PCM while the temperature drop was only 24.7°C with PCM. The results showed that PCM must be carefully selected with regards its melting

range and ensure its melting and solidification during compression and expansion processes, respectively. They concluded that latent heat storage could reduce air temperature drop during the process of expansion and make the air temperature close to isothermal.

Another study by Mazzucco, Rothuizen [127] also used PCM to demonstrate energy saving by capturing the heat during compression in order to reduce the energy needed in a hydrogen gas-fuelling system. Paraffin wax was placed on the inner wall (10 mm thickness) of a standard IV cylinder with operating pressure of 350 to 700 bar. The results showed that, during compression, the paraffin wax absorbed enough heat to reduce the air temperature inside the cylinder by approximately 20°C compared to the case without PCM.

As an improvement to the existing design, this research proposes a high-pressure ACAES, of up to 200 bar, and uses PCM as TES to capture and store the heat generated from the compressing process and give it back to the air while it expands. In many applications, both charging and discharging processes occur very fast, and hence the generated heat must be absorbed and released rapidly. For that reason, the work presented in this chapter focusses on the use of microencapsulated PCM inside the cylinder to provide the large surface area needed for accelerated heat transfer. This is a unique approach that allows fast compression and expansion to happen close to isothermal conditions and has not been addressed in previous research. In fact, none of previous workers have attempted to use of PCM microcapsules as thermal storage material in this application.

4.1.2 Encapsulation of phase change material

Encapsulation refers to the technique of covering a material with other materials as a coating or wrapping layer in a specific shape [90, 127]. In the term of encapsulation of PCM, the shell is usually made of plastic or metal and the core is PCM. According to the dimension, encapsulated PCMs can be divided into three main categories; macrocapsule (for typical dimensions above 1 mm), microcapsule (between 1 mm and 1 μm) and nanocapsule (lower than 1μm) [19].

Microencapsulation technology is already commercialised and has been proven successful for agrochemical, pharmaceutical, and textile industries as well as for PCM for use in building materials and other applications [2].

There are some advantages of using PCM microcapsules, such as minimising reaction with the environment, preventing PCM from leaking out and providing the large heat transfer area

needed for fast heat transfer [27]. PCM microcapsules could be utilised in many applications of energy storage through careful selection of the material and geometry of the capsule [25],

In some TES systems, which require heat to be stored and released fast, PCM was impregnated with a high thermal conductivity graphite [20] an approach which may be also used in CAES. In the work presented in this chapter, we choose to use microencapsulated PCM (Micronal® DS 5038X) since it can provide the large heat transfer area needed for fast heat transfer without any further modification.

4.2 Theoretical Modelling

A computational model is developed to forecast how air and cylinder's wall temperatures change during compression and expansion with and without PCM. The following assumptions were considered for the model developed in this work:

- The gas is assumed ideal,
- Closed system,
- No air leak and no heat losses to ambient during the process (well-insulated),
- Uniform temperature of the compressed air inside the cylinder (no stratification).

The steady-state energy balance for the air system can be writted as follow, based on the first law of thermodynamics [122]:

$$\Delta(mU) = H'\Delta m \quad \text{..... (17)}$$

$$(m_2U_2 - m_1U_1) = H'(m_2 - m_1) \quad \text{..... (18)}$$

where the initial and final mass of air are represented by m_1 and m_2, the initial and final internal energy by U_1 and U_2 and the enthalpy of the air entering the system by H′.

The theoretical modelling has been carried out by solving the two equations describing the transient change in temperature for air and the cylinder, which were developed based on equation (18). When PCM is used, the mass and heat capacity of PCM must be included in the heat balance equation as shown below:

Air heat balance:

$$m_2\,U_2 - m_1\,U_1 + \left\{\left(m\,C_p\right)_c\right\}\left(T_{c_2} - T_{c_1}\right) + \left\{\left(m\,C_p\right)_p\right\}\left(T_{p_2} - T_{p_2}\right) = (C_V T' + RT')(m_2 - m_1) \quad \text{..... (19)}$$

Since the microcapsules are very small, it is possible to assume that they are at equilibrium with the air, and therefore, the equation can be written as follows:

$$\left(m_2\, Cv_2 + m\, C_{p_{pcm}}\right) T_{a_2} - \left(m_1\, Cv_1 + m\, C_{p_{pcm}}\right)\, T_{a_1} + \left\{\left(m\, C_p\right)_c\right\}\left(T_{c_2} - T_{c_1}\right) + \left\{\left(m\, C_p\right)_p\right\}\left(T_{p_2} - T_{p_1}\right) = (CvT' + RT')(m_2 - m_1)$$

…… (20)

Specifically:

- $(CvT' + RT')(m_2 - m_1)$ is the energy input from the air entering the cylinder
- $(m_2\, Cv_2)T_{a_2} - (m_1\, Cv_1)\, T_{a_1}$ is the energy accumulation in the compressed air
- $\left(m\, C_{p_{pcm}}\right) T_{a_2} - \left(m\, C_{p_{pcm}}\right)\, T_{a_1}$ is the energy accumulation in the PCM
- $\left\{\left(m\, C_p\right)_c\right\}\left(T_{c_2} - T_{c_1}\right)$ is energy accumulation in the cylinder's wall
- $\left\{\left(m\, C_p\right)_p\right\}\left(T_{p_2} - T_{p_1}\right)$ is the energy accumulation in the thermocouple probe

It is to be noted that $C_{p_{pcm}}$ is the effective specific heat capacity of the PCM, which includes the latent heat effect as will be explained in section 4.4.1.

Cylinder heat balance:

$$h_1\, A_1 \left[\left(\frac{T_2+T_1}{2}\right) - \left(\frac{T_{c2}+T_{c1}}{2}\right)\right] \Delta t = (m\, Cp)_t (T_{c2} - T_{c1}) \qquad \text{…….(21)}$$

Specifically:

- $h_1\, A_1 \left[\left(\frac{T_2+T_1}{2}\right) - \left(\frac{T_{c2}+T_{c1}}{2}\right)\right] \Delta t$ is the energy transferred from the air to the cylinder
- $(m\, Cp)_c (T_{c2} - T_{c1})$ is energy accumulation in the cylinder's wall
- h is the heat transfer coefficient
- A_1 is the surface area of the cylinder's wall and Δt is the time difference

For temperature measurements, PT 100 (310 mm long, 6 mm in diameter) was used, which is capable of operating at high pressure (200 bar). Unfortunately, this temperature probe has a large thermal mass and hence exhibits low transient response compared to the rate at which pressure and temperature change during compression and expansion. Therefore, the measured air temperature using this probe is corrected based on its transient response defined by equation (22).

$$h_2\, A_2 \left[\left(\frac{T_2+T_1}{2}\right) - \left(\frac{T_{p2}+T_{p1}}{2}\right)\right] \Delta t = (m\, Cp)_{probe} \left(T_{p2} - T_{p1}\right) \qquad \text{…….. (22)}$$

where $h_2\ A_2\ \left[\left(\frac{T_2+T_1}{2}\right)-\left(\frac{T_{p2}+T_{p1}}{2}\right)\right]\ \Delta t$ is the energy transferred from air to the probe and $(m\ Cp)_{probe}(T_{p2}-T_{p1})$ is the energy accumulation in the thermocouple probe and A_2 is the surface area of the temperature probe.

4.3 Experimental Method

The experimental design is shown in the following diagram; the main equipment consists of a high-pressure compressor, a big cylinder (25 L), a small cylinder (2 L), a data logger and a personal computer.

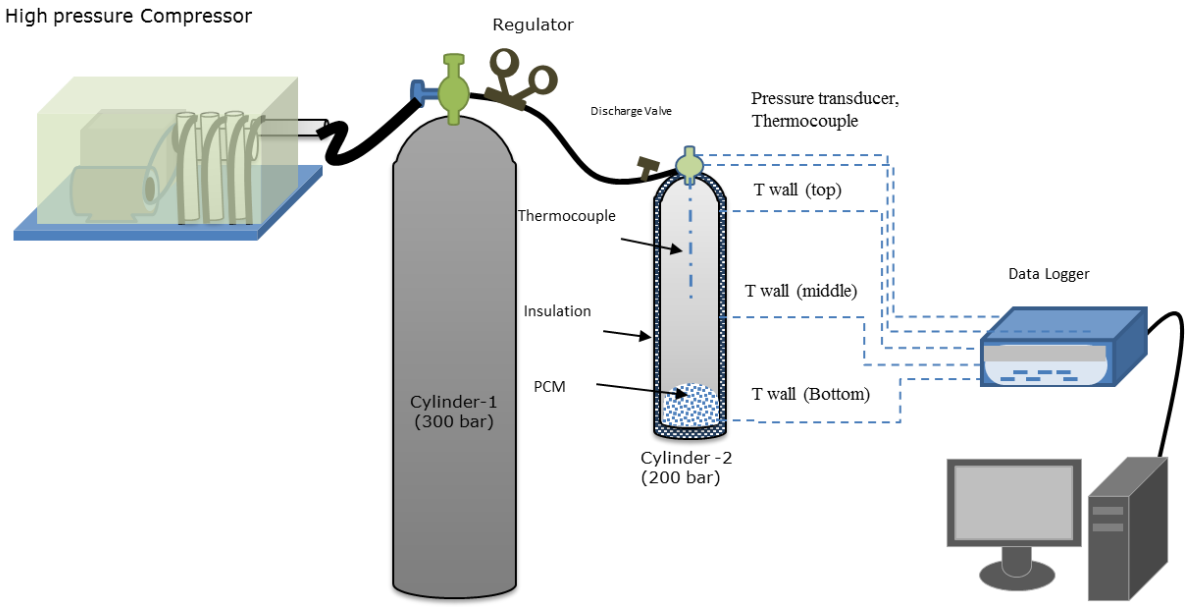

Figure 4.3 Experimental flow scheme design.

As seen in Figure 4.3, the compressor compresses the air and stores it in the big cylinder (300 bar, 25L), which acts as the reservoir in this system. The compressor is not capable of compressing air fast enough and hence, during air charge to the small cylinder (200bar, 2L), the large cylinder is used as the compressor since its pressure will change only a little (approximately 5 to 10 %). The safety factor is the main reason to use the big cylinder as compressor, since the direct and fast charging from the high pressure compressor to small cylinder could blow up the cylinder. Furthermore, the cooling system on the compressor will effect on the heat generated during compression process. During the discharging process, the high-pressure valve releases the air from the small cylinder to the environment. In this experiment, the PCM microcapsules (150 gram) were placed inside the small cylinder which was heavily insulated with ceramic fibre.

To acquire the experimental data, the test rig is equipped with temperature and pressure sensors. The pressure transducer is installed to measure the pressure inside the cylinder. Three thermocouples are assembled to measure the temperature of the cylinder's wall, at the bottom, middle and top. The air temperature inside the cylinder is measured accurately by RTD PT 100, type TR33 provided by WIKA Instruments. It can measure the liquid or gas media temperature in the range of -50 to +250°C with a pressure up to 270 bar. It is made from very thin platinum film which is applied to a ceramic carrier and stainless-steel case (manufacturer data sheet). This platinum sensor has very good accuracy and stability compared to other materials [121]. The small-cylinder specifications are shown in Table 3.1. All sensors were attached to a data logger which was linked to the computer.

4.4 Results and Discussion

4.4.1 Thermal Properties of phase change material (Micronal® DS 5038X).

In this research, the system without PCM shows an air temperature rise from 17.6°C to 60.6°C during compression. Subsequently, in the discharging process, the air temperature drops to approximately -20 °C from the ambient temperature. Therefore, a PCM that has a melting point between ambient temperature and compressed air temperature must be selected. For this reason, Micronal® DS 5038X (manufactured by BASF, Berlin, Germany) was selected, as it has a melting point in the range of 23°C to 28°C.

The physical properties of Micronal® DS 5038X, according to the manufacturer's datasheet, are a melting point at 25°C and heat-storage capacity of 100 kJ/kg. Additionally, the liquid and solid density of the encapsulated PCM are 0.86 g/ml and 0.95 g/ml respectively, and the liquid and solid specific heat are 2.22 J/g˚C and 1.80 J/g˚C respectively [8].

A differential scanning calorimetry (Shimadzu DSC-60) is used to determine the thermal characteristic of the PCM sample. The sample mass is kept in the range of 4 to 6 mg, with the aim to minimise error caused by temperature distribution in the sample [91] and at the same time to maximise the accuracy of the measurements. The heating and cooling rate is 2°C/min.

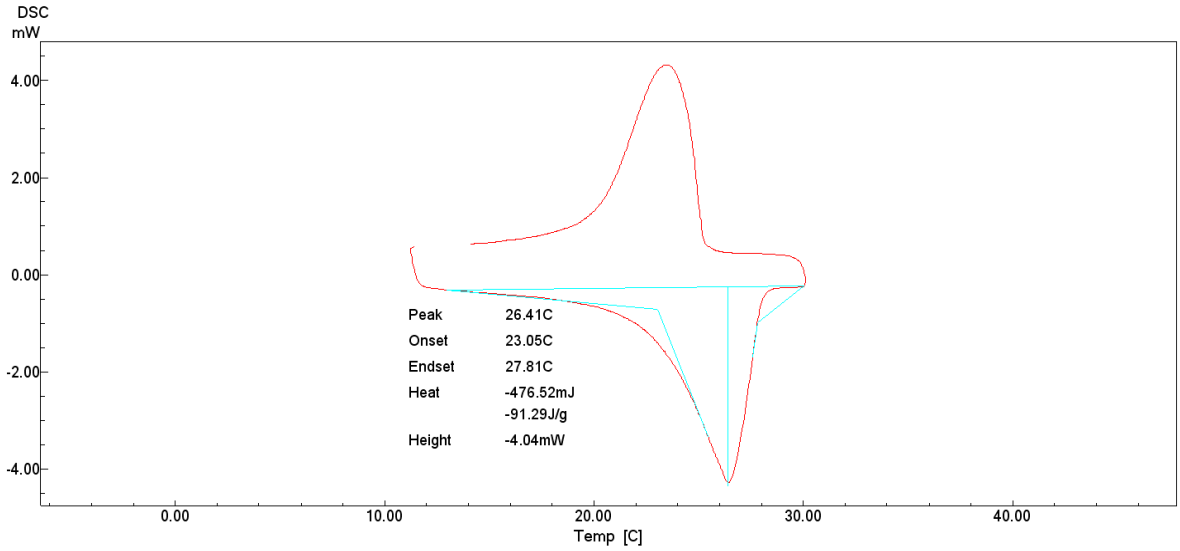

Figure 4.4 DSC analysis for Micronal® DS 5038X.

As shown in Figure 4.4, the melting starts at 23.05°C and completes at 27.82 °C. The amount of heat storage is 91.29 J/g, which is slightly lower than what is reported by the manufacturer.

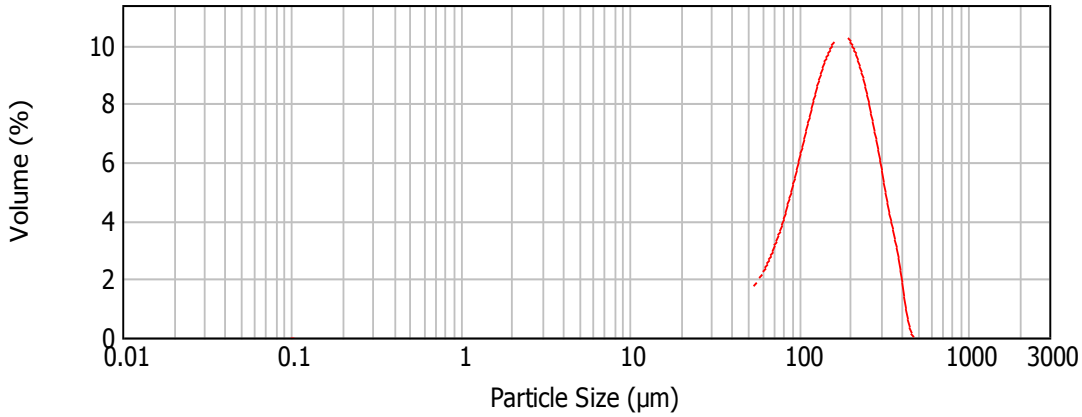

Figure 4.5 Particle size analyser result for Micronal® DS 5038X.

Figure 4.5 shows the particle size distribution of Micronal® DS 5038 X as measured by Mastersizer 2000 from Malvern Instruments. The average size distribution is about 150.6 µm, which suggests that these are clusters of small particles. This kind of microcapsule clusters ware synthesised through an agglomeration process, probably for safety reasons [128].

Modelling the latent heat storage is challenging due to the inclusion of the latent heat. However, it can be resolved by using an effective heat capacity method, which includes both specific heat and latent heat of PCM as described by Farid [129] and later by others [40, 130]. The method from Palanisamy and Niyas [40] is correlated below:

$$Cp\ effective = \begin{cases} Cp\ s\ , T < T_1 \\ \dfrac{L}{2(T_1 - T_2)} + Cp_{tr}\ , T_1 \leq T \leq T_2 \\ Cp\ l, \qquad T > T_2 \end{cases}$$

…….. (23)

Where: Cp_s is heat capacity in solid, Cp_l is heat capacity in liquid, Cp_{tr} is heat capacity in transition, assumed equal to $(Cp_s+CP_l)/2$ [40] and $T_1 \leq T \leq T_2$ is melting range temperature adapted from DSC analysis (Figure 4.4). Therefore, the effective heat capacity for Micronal® DS 5038X is calculated as follow:

$$Cp\ \ effective\ = \begin{cases} 2220\,\frac{j}{kgK}, T < 296\ K \\ 12010\,\frac{j}{KgK}, 296 \leq T \leq 301 \\ 1800\,\frac{j}{KgK},\ T > 301 \end{cases}$$

…….. (24)

4.4.2 Pressure change during charging and discharging processes.

The pressure variations during charging process in the system with and without PCM are described in the following graphs. In both systems (with and without PCM), the pressure increases quickly from 1 bar to approximately 200 bar, with charging time less than 15 seconds for both systems (Figure 4.6).

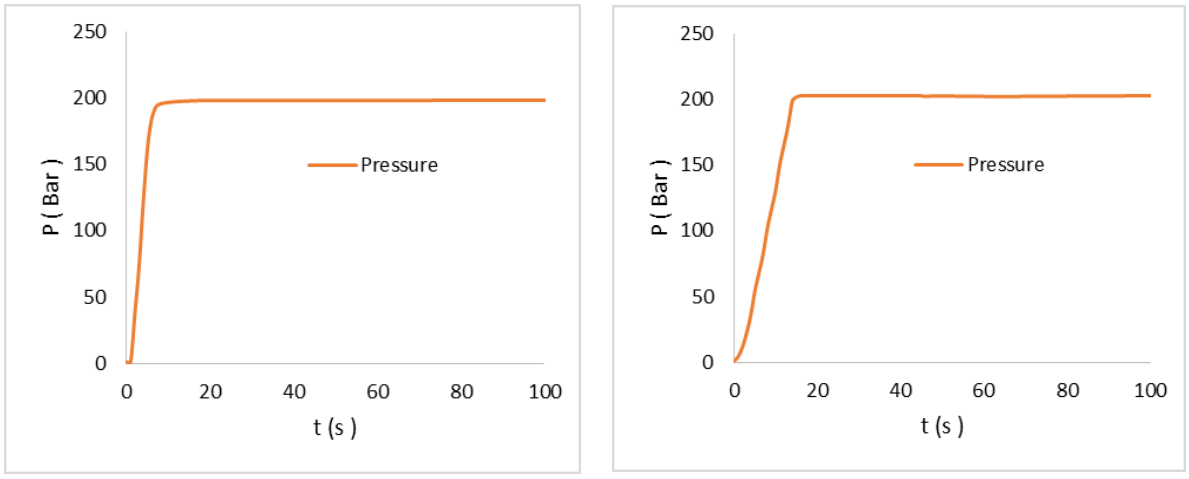

(a) **(b)**

Figure 4.6 Pressure change during charging and storing processes, with PCM (a) and without PCM (b).

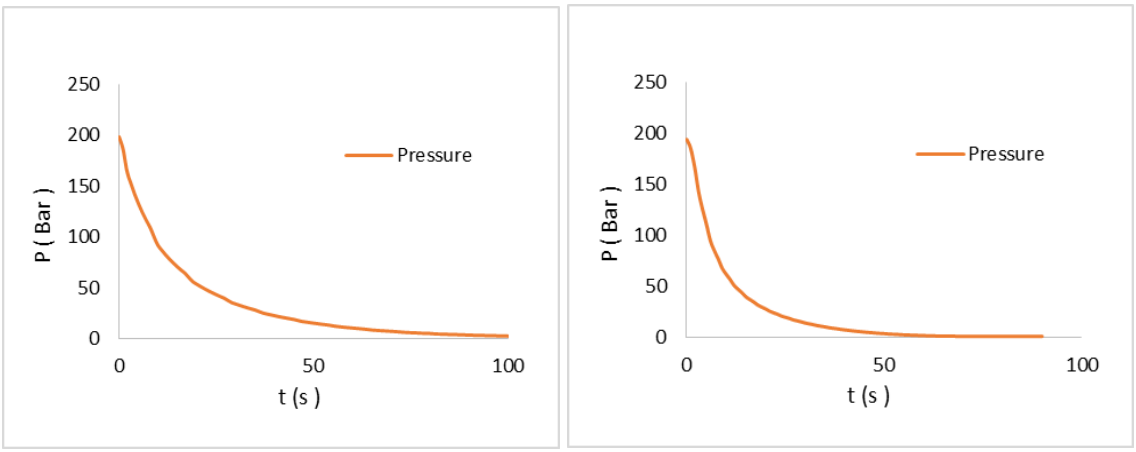

(a) **(b)**

Figure 4.7 Pressure change during discharging processes with PCM (a) and without PCM (b).

Meanwhile, Figure 4.7 shows the pressure variations during the discharging process of air from the cylinder into the environment. As shown in Figure 4.7, the pressure drops quickly in the first couple of minutes of the process and then tends to slow down until it reaches ambient pressure. Both systems follow fast discharging with not more than 100 s.

4.4.3 Heat transfer analysis

The heat transfer coefficient from the air during charging to the cylinder's wall depends on many factors that need to be considered, such as forced convection and natural convection; heat transfer must also be considered [108, 123]. This heat transfer phenomena also happens during the discharging process.

In this study, the heat transfer coefficient is calculated based on mixed forced and natural convection during the charging process, then followed by natural convection alone when the compression process is completed. Thus, heat transfer from air to cylinder's wall must be considered based on the mix convection referred earlier. The following equation developed by Woodfield, Monde [124] was used:

$$Nu_{mix} = 0.56\,Re^{0.67} + 0.104\,Ra^{0.352} \quad \text{..... (25)}$$

Nu is Nusselt number, Re is Reynolds number, and Ra is Rayleigh number.

After the charging process is completed, the following equation is used to define the natural convection heat transfer between the air and cylinder's wall [125]:

$$Nu = 0.55\,Ra_L^{1/4} \quad \text{..... (26)}$$

While the natural convection between the probe and air is assumed to follow the following equation developed for cylindrical geometry [126]:

$$Nu_L = \frac{4}{3}\left[\frac{7\,Ra_L\,Pr}{5\,(20+21Pr)}\right]^{1/4} + \frac{4(272+315Pr)L}{35\,(64+63Pr)D} \quad , \quad D \leq \frac{35\,L}{Gr_L^{1/4}} \tag{27}$$

The calculated heat transfer coefficient for the cylinder's wall system is shown in Figures 4.8 and 4.9.

The calculated heat transfer coefficient for both systems, with and without PCM, follow a similar trend. As can be seen in Figure 4.8, the heat transfer coefficient increases rapidly at the beginning of the process (to about 300 W/m^{2}C) due to the high air-flow rate. There is a small difference in the maximum heat transfer coefficient. The system with PCM has slightly lower heat transfer coefficient, this is because the heat is not only stored as sensible heat in the cylinder's wall but also stored as latent heat in the PCM. After the targeted pressure is reached, the heat transfer coefficient drops very fast to around 50 W/m^{2}K for both systems, as controlled by natural convection only and then slowly decreases until the air and cylinder temperature balances are at equilibrium.

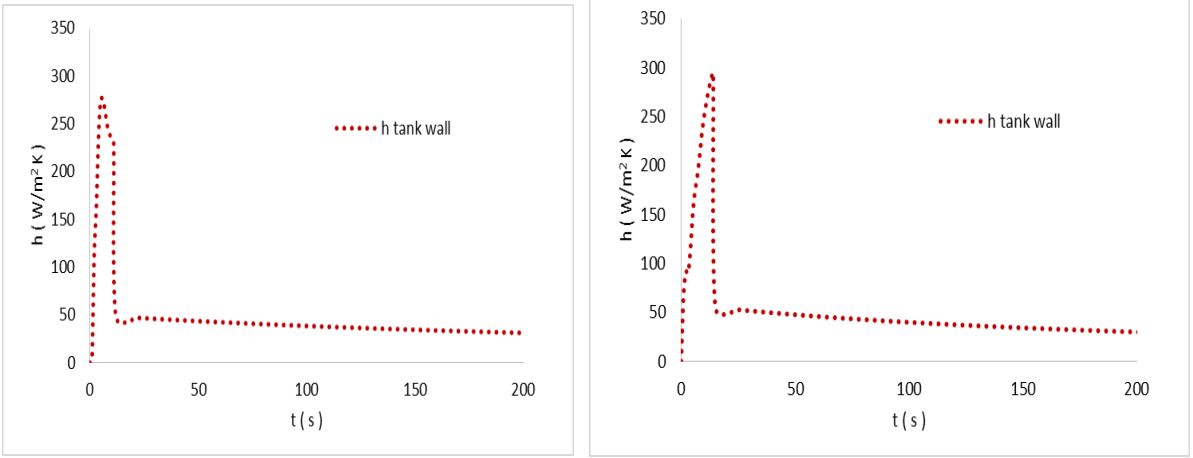

(a) (b)

Figure 4.8 Heat transfer coefficient during the charging process with PCM (a) and without PCM (b).

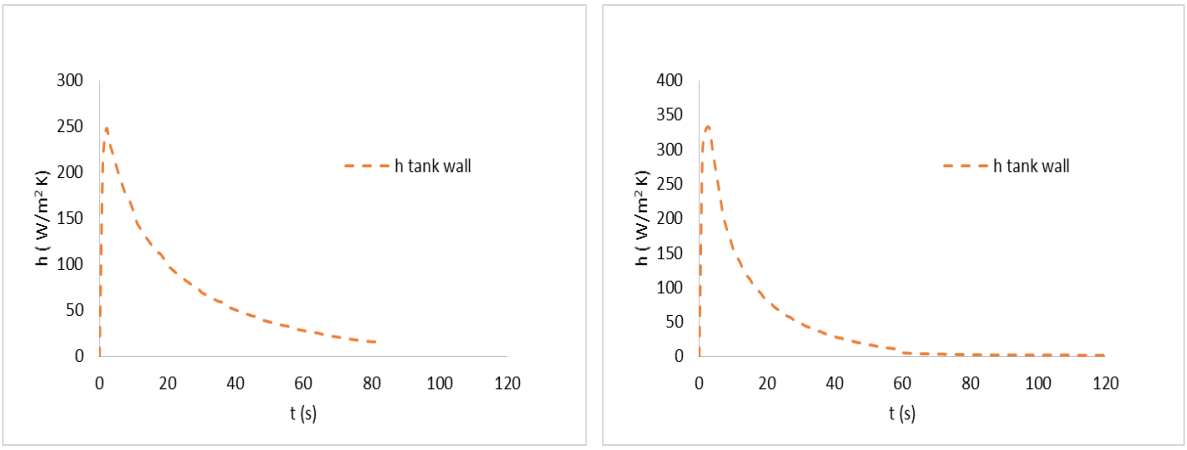

(a) (b)

Figure 4.9 Heat transfer coefficient during the discharging process with PCM (a) and without PCM (b).

A similar trend is also experienced in the discharging process. At the beginning of air discharge, the heat transfer coefficient rises rapidly and then slowly decreases to around 2 W/m^{2}K when the discharge process is completed. The heat transfer coefficient for the system with PCM is approximately 250 W/m^{2}K initially and gradually drops to around 2 W/m^{2}K as it is driven by natural convection only when discharging process has been completed (Figure 4.9 [a]). Similarly, in the system without PCM, the heat transfer coefficient gradually decreases from approximately 300 W/m^{2}K to 2 W/m^{2}K (Figure 4.9[b]). The maximum heat transfer coefficient for the system without PCM is higher than the system with PCM because in the system with PCM some amount of energy has already been absorbed by PCM. The cooling effect is caused by the expansion which has effect on the heat transfer coefficient during discharging.

Due to the complex nature of heat transfer in this system, researchers had to make simplifications to it. Kushnir, Dayan [108] and Xia, Zhou [109] simplified the heat transfer coefficient by using a constant value. Xia et al. [30] used h value of 30 W/m^{2}K according to their system, 59 bar on air storage chamber. Mazzucco, Rothuizen [127] simulated the gas-fuelling system (300-750 bar) by assuming constant h of 150 W/m^{2}K during the charging process, and 50 W/m^{2}K after filling is completed. These values are close to the maximum and minimum values calculated using the above-mentioned correlation

Raju and Khaitan [24] proposed that the heat transfer coefficient is a function of mass flow rate and proposed the value of h followed by the equation below:

$$h = 0.2356 + 0.0149\,[\,\dot{m}_{in} - \dot{m}_{out}]^{0.8}\ (W/m^2\ K) \qquad \ldots\ldots\ldots\ldots\ldots\ldots\ldots\ (28)$$

Hence, $\dot{m}_{in}$ represents the mass flow rate in and $\dot{m}_{out}$ is the mass flow rate out. As pressure and temperature are different in each CAES system, this equation may work only for their system but not for other systems. The correlation used in this chapter to define the heat transfer coefficient are general fundamental equations developed by others for very different geometries, which will provide a fair validation of our developed model against experimental measurements.

4.4.4 Temperature evaluation during charging and discharging process.

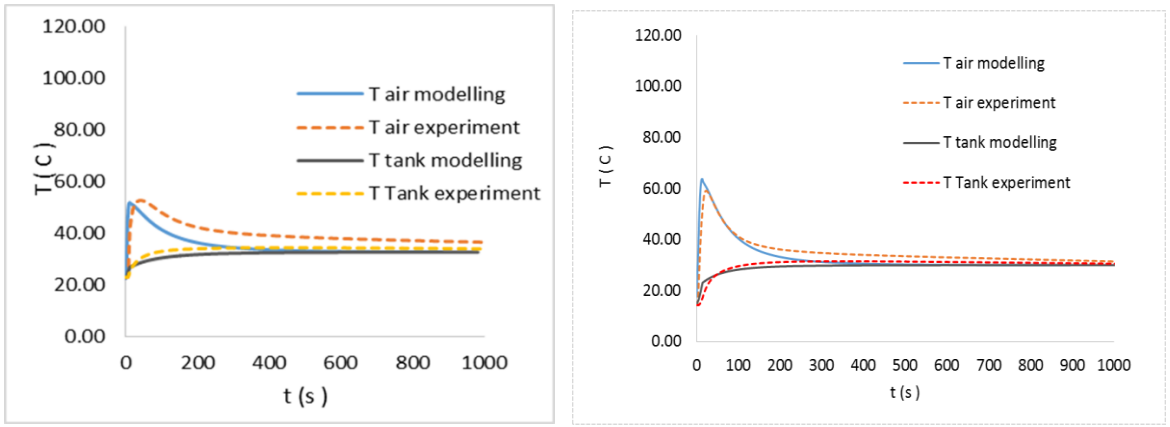

(a) (b)

Figure 4.10 Air and wall temperature comparison between simulation and experimental study on charging process for the system with PCM (a) and system without PCM (b).

Figure 4.10 reveals a sharp increase of the air temperature at the beginning of the charging process. In the system with PCM, the air temperature rises from 24°C to around 50°C, while it rises dramatically from 17 °C to approximately 62 °C when no PCM is used. In the presence of PCM, the heat is absorbed and stored in the PCM in the form of latent heat of melting. Both systems, with PCM and without PCM, show similar final steady-state air temperature, whereby air and cylinder's wall temperatures drop until they reach equilibrium.

The measured air profile and the predicted air profile have a small discrepancy (around 7%), especially for the system with PCM. This discrepancy could be attributed to many factors including the inaccurate prediction of heat transfer coefficient in such a complicated situation. Also, the model does not take into account air stratification and assumes that air temperature inside the cylinder is uniform, which may not be the case due to buoyancy. The air temperature in this system was only measured in the middle of the cylinder since it is not possible to have multiple thermocouples in this high-pressure system.

The temperature of the cylinder's wall was measured at the top, middle and the bottom. The average temperature measured at these three locations was used to define the cylinder's wall temperature, and it shows a reasonable agreement with the prediction of the model. In the system with PCM, the cylinder's wall temperature rises from 24°C to 32°C, while for the system without PCM the cylinder's wall temperature rises from 17°C to 34°C.

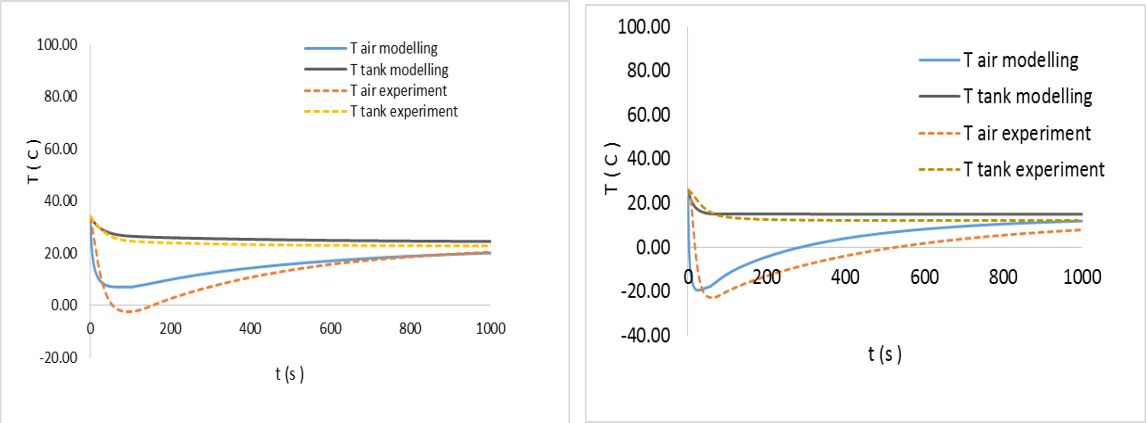

(a) (b)

Figure 4.11 Air and wall temperature comparison between simulation and experimental study on discharging process for system with PCM (a) and system without PCM (b).

Figure 4.11 presents a comparison between the measured and predicted air temperatures during the discharging process for the system with PCM (a) and without PCM (b). The air temperature drops dramatically to approximately -20°C (ΔT=48°C) in the system without PCM while only to about 6°C (ΔT=28°C) in the system with PCM. At the beginning of the process, the cooling effect from the expansion process was much faster than the heat transfer from the cylinder's wall. Based on measured data, PCM can reduce the drop in temperature from -20°C to only -2°C. The PCM microcapsule was successful in absorbing and releasing the latent heat at very high rate due to their large surface area.

In the system without PCM, Woodfield, Monde [124] reported a similar cooling effect phenomenon on hydrogen expansion at 100 bar system, which revealed a temperature drop from 30^0C to -30^0C in 10s. While although the expansion was done from 200bar, in the work presented in this chapter, air temperature drops from around 30°C to -20°C only, due to the longer expansion period of 60s and may be also due to the heavy thermal mass of the cylinder used.

In the system reported by Castellani *et al.* [97], a PCM based paraffin (RT18HC) is used, encapsulated in plastic disk (5 mm thickness), which were inserted into the cylinder. The results showed that ΔT for expansion decreased from 25.2 ^{0}C to 11 ^{0}C when PCM was used. This system was operated at 20 bar with an expansion period of 20 seconds so the rate of expansion was 1 bar/s. Using microcapsules of PCM allows expansion and compression at much higher rates such as the one applied in this work (3.33 bar/s). Simple transient heat transfer analysis on microcapsule shows that their time response is of the order of milliseconds and hence they could be used when expansion and compression need to be done at very high rates.

4.5 Summary

PCM is a potential candidate to improve thermal storage in ACAES, especially when it is used in the form of the microcapsule, due to the large surface area of the microcapsules, providing very fast heat transfer. Even though predicting the heat transfer coefficient in ACAES is complicated, it was possible to explain heat transfer using mix convection heat transfer during both charging and discharging processes. At the beginning of the process of charging and discharging, a high coefficient (up to around 300 W/m^{2}K) was obtained, that was mostly controlled by forced convection. Following that, it drops rapidly to around 50 W/m^{2}K when there is no more air flowing into the system and to under 5 W/m^{2}K after the expansion is completed due to the reduced temperature caused by expansion.

The method of using microcapsules as thermal storage in a compressed air system successfully stores the heat during compression and releases it during expansion and at very high rate. The maximum temperature difference in the presence of PCM drops to 26 °C from 45 °C (in the system without PCM). Subsequently, the minimum temperature drop in the presence of PCM is only 28 °C, compared to 48°C without PCM.

Chapter 5. Performance of metal and non-metal coated phase change materials microcapsules when used in compressed air energy storage system

Chapter Preface

Using phase change material microcapsules (PCMCs) in direct contact with a compressed air in an adiabatic compressed air energy storage system (ACAES) is an effective approach to capture the heat generated during air compression and to recover it later during expansion. In this work, three different PCMCs were investigated, including those coated with metal. The PCMCs were placed inside air-storage cylinder and compressed to 200bar. The PCMCs stability against air compression/expansion after 20x cycles was investigated using particle size distribution analyser (PSD), differential scanning calorimeter (DSC) and scanning electron microscope (SEM). The Micronal PCMCs show better thermal storing/releasing performance than other microcapsules showing no significant changes in its thermal behaviour after 20 cycles. In terms particle size distribution, Micronal 5038X and metal-coated Microtek24D MPCMCs retained their sizes after 20 cycles. From the DSC analysis, Micronal capsules show minor reduction in heat storage capacity after 20 cycle and retained good morphology based on SEM photo.

5.1 Introduction

Compressed air energy storage (CAES) is a promising energy storage system for coping with intermittency [46, 50, 131]. The air is compressed in an air storage container during electricity off-peak and it is used later to run gas turbines in order to generate electricity when it is required [131]. In this technology, after the compression, the air is allowed to cool and subsequently stored in a pressurized cylinder, normally underground cavern. During air expansion, the air temperature drops, and hence it has to be heated using fuel before it is transmitted to the power generation facilities. The need for extra heat in CAES plants makes the efficiency of the system relatively low and will not keep the process as an environmentally friendly [25, 132]. An adiabatic CAES (ACAES) is introduced to overcome these problems by combining CAES and thermal energy storage (TES). TES is introduced to store the heat generated during compression for later use during expansion. This TES is important as it can minimise the use

of non-renewable sources of energy and enhance the system efficiency up to around 70% [25, 28, 30].

Extensive research is conducted to improve ACAES system through the application of sensible energy storage. The common sensible heat-storage materials used are oil [32, 34], water [30, 35], rock bed [28, 38] and ceramic material [39]. Jubeh and Najjar [34] simulated the performance of ACAES using cavern as air storage chamber and oil as thermal storage material. The result showed that, with a high efficiency turbine and a high-capacity TES a round trip efficiency of approximately 70% could be achieved. Barbour et al. [38] developed a numerical model of an ACAES system with packed beds and validate it against analytical solutions. The estimated overall efficiency was around 70% and the main losses were found in the compressors and expanders (accounting for nearly 20% of the work input) rather than in the TES packed beds. Recently, Geissbühler et al. [133] presented experimental and numerical analysis of advanced adiabatic compressed air energy storage (AA-CAES) pilot-scale plant. The plant was built in an unused tunnel with a diameter of 4.9m and length of 120m. The sensible TES material was placed inside the cavern with a capacity of 12 MWh. The achievable compressed air gauge pressure is 7bar. The TES efficiency was determined to be between 76% and 90% however, the estimated round-trip efficiency was between 63–74%. The performance of a pilot plant of CAES system using water as thermal energy storage working medium was investigated [134]. The air is compressed inside a cylindrical stainless steel tank with a pressure of 93 bar. The total amount of heat absorbed was 565 kWh, while the storage water temperature reached 108.6°C in the TES system. The outcome was a round trip efficiency of 22.6%, which compares unfavourably with the usually quoted values of 60–75%.

Phase change materials (PCMs) are materials that melt and solidify at a nearly constant temperature, and are capable of storing and releasing large amounts of energy when they undergo phase change. Heat is absorbed or released when the material changes between the solid and liquid phases at a certain temperature, the phase change temperature, and vice versa. Selecting a proper storage media depends on the specific energy storage capacity, material cost and the expected temperature variation. Apparently, the use of latent heat storage based on phase change materials (PCMs) in a CAES application seems to be more viable in compared to sensible heat storage because of its higher energy storage density. Additional benefit of using PCM, involve the reduction of heat losses since heat could be stored close to ambient temperature. TES based on PCMs are used in many applications [4, 135], however, only few studies were reported in the literature on their use in CAES systems. Mazzucco, Rothuizen

[127] investigated the energy saving in a hydrogen gas fuelling system by storing the heat during compression using PCM. The operating conditions were set at 350 and 700 bar. The PCM used in this study is paraffin wax with melting temperature of 55°C, latent heat of 224.36 kJ/kg and placed between two walls (10 mm thickness). During air compression, the outcome showed that the PCM absorbed enough heat to reduce air temperature inside the tank from 118 to approximately 74°C. Castellani et al. [97] Investigated the expansion process in the ACAES by using PCM (RT18HC) at 20 and 30 bar. PCM was encapsulated in a plastic disk with 5 mm in thickness and inserted inside the air storage tank. In the system without PCM at 20 bar, the result showed that the air temperature drop was 25.2°C (from 27.7°C to 2.5°C) during the expansion. However, the temperature drop was only 11°C (from 24°C to 13°C) in the system with PCM. Similar findings were found at 30bar.

In an ACAES application, fast compression and expansion is experienced. Thus, PCM should have a high-thermal conductivity in order to absorb and release the heat at very high rates. Some methods provide means of increasing the effective thermal conductivity of PCM such as the use of PCM impregnation in a graphite matrix [136]and PCM microencapsulation [137]. The later can increase the rate of heat transfer by providing a large heat transfer surface area per unit volume of encapsulated PCM [40, 41]. For that reason, Saputro and Farid [138] investigated a novel approach of direct contact between compressed air and commercially available PCM microcapsules (PCMCs). Experimental measurements and simulation showed that the use of PCMCs reduces the maximum increase in air temperature from approximately 45 to 27°C during compression. While during expansion, the maximum decrease in temperature was reduced from 48 to 28°C, which prevented air temperature from dropping to below 0°C. In previous publication [139], the rate of heat transfer in microchannel heat exchanger was increased by 10% when metal-coated PCMCs slurry was used, compared to non-metal coated. In this chapter, the developed metal-coated PCMCs are tested in an ACAES system for the first time and compare the capsule thermal performance and stability with those non-metal coated PCMCs. Furthermore, the PCMCs particle size distribution, surface morphology and thermal properties before and after 20x cycles are investigated thoroughly.

5.2 Experimental work

5.2.1 Materials

Commercial Micronal DS 5038X (BASF, Germany) and Microtek 24D (Microtek Laboratories, USA) PCM microcapsules were used. The core materials for both PCM microcapsules are made out of paraffin. However, Micronal DS-5038X is microencapsulated with a hybrid shell (crosslinked polymethylmethacrylate and silica) and Microtek-24D with melamine resin. The thermos-physical properties of PCM microcapsules are listed in Table 5.1.

Table 5. 1: Thermo-physical properties of PCM microcapsules used in this study.

Thermo-physical properties	**Micronal DS 5038X**	**Microtek 24D**
Physical form	Powder	Powder
Particle size	50-300µm	15-30µm
Bulk density	300-400kg/m^3	-
Solubility in water	Insoluble- dispersible in water	Insoluble- dispersible in water
Phase change (melting)	25^{o}C (main peak)	24^{o}C (main peak)
Latent heat capacity	110J/g	154-164J/g

5.2.2 Preparation of metal coated PCM microcapsules

The electroless plating method is used to coat the Microtek 24D PCMCs. Initially, the PCMCs were coated with polydopamine (PDA) in order to activate the surface needed for the later process, the electroless plating. The chemicals used for the preparation of metal-coated PCMCs and the experimental procedure used to develop them are well explained in previous publication [91].

5.2.3 Surface activation of PCM microcapsules

The first step in the coating procedure is surface activation of PCM microcapsules by forming and depositing PDA on the surface of the PCM microcapsules. The procedure is described in previous publications [91, 139] as follows:

1. 5 L of dopamine solution was prepared by dissolving 10 g of dopamine into 6.057 g of tris (hydroxymethyl) aminomethane solution (10 mM).

2. The dopamine solution pH was adjusted to 8.5 by adding sodium hydroxide solution (1M) or hydrochloric acid solution (1M) stepwise in order to control the pH of the dopamine solution.
3. 200 g of PCM microcapsules were suspended in the 5 L of dopamine solution under stirring for 24 hours at room conditions.
4. The PCMs-DPA PCM microcapsules were filtered and washed three times with deionised distilled water and then placed in an oven at 50°C for 24 hours for drying before conducting the silver electroless plating.

5.2.4 Electroless plating

The second step of the coating procedure is electroless plating of silver on the surface of PCM microcapsules, following the procedure below:

1. The silver nitrate ($AgNO_3$) solution was prepared by dissolving 20 g of $AgNO_3$ into 2 L of deionised distilled water under magnetic stirring. Several drops of ammonia were added stepwise into silver nitrate solution until the colour changed from dark to transparent.
2. 50 g of PCMs-DPA PCM microcapsules were added to the $AgNO_3$ solution and stirring was maintained for 30 minutes to give a chance for the $AgNO_3$ ions to be absorbed on the surface of PCMs-DPA PCM microcapsules by the catechol and amino groups present in the PDA.
3. The reducing agent solution was prepared separately by dissolving 10 g of glucose (reducing agent) into 2 L of deionised distilled water. In addition to the glucose, 0.8 g of ethanol and 0.8 g of polyvinylpyrrolidone (PVP) were added.
4. The reducing agent solution was added slowly to the PCMs-DPA PCM microcapsules $AgNO_3$ solution under stirring, and then the electroless bath solution was continually stirred for 30 minutes. The PCMs-Ag PCM microcapsules were separated and rinsed three times with distilled water and then placed in an oven at 50°C for 24 hours for drying prior to use in CAES.

5.2.5 Air compression process

The experiments were carried out in a well-insulated stainless-steel air-storage cylinder-2 (2 L-200bar) equipped with pressure regulator and discharge valve. The cylinder is insulated using ceramic fibre insulation to minimize heat loses. The air-pressure compressor is connected to the stainless-steel air-storage cylinder-1 (25 L-300bar) as shown in Figure 5.1. The PCM microcapsules (150 g) are placed into the air-storage cylinder-2 and then pressurised air is transferred from cylinder-1 to cylinder-2 and stored at 200 bar until the air and wall temperatures reach a steady-state condition before it is released to the environment. This experiment is monitored by measuring temperature and pressure using sensors that are installed in cylinder-2. Three thermocouples are assembled to measure the temperature of the cylinder wall, and are located at the bottom, middle and top of the cylinder. The air centre temperature inside the cylinder is measured accurately by RTD PT 100, type TR33 especially designed to work at high-pressure and is provided by WIKA Company. The thermocouples are connected to the data acquisition system (PicoLog Thermocouple Data Logger-Model TC-08) which is connected to a computer for continuous temperature measurements.

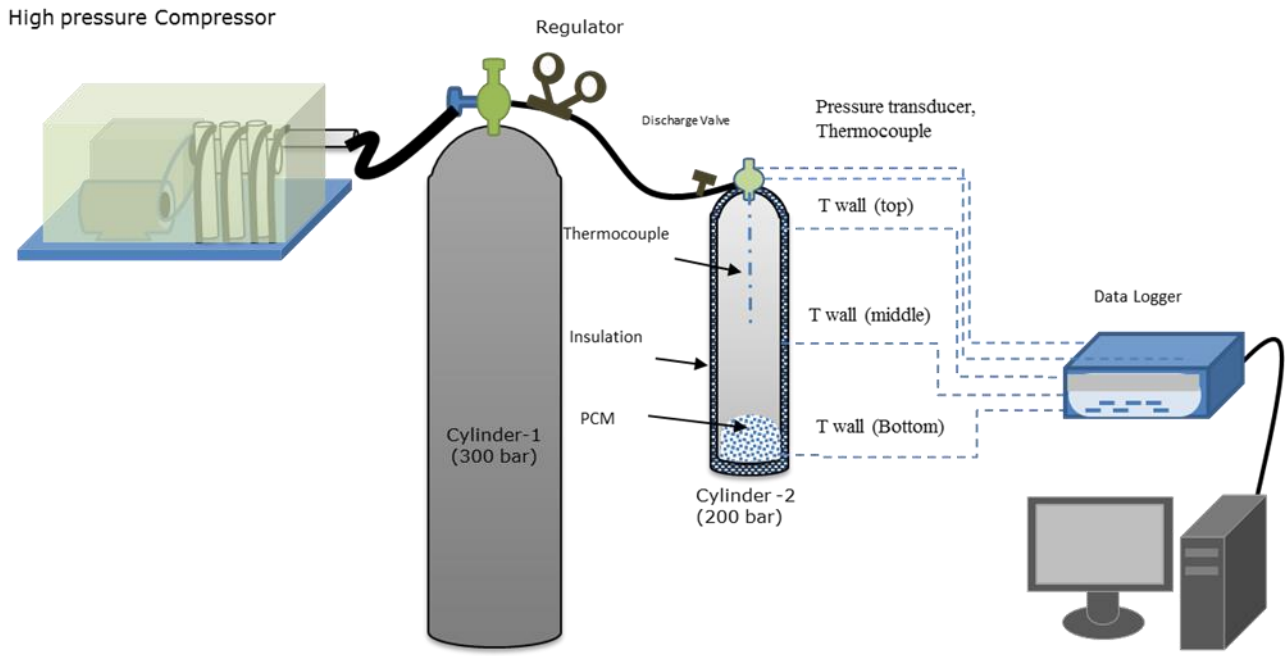

Figure 5.1 Schematic setup of ACAES

5.2.6 PCM microcapsules Characterizations

5.2.6.1 Particle size distribution (PSD)

The particle size analyser ((Mastersizer 2000, Malvern, UK) was used to measure the particles size and size distribution of the PCMCs before and after 20x cycles of air compression/expansion.

5.2.6.2 Differential Scanning Calorimetry (DSC)

The phase change properties in terms of melting and solidification temperatures and their phase change enthalpies of the metal and non-metal-coated PCM microcapsules, initially and after 20 air cycles were measured using differential scanning calorimetry (Perkin Elmer DSC8500). The measurements were performed by varying the temperature from -5 to 35°C with a heating and cooling rate of 2°C/min and under nitrogen purge of 20 mL/min.

5.2.6.3 Scanning Electron Microscope (SEM)

The surface morphology of the fresh PCM microcapsules and after 20 air cycles was observed using an SEM (Quanta eSEM) conducted under low vacuum pressure of 0.4–0.5 torr and temperature of -5°C.The encapsulated PCM is in its maintained in its solid state during SEM testing.

Figure 5.2 summarized the experimental steps for the manufacturing metal-coated PCMCs and the experiment design for testing PCMCs in an ACAES system.

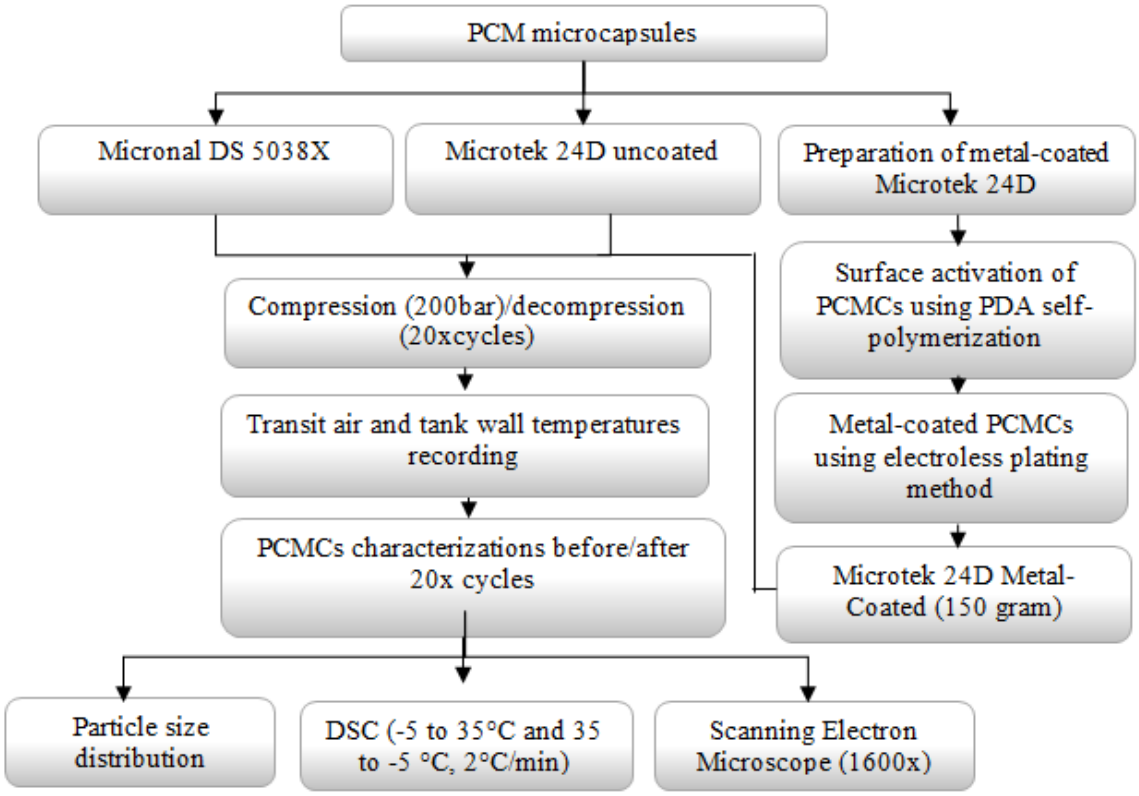

Figure 5.2 Flow chart diagram of the experimental steps

5.3 Result and Discussion

5.3.1 Thermal performance of ACAES system.

Experiments were conducted at constant rate of air compression and different rates of expansion, 60 (fast) and 1600 (slow) seconds. Figure 5.3 shows the wall and air temperatures and pressure variations at different rates of expansion. The maximum air temperature reached 60^{o}C during air compression then dropped to 5 and -20^{o}C when slow and fast expansions are performed respectively as shown in Figure 3. Slow expansion prevents air temperature from dropping below 0^{o}C thus avoid ice formation, however such slow expansion cannot be assured in all practical applications.

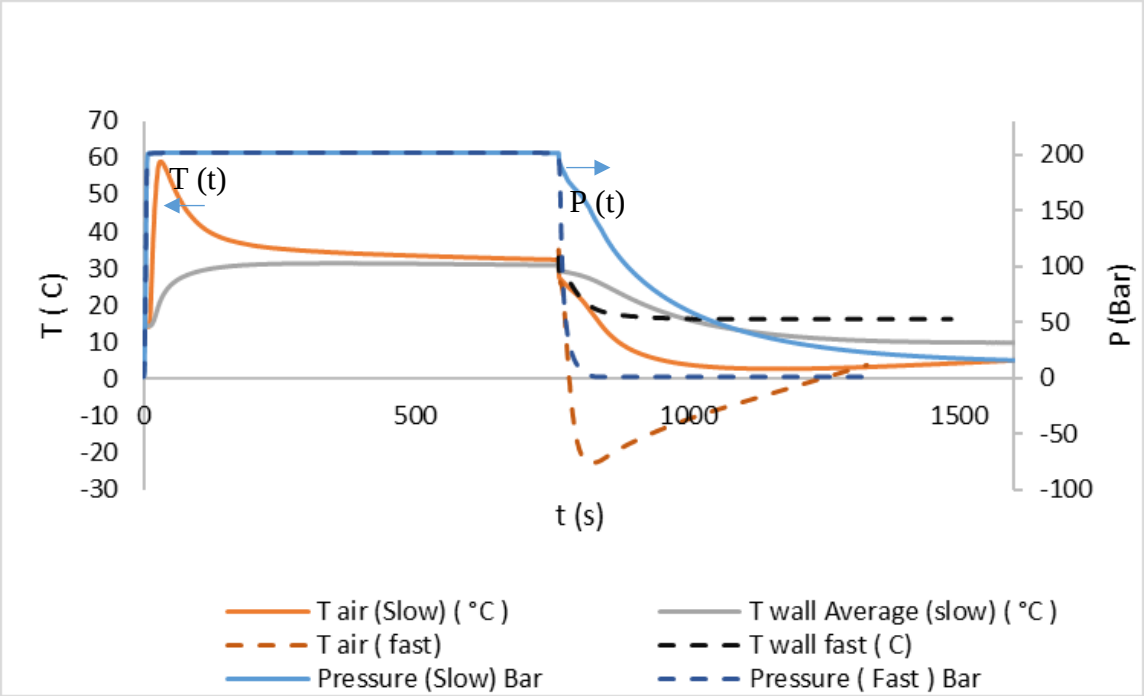

Figure 5.3 Temperature and pressure profiles at fast and slow air expansion.

The heat-recovered efficiency (the ratio of output thermal energy recovered to the input thermal energy supplied) is calculated as follow:

$$\eta = \frac{Q_{release}}{Q_{absorb}} \qquad \text{..... (29)}$$

Where Q absorb (kJ) is the input thermal energy supplied during air compression, while Q release (kJ) is the thermal energy recovered during expansion. The calculated values of thermal efficiency are 85 and 78% when slow and fast expansion are accomplish respectively. The slow expansion allows more time for the wall cylinder to transfer the absorbed heat to the air.

In an attempt to capture and reuse the waste heat generated during air compression, PCMCs were placed inside an air cyclinder-2. From now and on, the fast expansion is applied. Figure 5.4 shows the air and average wall temperatures viarations during air compression and expansion at first cycle. Four systems were tested: (1) no PCMCs, (2) Micronal 5038X PCMCs, (3) Microtek 24D PCMCs and (4) silver-coated Microtek 24D PCMCs. In this study, the weight of PCMCs was kept constant for all samples (150 g) and the initial temperature of the PCMCs was kept below the melting temperatures of the encapsulated PCM (solid state).

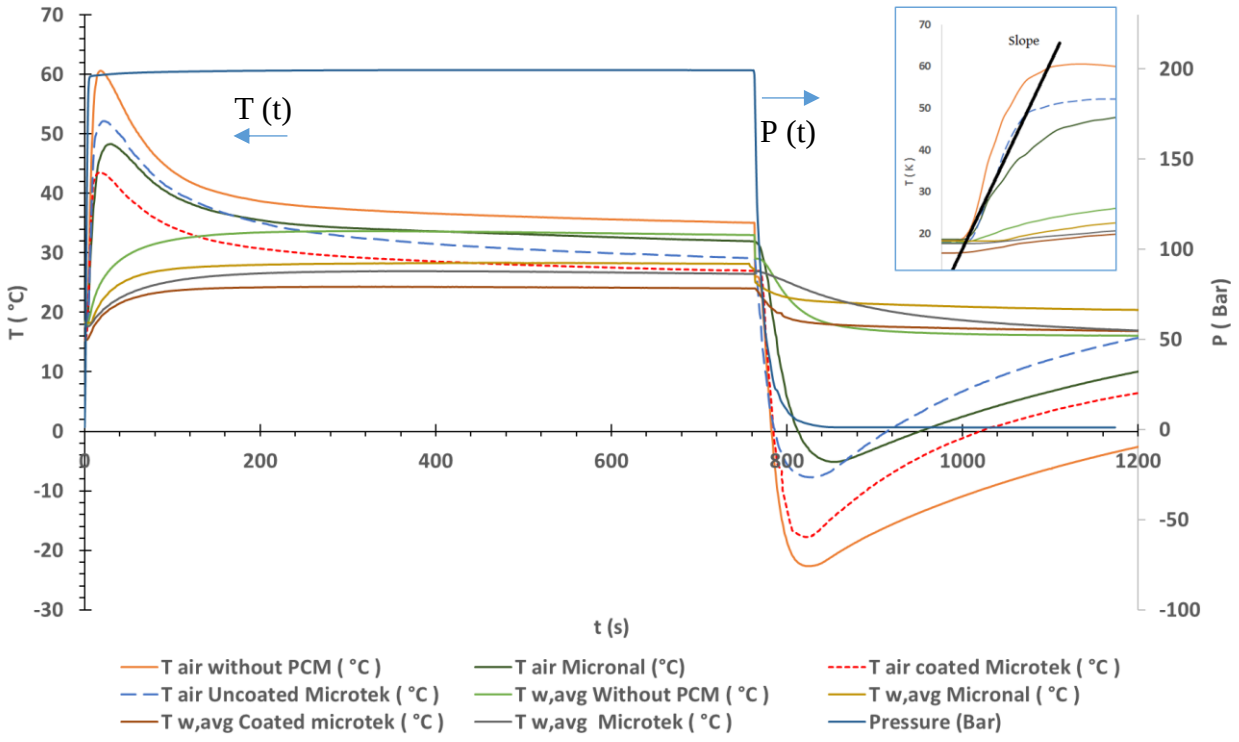

Figure 5.4 Air and wall temperatures variations during air compression/expansion-first cycle

In the system without PCMCs, the air temperature increases by around 42^{o}C, while when Micronal 5038X and Microtek 24D were used it increases by only 30^{o}C and 35^{o}C respectively. Micronal-5038X PCMCs has a remarkable effect on the thermal performance of the CAES system. The rate of PCM melting in Micronal-5038X is higher than the Microtek-24D PCMCs probably due to the presence of the high-thermal conductive silica shell [140]. The average rate of air temperature change when Micronal-5038X and Microtek 24D PCMCs were used are 3.2, 3.7°C/sec respectively, however it is 4.7°C/sec with no PCMCs. In expansion, the air temperature for the system without PCM is dropped 55^{o}C while when Micronal 5038X and Microtek 24D were used the air temperature dropped by only 35 and 40^{o}C respectively. PCMCs provide large surface area needed for fast heat transfer.

One of the objectives of this study is to look into the effect of using metal-coated PCMCs on the thermal performance of the ACAES system. The electroless metal-coating process for Microtek 24D is successful and the PCMCs are completely covered with silver naoparticles metal as shown in Figure 9E. However, it's difficult to metal coat Micronal capsules since they are clusters of nano capsules. The result from Figure 4 shows that the metal-coated Microtek

24D PCMCs have a 7°C further decrease in air temperature compared to the non-metal-coated PCMCs during compression. The effect of metal coating is more pronounced due to the increase in the PCMCs thermal capacity, sensible heat, caused by silver metal and also through the enhance heat transfer caused by micro-mixing of the metal-coated PCMCs. The significant effect of metal-coated PCMCs on the rate of PCM melting is observed by the delayed increase of air temperature as shown in Figure 5.4.

According to equation 29, the calculated thermal efficiencies of the system with Micronal 5038X, Microtek 24D and metal-coated Microtek 24D PCMCs are 96.3, 94.1 and 92.6% respectively. These values of efficiency are higher when compared with the system having no PCMCs. This is due to the low rate of heat release from the stored heat in the cylinder's wall compared to that from the capsules. Additional benefit of using PCM involves the reduction of heat losses to the environment since the heat is stored at close to ambient temperature.

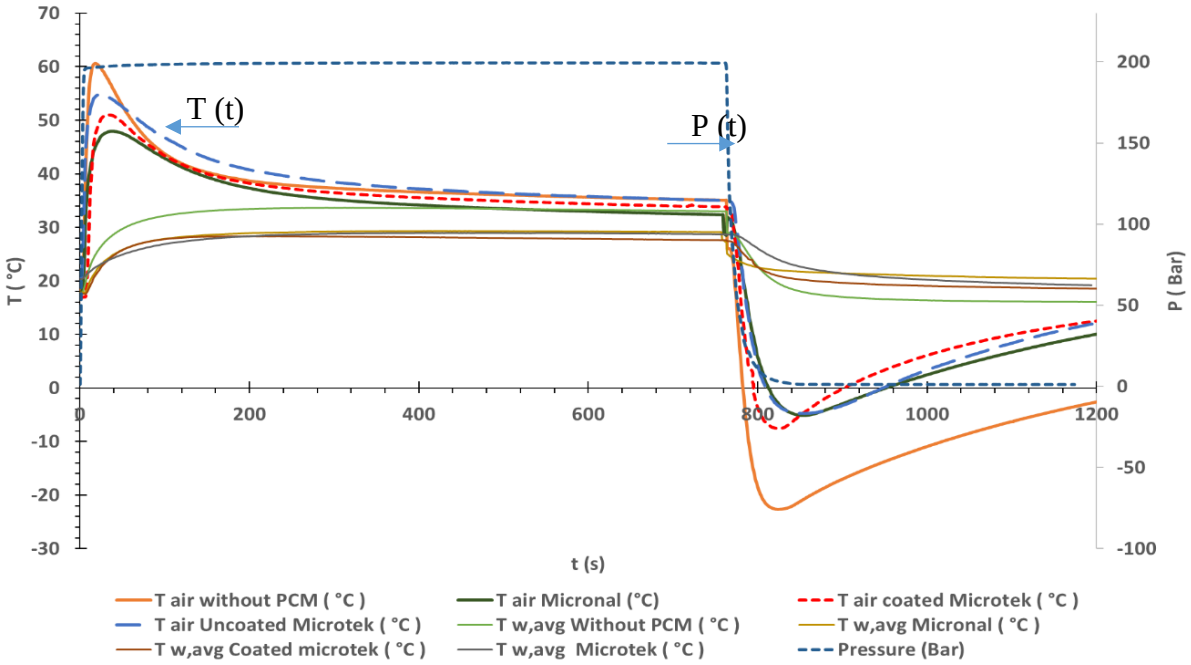

Figure 5.5 Air and wall temperature variations during air compression/expansion-20x cycles

Figure 5.5 shows the profiles of air and wall cylinder temperatures after 20x cycles. In the compression process, Micronal has the lowest temperature increase ($\Delta T=30^{o}C$) compared to the temperature increase of 35 and 40°C in the system of non-metal and metal coated Microtek 24D respectively. In expansion, Micronal has the lowest dropping temperature ($\Delta T=35^{o}C$) compared to the system with metal coated and non–coated Microtek 24D, which showed drop

of 37 and 40°C respectively. Micronal PCMCs retained their thermal performance after 20x cycles. This indicates Micronal PCMCs have a better stability than other PCMCs. The drop in the performance of metal coated after 20x cycles is probably due to the metal coated layer start falling because of the compression/ expansion process as confirmed by SEM photo in Figure 10F.

5.3.2 PCM microcapsules life assessment

5.3.2.1 Particle size distribution (PSD)

Figure 6 shows the particle size and size distributions for the three PCMCs samples before and after 20x cycles. The fresh Micronal® DS 5038X PCMCS has an average size of about 150.6 µm, which suggests that they are clusters of submicrons particles as shown in the SEM image (see Figure 10A**)**. This kind of microcapsule cluster was synthesised through an agglomeration process probably for safety reasons related to the use of nano-particles [128]. The fresh particle size for the non-metal-coated Microtek 24D is in the range of 15 to 30µm with an average diameter of 22µm while the metal-coated Microtek 24D has an average diameter of 32µm. After 20x cycles, the particles size and size distribution for Micronal and metal-coated Microtek 24D PCMCs are slightly shifted, while the non-metal coated Microtek 24D PCMCs show multiple peaks with significant shifting in their size. This could be due to capsules being cracked and sticking together.

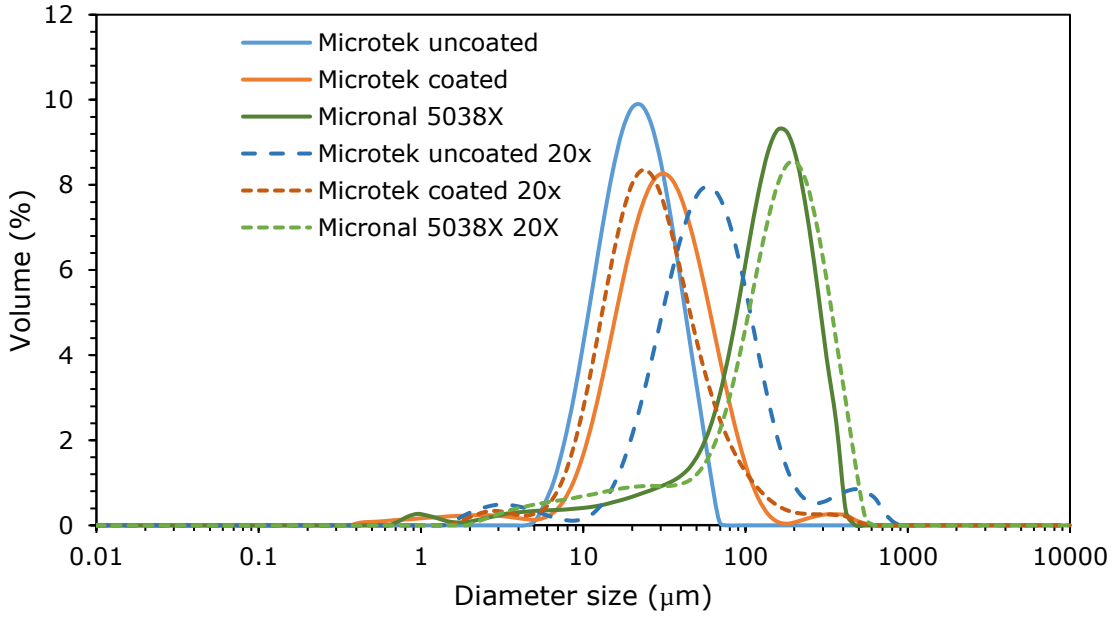

Figure 5.6 Particle size distribution before and after 20x cycles.

5.3.2.2 DSC analysis of PCMCs

Long performance of the PCMCs and the number of thermal cycles they can withstand with insignificant changes in their thermo-physical properties are key parameters in deciding the potential use of PCMCs in an ACAES system. The DSC result reveals that there are no changes in phase transition temperatures and heat-storage capacity of the Micronal DS 5038X PCMCs after 20x cycles as shown in Figure 5.7a. However, Microtek 24D PCMCs showed shifting in the peak melting temperature from 23 to 25^{o}C with some reduction in latent heat from 139.6 J/g to 135.4 J/g as shown in Figure 5.7b. The hybrid shell of the Micronal DS 5038X PCMCs gives a good mechanical strength of the shell particles; thus retained their thermal performance after 20x cycles.

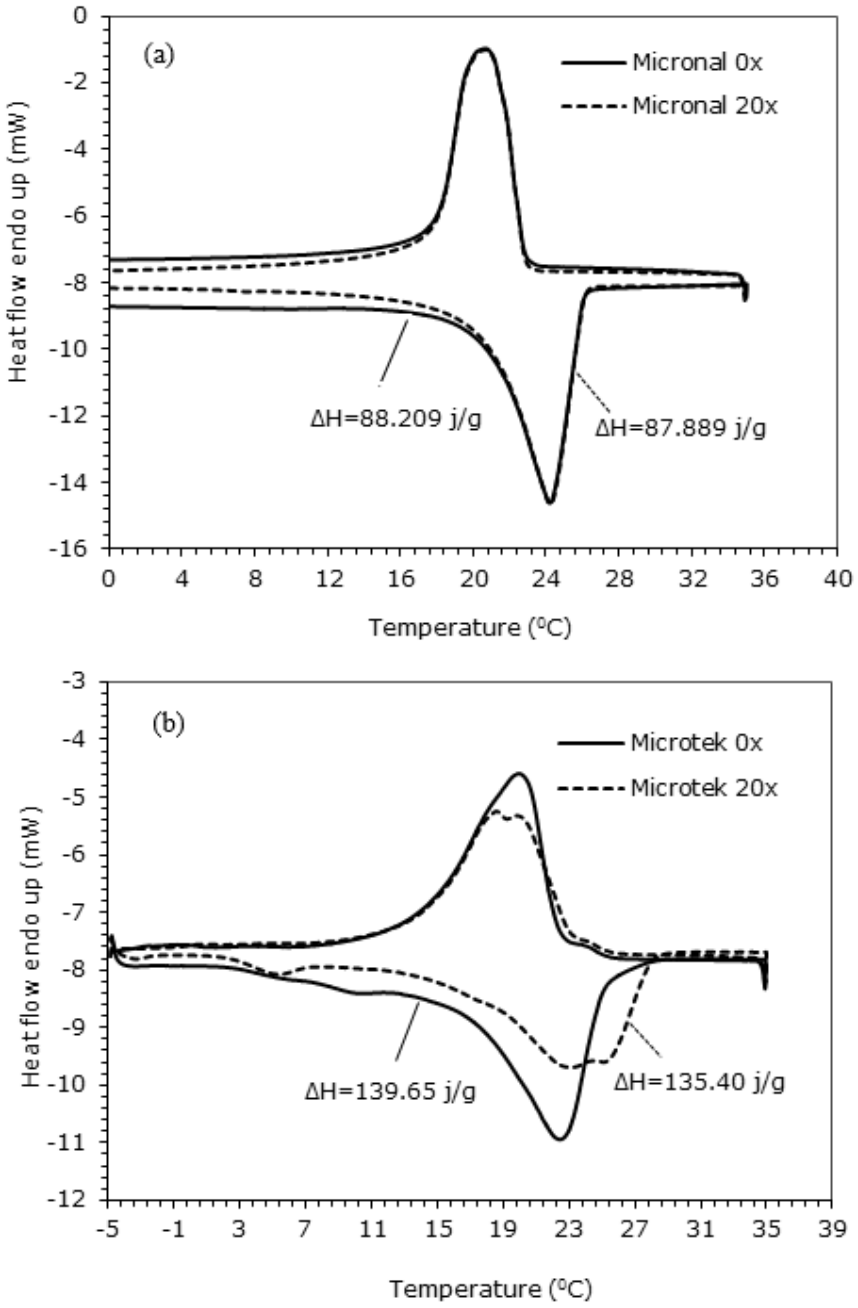

Figure 5.7 DSC measurements of (a) Micronal DS 5038X and (b) Microtek 24D before and after 20x cycles

The DSC result of metal-coated Microtek 24D PCMCs shows that the phase transition temperatures remain almost the same with minor reduction in specific heat capcity from 97.4 J/g to 96.4 J/g after 20 cycles as shown in Figure 5.8. The application of metal coating on the surface of PCMCs enhances the thermal performance and stability of the PCMCs in the ACAES system. In fact, the Micronal DS 5038X PCMCs showed a better thermal stability among metal and non-metal coated Microtek 24D PCMCs.

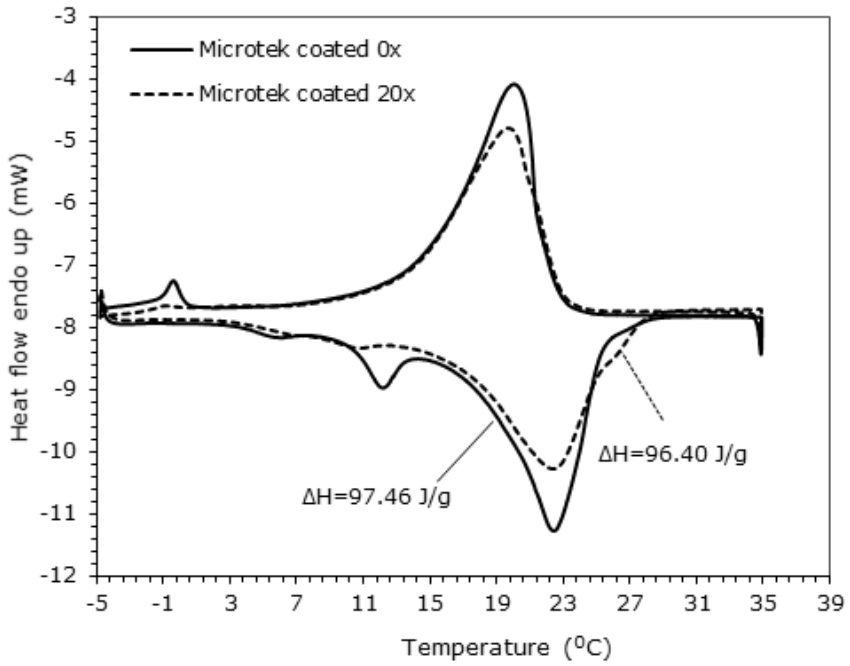

Figure 5.8 DSC measurements of metal-coated Microtek 24D PCMCs before and after 20x cycles

3.2.1 Scanning electron microscope (SEM)

In practical applications, especially in the ACAES system, the shell of PCMCs must have enough robustness to endure the high pressure caused by compressed air. In this work, three different PCMCs with different morphologies including, cluster of sub-micron particles (Micronal DS 5038X), non-metal and metal-coated Microtek 24D PCMCs were investigated. Micronal 5038X and Microtek 24D was coated with silver following the same procedures. Figure 5.9 shows that the surface is not coated properly and hence the metal coated Micronal 5038X were not tested during cycling.

Figure 5.10A shows the original Micronal DS 5038X PCMCs surface morphology. The PCMCs is in the form of a cluster of submicron particles (1-2µm) with an average diameter of 150µm. The agglomerated sub-micron PCMCs provide extra secure protection of PCMCs. Figure 5.10B shows the surface morphology of Micronal DS 5038X PCMCs after 20x cycles. The pressure disintegrate the clusters of nano capsules which contain the PCM (Figure 5.10B). The nano capsules of Micronal PCMCs seem to stay in its orginal shape with no PCM leaking and this is confirmed by the DSC mesurements before and after 20x cycles (Figure 5.7A).

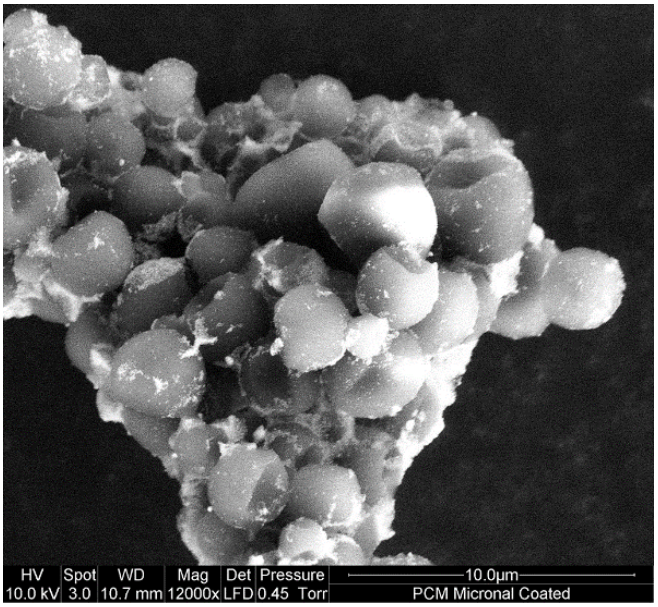

Figure 5.9 Micronal 5038X metal-coated.

Microtek 24D PCMCs with an average particle size of 20µm was also invistigated. The shell and core materials are made from melamine-formaldehyde resin and paraffin wax respectively. The Microtek 24D PCMCs manufacturer confirms the core-shell structure morphology. Figure 5.10F shows the internal feature of core-shell structure of PCMCs. The SEM image in Figure 5.10C shows that the Microtek 24D is in spherical shape with few dents on the surface. However, the number and the size of the dents are increased after 20x cycles as shown in Figure 5.10D. In addition, break shell fragments are observed.

Figure 5.10E shows the surface morphology of the metal-coated Microtek 24D. The metal-coating process for Microtek 24D is successful and the PCMCs are completely covered with silver naoparticles metal as shown in Figure 5.10E. However, it was difficult to metal coat Micronal DS 5038X sample being a cluster of nano capsules. Metal-coated Microtek 24D is exposed to 20x cycles of air compression/expansion. The shape of the metal-coated PCMCs after 20x cycles remains the same with few dents observed on the surface. However, the metal coating in some capsules is removed and some PCMCs are found ruptured as shown in Figure 5.10F. Thus, there is a need to design PCMCs with optimum polymer and metal shells thicknesses to provide a reasonable strength for the PCMCs

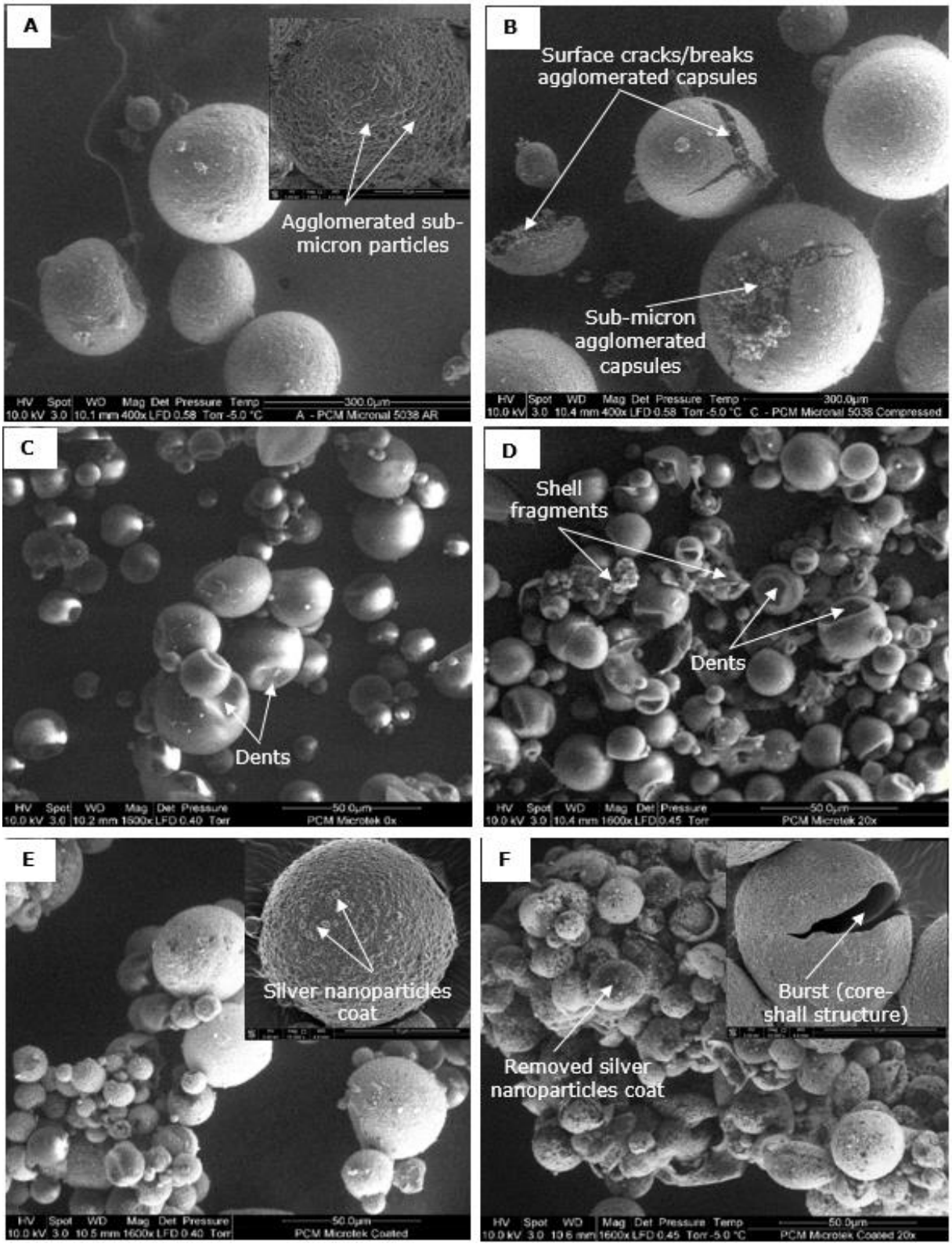

Figure 5.10 SEM images of (A) original Micronal DS 5038X PCMCs (B) Micronal DS 5038X PCMCs-20x cycles (C) original non-metal-coated Microtek 24D PCMCs (D) non-metal-coated Microtek 24D PCMCs-20x cycles (E) original metal-coated Microtek 24D PCMCs and (F) metal-coated Microtek 24D PCMCs-20x cycles

5.4 Scale-up challenges for CAES.

The large-scale compressed air energy storage system is one of the promising technologies to cope with intermittency in the power network. Since the Huntorf and Mcintosh plants, there have been some projects that have a set up CAES on a large scale such as: the Norton-Ohio project [23], Iowa project [24] and the Adiabatic CAES (Adele project). Unfortunately, these large-scale projects have been stopped due to technical and economic aspects.

5.4.1 Technology aspect.

Industrial compressors are already used at the two existing CAES plants. However, operating a big compressor/turbine on a large scale CAES is one of the technical problems that need to be addressed when setting up this system [45].The most promising compressor design so far includes a multi-stage–stage compressor and usually a combined axial-flow compressor and centrifugal compressor [141]. In regard to compressed air storage facility, a cavern seems to be the best option to store the high-pressure air. Indeed, for a small-scale application it may be possible to use pressurised cylinders [141].

5.4.2 Economic aspect

The estimated cost for a small CAES system, in 2015, with a maximum power of 33kw is around €17,000; for 100kW the value would be €30,000 [142]. In addition, the predicted capital cost for large-scale CAES (around 100MW) is around €13,530,000 [143]. In adiabatic CAES, the thermal storage material is important, the cost for sensible heat storage ranges is between €0.1–10/kWh, while the cost of latent heat storage systems based on PCM are estimated to be between €10–50/kWh [144]. The use of PCM encapsulation could be the solution to avoid using an expensive heat exchanger system. For instance; in a building structure (e.g., gypsum boards), where micro-encapsulated paraffin is used for the cooling system, the cost of the micro-encapsulated material is €13/kg and the price of paraffin is about €5/kg [144]. However, these prices are only for small quantities and it can be expected that the cost of PCM microcapsules is lower in larger quantities. The material cost for PCM microcapsules metal coating used in this research is around € 0.1/g which suggest that coating should with other metal, such as: copper.

5.4.3 Proposed large scale design using PCM Microcapsules as TES.

According to this research, the PCM Microcapsules has potential to use as thermal storage in the compressed air system. There are two possibilities design for applying PCM Microcapsule in large scale CAES system:

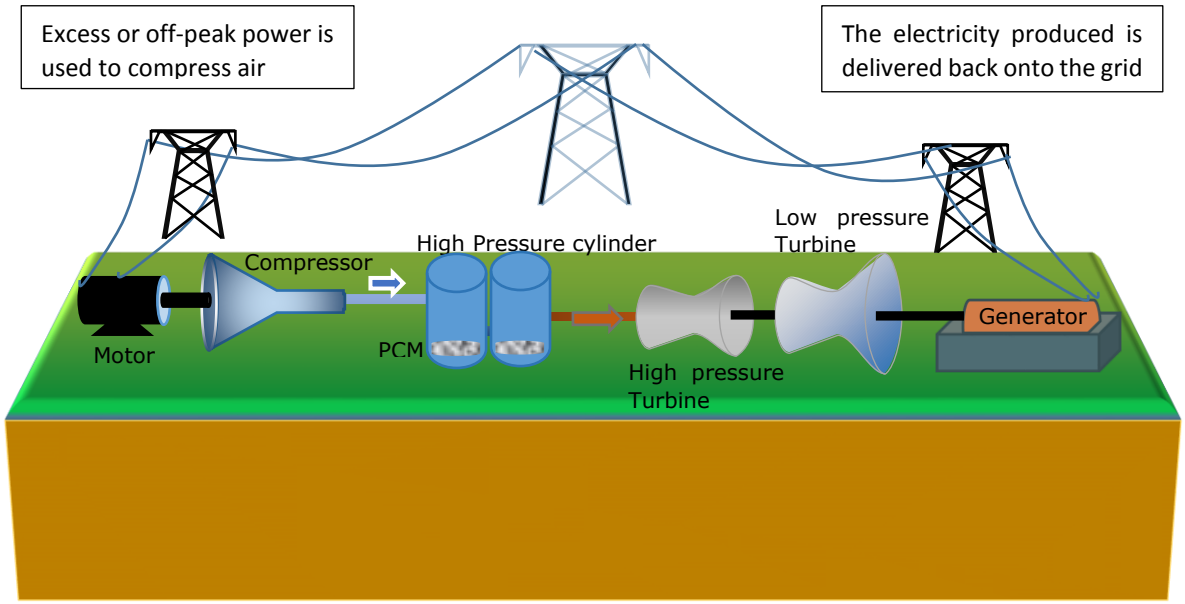

(a)

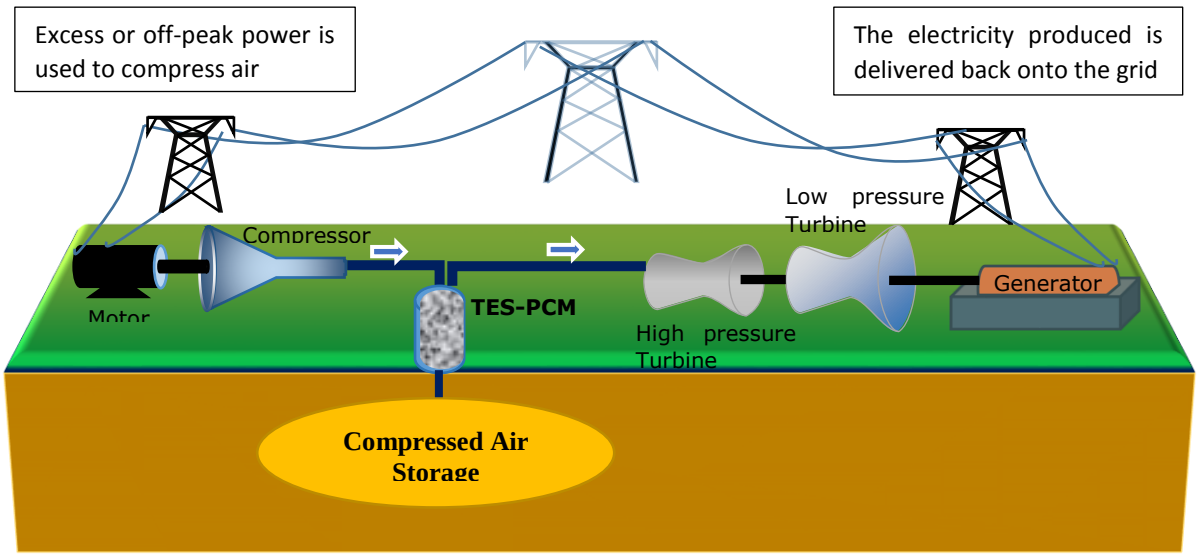

(b)

Figure 5.11 Application of PCM Microcapsule at CAES, (a) integrated with air storage, (b) special thermal storage facility.

In the first design, the PCM microcapsule is set up inside the high-pressure cylinder (Fig. 5.11 [a]). The idea of this design is to integrate the air storage and thermal storage. However, this may need a special cylinder to accommodate the PCM inside. The second design is to set up the thermal storage facility differently with an air-storage facility (Fig. 5.11 [b]). However, long period of operation for this design may cause the PCM to leave out of the cylinder during expansion. This problem can be minimised by applying a microfilter to prevent the microcapsules leaving from the storage during expansion.

5.5 Summary

Different types of PCMC were used for thermal storage in compressed air system and the performances of these PCMCs can be concluded as follow:

- The air temperature increase is reduced during compression and decreased during expansion when PCMCs is applied. The heat-recovered efficiency is improved from 78 to 96.4% when Micronal DS 5038X PCMCs is used.
- The application of metal coating on the surface of PCMCs enhances the thermal performance and stability of the PCMCs in the ACAES system. In fact, the Micronal DS 5038X PCMCs showed a better thermal stability among metal and non-metal coated Microtek 24D PCMCs.
- The shape of the metal-coated Microtek 24D PCMCs after 20x cycles remains the same with few dents observed on the surface. However, some PCMCs are found ruptured. In the Micronal DS 5038X sample, the pressure disintegrate the clusters of nano capsules which contain the PCM but these nano particles seem to stay in its orginal shape with no PCM leaking.

Chapter 6. Conclusions and Future Research Work

6.1 Author's Contributions

1. Developed a conceptual model to predict the transient change of both air temperature and cylinder's wall temperature in a small-scale compressed air energy storage system (CAES).
2. Designed a small-scale CAES using a high-pressure cylinder (2 L) to validate the conceptual model.
3. Invented a simple and efficient method for storing thermal energy in CAES through the use of PCM microcapsules to store the heat generated from compression and releasing it back during expansion.
4. Implemented a metal-coating PCM microcapsules to improve rate of charge/discharge of heat.
5. Identified the effect of high-pressure compressing on the stability of PCM microcapsules, their morphology and thermal characteristics.

6.2 Conclusions

A novel approach for storing the generated heat during compression and releasing it during expansion in CAES was successfully invented, modelled, implemented and discussed in this thesis.

Firstly, in this research, a model was developed to describe the transient change of air and the cylinder's wall temperature in air storage and was validated using a small CAES system. Although it is challenging to predict the heat transfer rate accurately in compressed air storage, it was possible to explain using mixed forced and free convection heat transfer during both charging and discharging processes. The heat absorbed by the cylinder wall's temperature was included in the model. The result showed that the air and cylinder's wall temperature of the high-pressure cylinder can be predicted successfully during both compression and expansion processes. For the 100 bar system, the calculated heat transfer coefficient rose to around 150 W/m^2K at the beginning of the compression process and dropped to around 2 W/m^2K when compression was completed. Meanwhile, in the 200 bar system, it rose to around 300 W/m^2K at the beginning of the compression and dropped to around 2 W/m^2K when the compression process was completed. During compression, at 100 bar, the air temperature rose from 24 °C to 60 °C, while at 200 bar it rose approximately from 17 °C to over 60 °C then dropped close to

wall temperature as the system approached equilibrium. During expansion, air temperature dropped to approximately 5 °C from starting pressure of 100 bar and reduced to -20 °C from starting pressure of 200 bar.

Secondly, this project successfully upgraded the small compressed air energy storage system to adiabatic compressed air energy storage system by using PCM microcapsules (Micronal DS 5038X) for thermal storage. PCM is a potential candidate to improve thermal storage in ACAES, especially when it is used in the form of microcapsules, providing the large surface area needed for more efficient heat transfer. The model was modified to include the effect of using PCM microcapsules. The result shows that the model has a good agreement with the experimental measurements. The maximum temperature difference in the presence of PCM is 26 °C compared to 45°C for the system without PCM. Subsequently, the minimum temperature drop in the presence of PCM is only 28 °C compared to 48 °C without PCM. The use of PCM microcapsules as thermal storage in the ACAES system successfully stores the heat during compression and releases it back during expansion at a very high rate.

Finally, the microcapsules used in this research were assessed for stability at their initial condition and after 20 compression-expansion cycles. The result showed that Micronal DS 5038X has a better stability than Microtek 24D since these microcapsules are a clusters of very small capsules. According to DSC analysis, after the cycles, Micronal DS 5038X have lost 0.3% of its energy storage density compared to Microtek 24D (3.5 %). However, the performance of Microtek 24D improved when metal coating was applied to the capsules, with a loss of only 1% after the 20 cycles. Based on SEM images, the cycles only affected the clusters of Micronal DS 5038X and not the capsules, but Microtek 24D showed some fragments and big dimples on the surface. However, SEM images revealed that Microtek 24D metal-coated remained the same after 20 cycles.

6.3 General Conclusion

This research have demonstrated that the PCM microcapsules are capable to absorb the heat during compression and release it during expansion in very high rate. Micronal DS 5038X showed a better stability against air cycling compare to coated and non-coated Microtek 24D. The performance of Microtek 24D is improved when metal-coating is applied.

6.4 Recommendations for Future Research Work

1. Investigate the optimum PCM for ACAES application, regarding the PCM type, capsule size (macro, micro, and nano) and the mass ratio of PCM.
2. Investigate the CAES by using thinner or lighter cylinder storage that is strong enough to operate in a high-pressure condition.
3. Modify the air storage chamber by inserting the PCM in the wall chamber as applied in building material.
4. Improve the strength of the microcapsules by applying metal coatings with different thickness and material.
5. Study the stability of PCM microcapsules at a higher number of cycles (compression and expansion).
6. Analyse the economics aspect for a small CAES system to determine its optimum capacity.
7. Use multiple PCM with different melting points to improve the performance of thermal storage.
8. Assess the environmental viability of the system using LCA approach.

References

[1] E.A.S.E., *European Energy Storage Technology Development Roadmap Towards 2030*. 2014, European Association for Storage of Energy EASE/EERA: Europ.

[2] Chen, H., T.N. Cong, W. Yang, C. Tan, Y. Li, and Y. Ding, *Progress in electrical energy storage system: A critical review.* Progress in Natural Science, 2009. **19**(3): p. 291-312.

[3] I.E.C, *Electrical Energy Storage*. 2011, International Electrotechnical Commision: Switzerland.

[4] Farid, M.M., A.M. Khudhair, S.A.K. Razack, and S. Al-Hallaj, *A review on phase change energy storage: Materials and applications.* Energy Conversion and Management, 2004. **45**(9-10): p. 1597-1615.

[5] Hadjipaschalis, I., A. Poullikkas, and V. Efthimiou, *Overview of current and future energy storage technologies for electric power applications.* Renewable and Sustainable Energy Reviews, 2009. **13**(6–7): p. 1513-1522.

[6] GWEC, *Global Wind Statistic 2015*. 2016.

[7] IHS-Technology, *Top-Solar-Power-Industry-Trends-for-2015*. 2015.

[8] Ren, P., *Renewables 2015 global status report.* REN21 Secretariat: Paris, France, 2015.

[9] Mahlia, T.M.I., T.J. Saktisahdan, A. Jannifar, M.H. Hasan, and H.S.C. Matseelar, *A review of available methods and development on energy storage; technology update.* Renewable and Sustainable Energy Reviews, 2014. **33**: p. 532-545.

[10] Ferreira, H.L., R. Garde, G. Fulli, W. Kling, and J.P. Lopes, *Characterisation of electrical energy storage technologies.* Energy, 2013. **53**: p. 288-298.

[11] Hameer, S. and J.L. Niekerk, *A review of large-scale electrical energy storage.* International Journal of Energy Research, 2015. **39**: p. 1179-1195.

[12] Helsingen, E.M., *Adiabatic compressed air energy storage*. 2015, NTNU.

[13] Lund, H. and G. Salgi, *The role of compressed air energy storage (CAES) in future sustainable energy systems.* Energy Conversion and Management, 2009. **50**(5): p. 1172-1179.

[14] Mason, J.E. and C.L. Archer, *Baseload electricity from wind via compressed air energy storage (CAES).* Renewable and Sustainable Energy Reviews, 2012. **16**(2): p. 1099-1109.

[15] Succar, S. and R.H. Williams, *Compressed air energy storage: theory, resources, and applications for wind power.* Princeton environmental institute report, 2008. **8**.

[16] Sundararagavan, S. and E. Baker, *Evaluating energy storage technologies for wind power integration.* Solar Energy, 2012. **86**(9): p. 2707-2717.

[17] Tallini, A., F. Rispoli, L.d. Santoli, A. Tallini, A. Vallati, and L. Cedola, *70th Conference of the Italian Thermal Machines Engineering Association, ATI2015Applications of Micro-CAES Systems: Energy and Economic Analysis.* Energy Procedia, 2015. **82**: p. 797-804.

[18] Ibrahim, H., A. Ilinca, and J. Perron, *Energy storage systems—Characteristics and comparisons.* Renewable and Sustainable Energy Reviews, 2008. **12**(5): p. 1221-1250.

[19] Budt, M., D. Wolf, R. Span, and J. Yan, *A review on compressed air energy storage: Basic principles, past milestones and recent developments.* Applied Energy, 2016. **170**: p. 250-268.

[20] Davidson, B.J., I. Glendenning, R.D. Harman, A.B. Hart, B.J. Maddock, R.D. Moffitt, . . . J.K. Wright, *LARGE-SCALE ELECTRICAL ENERGY STORAGE.* IEE Proceedings A: Physical Science. Measurement and Instrumentation. Management and Education. Reviews, 1980. **127**(6): p. 345-385.

[21] Bouman, E.A., M.M. Øberg, and E.G. Hertwich. *LIFE CYCLE ASSESSMENT OF COMPRESSED AIR ENERGY STORAGE (CAES)*. in *LCM 2013*. 2013.

[22] Lim, S.D., A.P. Mazzoleni, J.-k. Park, P.I. Ro, and B. Quinlan. *Conceptual design of ocean compressed air energy storage system*. in *Oceans, 2012*. 2012. IEEE.

[23] Luo, X., J. Wang, M. Dooner, J. Clarke, and C. Krupke, *Overview of Current Development in Compressed Air Energy Storage Technology.* Energy Procedia, 2014. **62**: p. 603-611.

[24] Isaac S, Dan W, and B.S. Haifa, *Compressed air energy storage method and system.* Renewable Energy, 1997. **11**(2): p. 282.
[25] Mozayeni, H., M. Negnevitsky, X. Wang, F. Cao, and X. Peng, *Performance Study of an Advanced Adiabatic Compressed Air Energy Storage System.* Energy Procedia, 2017. **110**: p. 71-76.
[26] Sciacovelli, A., Y. Li, H. Chen, Y. Wu, J. Wang, S. Garvey, and Y. Ding, *Dynamic simulation of Adiabatic Compressed Air Energy Storage (A-CAES) plant with integrated thermal storage – Link between components performance and plant performance.* Applied Energy, 2017. **185**: p. 16-28.
[27] Gulagi, A., A. Aghahosseini, D. Bogdanov, and C.B. Ch, *Comparision Of The Potential Role Of Adiabatic Compressed Air Energy Storage (A-Caes) For A Fully Sustainable Energy System In A Region Of Significant And Low Seasonal Variations.* 10th IRES, 2016: p. 15-17.
[28] Ortega-Fernández, I., S.A. Zavattoni, J. Rodríguez-Aseguinolaza, B. D'Aguanno, and M.C. Barbato, *Analysis of an integrated packed bed thermal energy storage system for heat recovery in compressed air energy storage technology.* Applied Energy, 2017. **205**(Supplement C): p. 280-293.
[29] Viladegut Minguell, A., *Study of an adiabatic CAES plant for electricity storage in a photovoltaic plant/Phase changing materials*. 2013, Universitat Politècnica de Catalunya.
[30] Wolf, D. and M. Budt, *LTA-CAES – A low-temperature approach to Adiabatic Compressed Air Energy Storage.* Applied Energy, 2014. **125**: p. 158-164.
[31] CHEN, L., T. ZHENG, S. MEI, X. XUE, B. LIU, and Q. LU, *Review and prospect of compressed air energy storage system.* Journal of Modern Power Systems and Clean Energy, 2016. **4**(4): p. 529-541.
[32] De Biasi, V., *Fundamental analyses to optimize adiabatic CAES plant efficiencies.* Gas Turbine World, 2009. **39**(5): p. 26-28.
[33] Freund, S., R. Schainker, and R. Moreau, *Commercial concepts for adiabatic compressed air energy storage.* proceedings of IRES 2012, 2012: p. 558.
[34] Jubeh, N.M. and Y.S. Najjar, *Green solution for power generation by adoption of adiabatic CAES system.* Applied Thermal Engineering, 2012. **44**: p. 85-89.
[35] Grazzini, G. and A. Milazzo, *A thermodynamic analysis of multistage adiabatic CAES.* Proceedings of the IEEE, 2012. **100**(2): p. 461-472.
[36] Yang, K., Y. Zhang, X.M. Li, and J.Z. Xu, *Design and calculation of advanced adiabatic compressed air energy storage system.* Kung Cheng Je Wu Li Hsueh Pao/Journal of Engineering Thermophysics, 2012. **33**(5): p. 725-728.
[37] Park, J.-W., D. Park, D.-W. Ryu, B.-H. Choi, and E.-S. Park, *Analysis on heat transfer and heat loss characteristics of rock cavern thermal energy storage.* Engineering Geology, 2014. **181**: p. 142-156.
[38] Barbour, E., D. Mignard, Y. Ding, and Y. Li, *Adiabatic Compressed Air Energy Storage with packed bed thermal energy storage.* Applied Energy, 2015. **155**: p. 804-815.
[39] Kere, A., N. Sadiki, X. Py, and V. Goetz, *Applicability of thermal energy storage recycled ceramics to high temperature and compressed air operating conditions.* Energy Conversion and Management, 2014. **88**: p. 113-119.
[40] Palanisamy, M. and H. Niyas, *Comparison of Thermal Characteristics of Sensible and Latent Heat Storage Materials Encapsulated in Different Capsule Configurations*, in *Concentrated Solar Thermal Energy Technologies*. 2018, Springer. p. 11-20.
[41] Mathur, A., R. Kasetty, J. Oxley, J. Mendez, and K. Nithyanandam, *Using Encapsulated Phase Change Salts for Concentrated Solar Power Plant.* Proceedings of the SolarPACES 2013 International Conference, 2014. **49**(0): p. 908-915.
[42] REN21, *Renewables 2017 global status report.* REN21 Secretariat: Paris, France, 2017.
[43] Stark, C., J. Pless, J. Logan, E. Zhou, and D.J. Arent, *Renewable Electricity: Insights for the Coming Decade*. 2015, National Renewable Energy Lab.(NREL), Golden, CO (United States).

[44] Chen, H., X. Zhang, J. Liu, and C. T, *Compressed Air Energy Storage.* 2013.
[45] Bullough, C., C. Gatzen, C. Jakiel, M. Koller, A. Nowi, and S. Zunft. *Advanced adiabatic compressed air energy storage for the integration of wind energy*. in *Proceedings of the European Wind Energy Conference, EWEC*. 2004.
[46] Zhang, Y., K. Yang, X. Li, and J. Xu, *Thermodynamic analysis of energy conversion and transfer in hybrid system consisting of wind turbine and advanced adiabatic compressed air energy storage.* Energy, 2014. **77**: p. 460-477.
[47] Robb, D., *The CAES for wind.* Renewable Energy Focus, 2011. **12**(1): p. 18-19.
[48] Ramadan, O., S. Omer, M. Jradi, H. Sabir, and S. Riffat, *Analysis of compressed air energy storage for large-scale wind energy in Suez, Egypt.* International Journal of Low-Carbon Technologies, 2016. **11**(4): p. 476-488.
[49] Manchester, S. and L. Swan, *Compressed Air Storage and Wind Energy for Time-of-day Electricity Markets.* Procedia Computer Science, 2013. **19**: p. 720-727.
[50] Fertig, E. and J. Apt, *Economics of compressed air energy storage to integrate wind power: A case study in ERCOT.* Energy Policy, 2011. **39**(5): p. 2330-2342.
[51] Wang, Z., W. Xiong, D.S.K. Ting, R. Carriveau, and Z. Wang, *Comparison of underwater and underground CAES systems for integrating floating offshore wind farms.* Journal of Energy Storage, 2017. **14**: p. 276-282.
[52] Flynn, G.T. and J.L. Nash-Webber, *Application and design studies of compressed-air energy storage for solar applications, final report.* 1979.
[53] Setiawan, A., A. Priyadi, M. Pujiantara, and M.H. Purnomo. *Sizing compressed-air energy storage tanks for solar home systems*. in *2015 IEEE International Conference on Computational Intelligence and Virtual Environments for Measurement Systems and Applications (CIVEMSA)*. 2015.
[54] Cazzaniga, R., M. Cicu, M. Rosa-Clot, P. Rosa-Clot, G.M. Tina, and C. Ventura, *Compressed air energy storage integrated with floating photovoltaic plant.* Journal of Energy Storage, 2017. **13**: p. 48-57.
[55] Nakhamkin, M. and R.B. Schainker. *ADVANCED COMPRESSED AIR ENERGY STORAGE PLANTS WITH UTILIZATION OF THERMAL ENERGY STORAGE SYSTEMS*. in *American Society of Mechanical Engineers* 1986.
[56] Nakhamkin, M., E. Swensen, R. Schainker, and R. Pollak. *Compressed air energy storage: survey of advanced CAES development*. in *American Society of Mechanical Engineers* 1991.
[57] Hartmann, N., O. Vöhringer, C. Kruck, and L. Eltrop, *Simulation and analysis of different adiabatic Compressed Air Energy Storage plant configurations.* Applied Energy, 2012. **93**: p. 541-548.
[58] Kim, Y.M., D.G. Shin, and D. Favrat, *Operating characteristics of constant-pressure compressed air energy storage (CAES) system combined with pumped hydro storage based on energy and exergy analysis.* Energy, 2011. **36**(10): p. 6220-6233.
[59] Odukomaiya, A., A. Abu-Heiba, K.R. Gluesenkamp, O. Abdelaziz, R.K. Jackson, C. Daniel, . . . A.M. Momen, *Thermal analysis of near-isothermal compressed gas energy storage system.* Applied Energy, 2016. **179**: p. 948-960.
[60] Odukomaiya, A., E. Kokou, Z. Hussein, A. Abu-Heiba, S. Graham, and A.M. Momen, *Near-isothermal-isobaric compressed gas energy storage.* Journal of Energy Storage, 2017. **12**: p. 276-287.
[61] Zhang, X., Y. Xu, X. Zhou, Y. Zhang, W. Li, Z. Zuo, . . . H. Chen, *A near-isothermal expander for isothermal compressed air energy storage system.* Applied Energy, 2018. **225**: p. 955-964.
[62] McBride, T., A. Bell, and D. Kepshire, *ICAES innovation: Foam-based heat exchange.* Seabrook, TX, USA, 2013.
[63] Abdo, R.F., H.T.C. Pedro, R.N.N. Koury, L. Machado, C.F.M. Coimbra, and M.P. Porto, *Performance evaluation of various cryogenic energy storage systems.* Energy, 2015. **90**: p. 1024-1032.

[64] Antonelli, M., U. Desideri, R. Giglioli, F. Paganucci, and G. Pasini, *Liquid Air Energy Storage: A Potential Low Emissions and Efficient Storage System.* Energy Procedia, 2016. **88**: p. 693-697.
[65] Wang, S.X., X.D. Xue, X.L. Zhang, J. Guo, Y. Zhou, and J.J. Wang, *The Application of Cryogens in Liquid Fluid Energy Storage Systems.* Physics Procedia, 2015. **67**: p. 728-732.
[66] Cárdenas, B., A.J. Pimm, B. Kantharaj, M.C. Simpson, J.A. Garvey, and S.D. Garvey, *Lowering the cost of large-scale energy storage: High temperature adiabatic compressed air energy storage.* Propulsion and Power Research, 2017. **6**(2): p. 126-133.
[67] Chen, L.X., M.N. Xie, P.P. Zhao, F.X. Wang, P. Hu, and D.X. Wang, *A novel isobaric adiabatic compressed air energy storage (IA-CAES) system on the base of volatile fluid.* Applied Energy, 2018. **210**: p. 198-210.
[68] Gil, A., M. Medrano, I. Martorell, A. Lázaro, P. Dolado, B. Zalba, and L.F. Cabeza, *State of the art on high temperature thermal energy storage for power generation. Part 1—Concepts, materials and modellization.* Renewable and Sustainable Energy Reviews, 2010. **14**(1): p. 31-55.
[69] Kuravi, S., J. Trahan, D.Y. Goswami, M.M. Rahman, and E.K. Stefanakos, *Thermal energy storage technologies and systems for concentrating solar power plants.* Progress in Energy and Combustion Science, 2013. **39**(4): p. 285-319.
[70] Chiu, J.N., *Heat transfer aspects of using phase change material in thermal energy storage applications*. 2011, KTH Royal Institute of Technology.
[71] Sharma, A., V.V. Tyagi, C.R. Chen, and D. Buddhi, *Review on thermal energy storage with phase change materials and applications.* Renewable and Sustainable Energy Reviews, 2009. **13**(2): p. 318-345.
[72] Tian, Y. and C.Y. Zhao, *A review of solar collectors and thermal energy storage in solar thermal applications.* Applied Energy, 2013. **104**(Supplement C): p. 538-553.
[73] Zalba, B., J.M. Marín, L.F. Cabeza, and H. Mehling, *Review on thermal energy storage with phase change: materials, heat transfer analysis and applications.* Applied Thermal Engineering, 2003. **23**(3): p. 251-283.
[74] H Abedin, A. and M. A Rosen, *A critical review of thermochemical energy storage systems.* The Open Renewable Energy Journal, 2011. **4**(1).
[75] Budt, M., D. Wolf, and R. Span, *Modeling a Low-temperature Compressed Air Energy Storage with Modelica.* 2012. **76**: p. 791-800.
[76] Pickard, W.F., N.J. Hansing, and A.Q. Shen, *Can large-scale advanced-adiabatic compressed air energy storage be justified economically in an age of sustainable energy?* Journal of Renewable and Sustainable Energy, 2009. **1**(3): p. 033102.
[77] SigmaAldrich. *Product*. 2018 [cited 2018 24 Oct]; Available from: https://www.sigmaaldrich.com/catalog/search?term=Si&interface=Molecular%20Formula&N=0&mode=match%20partialmax&lang=en&region=US&focus=product.
[78] Tessier, M.J., M.C. Floros, L. Bouzidi, and S.S. Narine, *Exergy analysis of an adiabatic compressed air energy storage system using a cascade of phase change materials.* Energy, 2016. **106**: p. 528-534.
[79] Pomianowski, M., P. Heiselberg, and Y. Zhang, *Review of thermal energy storage technologies based on PCM application in buildings.* Energy and Buildings, 2013. **67**(0): p. 56-69.
[80] Castell, A. and M.M. Farid, *Experimental validation of a methodology to assess PCM effectiveness in cooling building envelopes passively.* Energy and Buildings, 2014. **81**: p. 59-71.
[81] Khudhair, A.M. and M.M. Farid, *A review on energy conservation in building applications with thermal storage by latent heat using phase change materials.* Energy Conversion and Management, 2004. **45**(2): p. 263-275.
[82] Vautherot, M., F. Marechal, and M.M. Farid, *Analysis of energy requirements versus comfort levels for the integration of phase change materials in buildings.* Journal of Building Engineering, 2015. **1**(1): p. 53-62.

[83] Baetens, R., B.P. Jelle, and A. Gustavsen, *Phase change materials for building applications: A state-of-the-art review.* Energy and Buildings, 2010. **42**(9): p. 1361-1368.
[84] Oró, E., A. de Gracia, A. Castell, M.M. Farid, and L.F. Cabeza, *Review on phase change materials (PCMs) for cold thermal energy storage applications.* Applied Energy, 2012. **99**: p. 513-533.
[85] Juárez, D., R. Balart, S. Ferrándiz, and M. Peydró. *Classification of phase change materials and his behaviour in SEBS/PCM blends*. in *Proceedings of the 5th Manufacturing Engineering Society International Conference–Zaragoza*. 2013.
[86] Tatsidjodoung, P., N. Le Pierrès, and L. Luo, *A review of potential materials for thermal energy storage in building applications.* Renewable and Sustainable Energy Reviews, 2013. **18**: p. 327-349.
[87] Mohamed, S.A., F.A. Al-Sulaiman, N.I. Ibrahim, M.H. Zahir, A. Al-Ahmed, R. Saidur, . . . A.Z. Sahin, *A review on current status and challenges of inorganic phase change materials for thermal energy storage systems.* Renewable and Sustainable Energy Reviews, 2017. **70**: p. 1072-1089.
[88] Zhang, Z. and X. Fang, *Study on paraffin/expanded graphite composite phase change thermal energy storage material.* Energy Conversion and Management, 2006. **47**(3): p. 303-310.
[89] Mills, A., M. Farid, J.R. Selman, and S. Al-Hallaj, *Thermal conductivity enhancement of phase change materials using a graphite matrix.* Applied Thermal Engineering, 2006. **26**(14-15): p. 1652-1661.
[90] Salunkhe, P.B. and P.S. Shembekar, *A review on effect of phase change material encapsulation on the thermal performance of a system.* Renewable and Sustainable Energy Reviews, 2012. **16**(8): p. 5603-5616.
[91] Al-Shannaq, R., J. Kurdi, S. Al-Muhtaseb, and M. Farid, *Innovative method of metal coating of microcapsules containing phase change materials.* Solar Energy, 2016. **129**: p. 54-64.
[92] Hasnain, S.M., *Review on sustainable thermal energy storage technologies, Part I: heat storage materials and techniques.* Energy Conversion and Management, 1998. **39**(11): p. 1127-1138.
[93] Jankowski, N.R. and F.P. McCluskey, *A review of phase change materials for vehicle component thermal buffering.* Applied Energy, 2014. **113**: p. 1525-1561.
[94] Pereira da Cunha, J. and P. Eames, *Thermal energy storage for low and medium temperature applications using phase change materials – A review.* Applied Energy, 2016. **177**: p. 227-238.
[95] Oró, E., A. Gil, L. Miró, G. Peiró, S. Álvarez, and L.F. Cabeza, *Thermal Energy Storage Implementation Using Phase Change Materials for Solar Cooling and Refrigeration Applications.* 1st International Conference on Solar Heating and Coolingfor Buildings and Industry (SHC 2012), 2012. **30**(0): p. 947-956.
[96] Liu, M., W. Saman, and F. Bruno, *Review on storage materials and thermal performance enhancement techniques for high temperature phase change thermal storage systems.* Renewable and Sustainable Energy Reviews, 2012. **16**(4): p. 2118-2132.
[97] Castellani, B., A. Presciutti, M. Filipponi, A. Nicolini, and F. Rossi, *Experimental investigation on the effect of phase change materials on compressed air expansion in CAES plants.* Sustainability, 2015. **7**(8): p. 9773-9786.
[98] Oró, E., C. Barreneche, M.M. Farid, and L.F. Cabeza, *Experimental study on the selection of phase change materials for low temperature applications.* Renewable Energy, 2013. **57**: p. 130-136.
[99] EntropySolutions. *Puretemp technical data sheets*. 2017 [cited 2017 17 october]; Available from: www.puretemp.com.
[100] RubithermTechnologies. *product*. 2017 [cited 2017 18 October]; Available from: www.rubitherm.eu.
[101] CrodaInternationalPLc. *Product*. 2017 [cited 2017 17 October]; Available from: www.crodatherm.com.
[102] CRISTOPIAEnergySystems. *Thermal Energy Storage Catalogue 2013*. 2017 [cited 2017 17 October]; Available from: www.cristopia.com.

[103] Teappcm. *Product Detail*. 2017 21 June 2015 [cited 2017 18 October]; Available from: www.teappcm.com.
[104] ClimatorSweden. *Product Data Sheet*. 2017 [cited 2017 17 october]; Available from: www.climator.com.
[105] PCMProductLtd. *PCM Product*. 2017 [cited 2017 18 October]; Available from: www.pcmproducts.net.
[106] Py, X., R. Olives, and S. Mauran, *Paraffin/porous-graphite-matrix composite as a high and constant power thermal storage material.* International Journal of Heat and Mass Transfer, 2001. **44**(14): p. 2727-2737.
[107] Najjar, Y.S.H. and A.M. Abubaker, *Using novel compressed-air energy storage systems as a green strategy in sustainable power generation–a review.* International Journal of Energy Research, 2016. **40**(12): p. 1595-1610.
[108] Kushnir, R., A. Dayan, and A. Ullmann, *Temperature and pressure variations within compressed air energy storage caverns.* International Journal of Heat and Mass Transfer, 2012. **55**(21-22): p. 5616-5630.
[109] Xia, C., Y. Zhou, S. Zhou, P. Zhang, and F. Wang, *A simplified and unified analytical solution for temperature and pressure variations in compressed air energy storage caverns.* Renewable Energy, 2015. **74**: p. 718-726.
[110] Khamis, A., Z.M. Badarudin, A. Ahmad, A. Ab Rahman, and M.H. Hairi. *Overview of mini scale compressed air energy storage system*. in *Power Engineering and Optimization Conference (PEOCO), 2010 4th International*. 2010. IEEE.
[111] Manfrida, G. and R. Secchi, *Performance prediction of a small-size adiabatic compressed air energy storage system.* International Journal of Thermodynamics, 2015. **18**(2): p. 111-119.
[112] Kiliç, M., Z.K. Kocabiçak, E.E. Topçu, and M. Mutlu, *Mathematical modeling of a small scale compressed air energy storage system*, in *Progress in Exergy, Energy, and the Environment*. 2014, Springer. p. 477-486.
[113] Baqari, F. and B. Vahidi, *Small-compressed air energy storage system integrated with induction generator for metropolises: A case study.* Renewable and Sustainable Energy Reviews, 2013. **21**: p. 365-370.
[114] Vongmanee, V. and V. Monyakul. *A new concept of small-compressed air energy storage system integrated with induction generator*. in *2008 IEEE International Conference on Sustainable Energy Technologies*. 2008. IEEE.
[115] Kaya, D., P. Phelan, D. Chau, and H. Ibrahim Sarac, *Energy conservation in compressed-air systems.* International Journal of Energy Research, 2002. **26**(9): p. 837-849.
[116] Zhang, L., S. Ahmari, M. Budhu, and B. Sternberg, *Feasibility study of compressed air energy storage using steel pipe piles.* GeoCongress 2012, 2012: p. 4272-4279.
[117] Khamis, A., Z.M. Badarudin, A. Ahmad, A. Ab Rahman, and N.A. Bakar. *Development of mini scale compressed air energy storage system*. in *Clean Energy and Technology (CET), 2011 IEEE First Conference on*. 2011. IEEE.
[118] Wang, S., G. Chen, M. Fang, and Q. Wang, *A new compressed air energy storage refrigeration system.* Energy Conversion and Management, 2006. **47**(18-19): p. 3408-3416.
[119] Kim, Y.-M., J.-H. Lee, S.-J. Kim, and D. Favrat, *Potential and evolution of compressed air energy storage: energy and exergy analyses.* Entropy, 2012. **14**(12): p. 1501-1521.
[120] Zhang, Y., K. Yang, X. Li, and J. Xu, *The thermodynamic effect of air storage chamber model on Advanced Adiabatic Compressed Air Energy Storage System.* Renewable Energy, 2013. **57**: p. 469-478.
[121] Button, V.L., *Chapter 4 - Temperature Transducers*, in *Principles of Measurement and Transduction of Biomedical Variables*. 2015, Academic Press: Oxford. p. 101-154.
[122] Smith, J., H. Van Ness, and M. Abbott, *Chemical engineering thermodynamics.* Sat, 1996. **18**: p. 1-3.

[123] Raju, M. and S. Kumar Khaitan, *Modeling and simulation of compressed air storage in caverns: A case study of the Huntorf plant.* Special issue on Thermal Energy Management in the Process Industries, 2012. **89**(1): p. 474-481.
[124] Woodfield, P.L., M. Monde, and Y. Mitsutake, *Measurement of Averaged Heat Transfer Coefficients in High-Pressure Vessel during Charging with Hydrogen, Nitrogen or Argon Gas.* Journal of Thermal Science and Technology, 2007. **2**(2): p. 180-191.
[125] Burmeister, L.C., *Convective heat transfer (2nd ed.)*. 1993: New York: Wiley.
[126] Bejan, A., *Convection heat transfer (4th.ed)*. 2013: Hoboken,NJ:Wiley.
[127] Mazzucco, A., E. Rothuizen, J.-E. Jørgensen, T.R. Jensen, and M. Rokni, *Integration of phase change materials in compressed hydrogen gas systems: Modelling and parametric analysis.* International Journal of Hydrogen Energy, 2016. **41**(2): p. 1060-1073.
[128] Giro-Paloma, J., R. Al-Shannaq, A.I. Fernández, and M.M. Farid, *Preparation and characterization of microencapsulated phase change materials for use in building applications.* Materials, 2015. **9**(1): p. 11.
[129] Farid, M.M., F.A. Hamad, and M. Abu-Arabi, *Melting and Solidification in Multi-Dimensional Geometry and Presence of More Than One Interface.* Energy Conversion and Management, 1998. **39**(8): p. 809-818.
[130] Khateeb, S.A., S. Amiruddin, M. Farid, J.R. Selman, and S. Al-Hallaj, *Thermal management of Li-ion battery with phase change material for electric scooters: experimental validation.* Journal of Power Sources, 2005. **142**(1-2): p. 345-353.
[131] Liu, X., Y. Zhang, J. Shen, S. Yao, and Z. Zhang, *Characteristics of air cooling for cold storage and power recovery of compressed air energy storage (CAES) with inter-cooling.* Applied Thermal Engineering, 2016. **107**: p. 1-9.
[132] Sciacovelli, A., Y. Li, H. Chen, Y. Wu, J. Wang, S. Garvey, and Y. Ding, *Dynamic simulation of Adiabatic Compressed Air Energy Storage (A-CAES) plant with integrated thermal storage – Link between components performance and plant performance.* Applied Energy, 2017. **185, Part 1**: p. 16-28.
[133] Geissbühler, L., V. Becattini, G. Zanganeh, S. Zavattoni, M. Barbato, A. Haselbacher, and A. Steinfeld, *Pilot-scale demonstration of advanced adiabatic compressed air energy storage, Part 1: Plant description and tests with sensible thermal-energy storage.* Journal of Energy Storage, 2018. **17**: p. 129-139.
[134] Wang, S., X. Zhang, L. Yang, Y. Zhou, and J. Wang, *Experimental study of compressed air energy storage system with thermal energy storage.* Energy, 2016. **103**: p. 182-191.
[135] Iqbal, K., A. Khan, D. Sun, M. Ashraf, A. Rehman, F. Safdar, . . . H.S. Maqsood, *Phase change materials, their synthesis and application in textiles—a review.* The Journal of The Textile Institute, 2019. **110**(4): p. 625-638.
[136] Al-Shannaq, R., B. Young, and M. Farid, *Cold energy storage in a packed bed of novel graphite/PCM composite spheres.* Energy, 2019. **171**: p. 296-305.
[137] Al Shannaq, R. and M.M. Farid, *10 - Microencapsulation of phase change materials (PCMs) for thermal energy storage systems*, in *Advances in Thermal Energy Storage Systems*, L.F. Cabeza, Editor. 2015, Woodhead Publishing. p. 247-284.
[138] Saputro, E.A. and M.M. Farid, *A novel approach of heat recovery system in compressed air energy storage (CAES).* Energy Conversion and Management, 2018. **178**: p. 217-225.
[139] Roberts, N.S., R. Al-Shannaq, J. Kurdi, S.A. Al-Muhtaseb, and M.M. Farid, *Efficacy of using slurry of metal-coated microencapsulated PCM for cooling in a micro-channel heat exchanger.* Applied Thermal Engineering, 2017. **122**: p. 11-18.
[140] Zhang, H., X. Wang, and D. Wu, *Silica encapsulation of n-octadecane via sol–gel process: A novel microencapsulated phase-change material with enhanced thermal conductivity and performance.* Journal of Colloid and Interface Science, 2010. **343**(1): p. 246-255.
[141] Wang, J., K. Lu, L. Ma, J. Wang, M. Dooner, S. Miao, . . . D. Wang, *Overview of compressed air energy storage and technology development.* Energies, 2017. **10**(7): p. 991.

[142] Tallini, A., A. Vallati, and L. Cedola, *Applications of micro-CAES systems: energy and economic analysis.* Energy Procedia, 2015. **82**: p. 797-804.
[143] Karellas, S. and N. Tzouganatos, *Comparison of the performance of compressed-air and hydrogen energy storage systems: Karpathos island case study.* Renewable and Sustainable Energy Reviews, 2014. **29**(0): p. 865-882.
[144] IEA-ETSAP, I., *Thermal energy storage: Technology brief e17.* 2013.

Appendices

A. Permission to use the figure (copyright)

Erwan Adi Saputro <eadi197@aucklanduni.ac.nz>
to Marcus

Dear
Marcus Budt

Thank for your reply,
Please see attachment is my redrawn ACAES including the citation that I want to use on my paper

Budt, Marcus <marcus.budt@umsicht.fraunhofer.de>
to Daniel, me

Dear Erwan Adi Saputro,

we permit use and redrawing of our figure using the citation you mentioned and are looking forward to reading your paper once it is published.
By the way, what is the special topic of your paper and what is your work on CAES about?

Best regards,
Marcus

****

Fraunhofer

Dr.-Ing. Marcus Budt
Energieanlagen / Fraunhofer UMSICHT
Osterfelder Str. 3 / 46047 Oberhausen
Telefon: +49 208 8598-1293

B. Manufacturer data sheet for PCM Microcapsules

B.1 Micronal DS 5038X

MICRONAL® DS 5038 X

Climate Control MICRONAL® PCM

Description

Micronal DS 5038 X is a purified paraffin, microencapsulated with highly crosslinked polymethylmethacrylate polymer wall. It is primarily used as a functional component in building materials, textiles, foams, and thermal management systems for temperature regulation.

Properties

Physical form	Powder; >98% SC
Particle size	ca. 50 – 300 µm
Bulk density	ca. 300-400 kg/m³
Solubility in water	Insoluble- Dispersable in water
Phase Change (Melting)	25 °C ± 1°C (main peak)
Phase Change (Crystallization)	24 °C ± 1°C (main peak)
Heat of Fusion (Int. 10-35 °C)	≥ 97 J/g

Applications

Phase Change Materials (PCMs) are widely used in building and construction, textiles, medical applications, transport containers, coatings, and in flexible and rigid foams. The different types of PCMs available vary considerably, but all work on the same principle of latent heat storage and release. Latent heat storage and release occurs when there is an absorption and release of energy, in the form of heat, during a change in phase (solid <-> liquid) of the PCM material. The use of phase change materials for passive thermal energy storage is particularly attractive due to their ability to provide high storage density of energy and thermal regulation at a constant temperature around the phase transition temperature of the material.

Microtek's Micronal DS 5038 X material consists of polymer microspheres that create a secure containment system for the high-purity paraffin wax core. This makes the direct use of microencapsulated PCMs in materials such as conventional and thick-layer plasters, plasterboard, fillers, floor screeds and concrete, possible. Micronal DS 5038 X can also be incorporated in wood products such as MDF and OSB, and in coatings such as acrylic paints. The distinguishing features of Micronal DS 5038 X are that it is acrylic based, low dusting and free of formaldehyde*, making it favorable for a wide range of applications.

As an example, Micronal DS 5038 X can be employed passively or in conjunction with an active cooling system. The maximum loads on heating and cooling systems can be reduced through the application of Micronal PCMs making buildings more energy-efficient. Micronal can be used in interior applications to maintain a more constant temperature in the range of ~24 °C- 25 °C. This leads to a significant increase in comfort inside of the room and reduces peak demands for heating and cooling systems throughout the year.

Processing

Because Micronal DS 5038 X is a dry powder, it can be handled like most solids in processes.

The easiest way to incorporate Micronal PCM is to premix it with system materials and directly add it to the product stream. It is recommended to add Micronal phase change materials to cementitious systems at up to ~ 15% v/v and to plaster-based systems at up to ~ 30% v/v. Thickeners may be added to formulations to help with structural viscosity.

The following points should be considered when cementitious formulations and plaster-based products are being developed:

- Formulations may require the use of more water when using Micronal PCMs
- Plasticizers can be used to counteract thickening effects
- Curing accelerators may be added as necessary, although Micronal PCM causes little delay to the curing process
- Defoamers may be added to reduce air that may become entrapped in the system
- Micronal PCMs can be considered filler particles with an individual capsule diameter of 1-5 um which are agglomerated to 50-300 um powder particles. Reduction in the proportion of additional filler particles in mixtures may be helpful for processing

** No formaldehyde intentionally added*

B.2 Microtek 24D

microtek laboratories, inc.

2400 E. River Rd.
Dayton, Ohio 45439
Tel: 937.236.2213 • Fax: 937.236.2217
e-mail: microtek@microteklabs.com
www.microteklabs.com

MPCM 24D

Microencapsulated Phase Change Material

Phase Change: 24°C, 75.2°F

DESCRIPTION

Microencapsulated phase change materials (MicroPCMs) are very small bi-component particles consisting of a core material, the PCM, and an outer shell or capsule wall. PCMs are low melting materials with melt points in the range of -30°C to 70°C that can absorb and release large amounts of heat. The capsule wall is an inert, stable polymer or plastic.

APPLICATIONS

Microencapsulated PCMs are used to regulate temperatures and for heat storage in a variety of applications.

A primary use of the microPCM products is in the coating of fabrics and foams for the textile industry. The coated materials have broad applications for use in various wearing apparel such as inner and outer garments, gloves and footwear. These end-use products containing microPCMs work by absorbing the body's excess heat, storing that heat, and releasing it back to the body as needed.

Microencapsulated PCMs are also finding widespread use in several other applicaton areas, including in:

- **Electronics** - for cooling electrical components in computers, increasing duty cycles in lasers, and helping maintain constant temperatures for scientific instrumentation and military equipment used in the field.
- **Building Materials** – to increase the energy efficiency of residential and commercial buildings. The materials are being used in combination with radiant heat and solar energy to extend the heating and cooling efficiencies of these systems. PCMs are also being incorporated in plasters, fiberboards, tiles, and insulation.
- **Storage Solutions** – to protect food, beverages, medical products, and temperature-sensitive chemicals in transit.

PROPERTIES

The MPCM 24D product exhibits the following general properties:

Typical Properties	
Appearance	White to slightly off-white color
Form	Dry Powder (≥97% Solids)
Capsule composition	85-90 wt.% PCM 10-15 wt.% polymer shell
Core material	Paraffin
Particle size (mean)	15 - 30micron
Melting Point	24°C (75.2°F)
Heat of Fusion	154 - 164 J/g
Specific Gravity	0.9
Temperature Stability	Extremely stable – less than 1% leakage when heated to 250°C
Thermal Cycling	Multiple

PACKAGING

This product is generally shipped in 50-gallon fiber drums of 140 pounds net weight. Sample quantities may be ordered for customers requiring smaller amounts of product.

HEALTH AND SAFETY

Please refer to the Safety Data Sheet (SDS) for necessary safety and handling precautions for this product.

MPDS3300-0026 Revision 0 Effective Date: 01/01/2017

C. Heat loss calculation

The insulation is made from ceramic fibre, the properties of insulation are as follow :

- k = 0.045 w/mK at 35°C.
- (1,5 cm thickness)

The specification of the insulation based on cylinder is:

- r1=9.8 cm, r2=11.3, L=40 cm
- T2 = 18.3 °C, T1 equilibrium = 35.2°C

Heat loss from conduction and convection

$$Qloss = \frac{(T1 - T2)}{\frac{\ln(\frac{r2}{r1})}{2\pi\, k\, L} + \frac{1}{hA}}$$

$$Qloss = \frac{(35.2 - 18.3)}{\frac{\ln(\frac{11.3}{9.8})}{2\pi\ 0.045\ 0.4} + \frac{1}{1.419}} = 8.7\ j/s$$

In 500 s = 0.0087 kJ/s x 500 = 4.3 kj.

Total Q in the system = 35.5 kj (system air + cylinder)

% Heat loss = 4.3/35.5 = 12.1 %

D. Experiment with graphite matrix.

Apart of using PCM Microcapsules, another approach for capturing the heat during compression is by using impregnated PCM in a graphite matrix.

Procedure:

1. Make small balls of graphite (diameter 1 cm) from a graphite block.
2. The small balls of graphite are impregnated with PCM PT29 following the coating process / followed by the coating process.
3. The balls are then put inside the small cylinder.
4. Flow the high-compressed air (200 bar) into the small cylinder.
5. Record the air temperature and wall cylinder temperature.

(a) (b) (c)

Figure Appendix D.1, (a) small cylinder, (b) small balls of graphite before compression, (c) after compression.

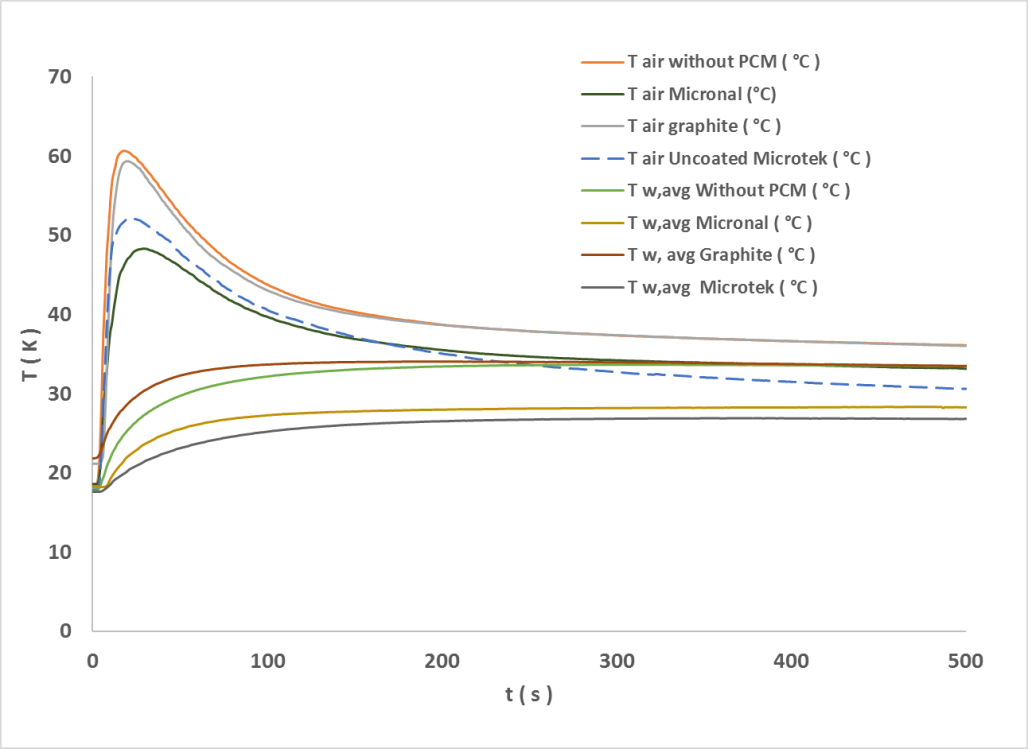

Figure Apendix D2. Air temperature profile during compression

The above graph shows the air temperature profile during compression in the system without PCM, with small balls of graphite, and with PCM microcapsules (Microtek and Micronal). As shown, the graphite balls have little effect on reducing air temperature, while the PCM microcapsules have a significant effect in minimizing increased temperatures during compressing. This indicates that the PCM inside the graphite may not be able to absorb the heat during the charging process at a high rate as the compression process is fast (10 seconds). Also after compression, many cracks were found in the graphite balls. In short, the use of PCM impregnated in a graphite matrix is not promising approach.